

NISTIR 89-4088

SURFACE FINISH METROLOGY TUTORIAL

**T. V. Vorburger
Supervisory Physicist
Center for Manufacturing
Engineering
National Institute of
Standards and Technology**

**J. Raja
Assistant Professor
Mechanical Engineering &
Engineering Mechanics
Department
Michigan Technological
University**

**U.S. DEPARTMENT OF COMMERCE
National Institute of Standards
and Technology
Gaithersburg, MD 20899**

JUNE 1990



**U.S. DEPARTMENT OF COMMERCE
Robert A. Mosbacher, Secretary
National Institute of Standards
and Technology
John W. Lyons, Director**

NOTICE

These notes contain figures reprinted with permission from other sources. The figures obtained from other sources may not be duplicated unless permission is obtained from the authors and publishers of the original documents.

DISCLAIMER

Certain commercial equipment, instruments, or materials are identified in this paper in order to specify adequately certain experimental procedures. Such identification does not imply recommendation or endorsement by the National Institute of Standards and Technology or Michigan Technological University nor does it imply that the materials or equipment are necessarily the best available for the purpose.

ACKNOWLEDGMENTS

These notes were developed for a tutorial presented at the October 1988 conference of the American Society for Precision Engineering held in Atlanta, Georgia.

We are grateful to a number of people who have contributed materials used in these notes and lectures. They include A. Tabenkin, D.E. Gilsinn, C.H.W. Giauque, F.E. Scire, E.C. Teague, J. Garbini, J.C. Wyant, R.A. Smythe, F. Mason, T.C. Bristow, J.M. Bennett, M.J. Downs, E.L. Church, R. Brodmann, R.A. Dragoset, U. Koehler, D.K. Biegelsen, J.A. Detrio, J. Zimmerman, D. Risko, B.J. Griffiths, R.D. Young, J. Bielle, B.B. Gloss, and P. Ackroyd. We are also grateful to F.F. Rudder, Jr., and E.P. Whinton for suggestions to clarify a number of explanations in the text. V.S. Gagne typed and edited the manuscript.

TABLE OF CONTENTS

	<u>Page</u>
1. INTRODUCTION	1
2. GENERAL IDEAS ABOUT SURFACES	2
References.	12
3. THE STYLUS TECHNIQUE	16
General	16
Transducers	16
Results	19
Key Properties.	19
Stylus Tips	26
Traverse Mechanisms and Reference Lines	31
Pitfalls.	33
R_a and R_q	35
Other Properties.	35
Drawing Terminology	37
Calibration	41
Sources of Uncertainty.	43
3-D Profiling	45
References.	47
4. PARAMETERS, FUNCTIONS, AND FILTERING	51
Introduction.	51
Constituents of Surface Texture	51
Measurement of Surface Profile.	53
Separation of Waviness and Roughness (Filtering).	57
Surface Texture Parameters.	65
Statistical Functions	73
Other Descriptors	78
References.	80
5. SURVEY OF PROFILING TECHNIQUES	83
Fringe-Field Capacitance	83
Optical Sectioning.	83
Interferometry.	85
Recent Interferometers.	87
Focus Detection	98
STM and AFM	98
References.	106
6. AREA TECHNIQUES.	110
Optical Scattering.	110
Ultrasonics	122
Areal Capacitance	124
References.	129
7. FUNCTION	132
Optics.	132
Hydrodynamic Drag	134
Aerodynamic Drag.	134
Metalworking.	137
A Surface Texture Information System.	146
References.	150
APPENDIX A	153

SECTION 1

INTRODUCTION

The surface finish is important to the function of many kinds of industrial products ranging from optics to highways, but there is a bewildering variety of techniques for measuring surface finish. In this tutorial, we will present a review of the field, hopefully a fairly inclusive one, and at the same time try to give some insight into the various classes of techniques for measuring surfaces and their uses.

The contents of our discussion today are as follows. Section 2 has some general ideas about surface roughness. This is followed by a section on the stylus technique, which is probably the most widely used class of instrument. After that we will discuss surface parameters, statistical functions, and filtering. Then we will survey other types of profiling techniques besides the stylus technique and area techniques as well, and finally we will discuss some examples of how surface finish affects surface function.

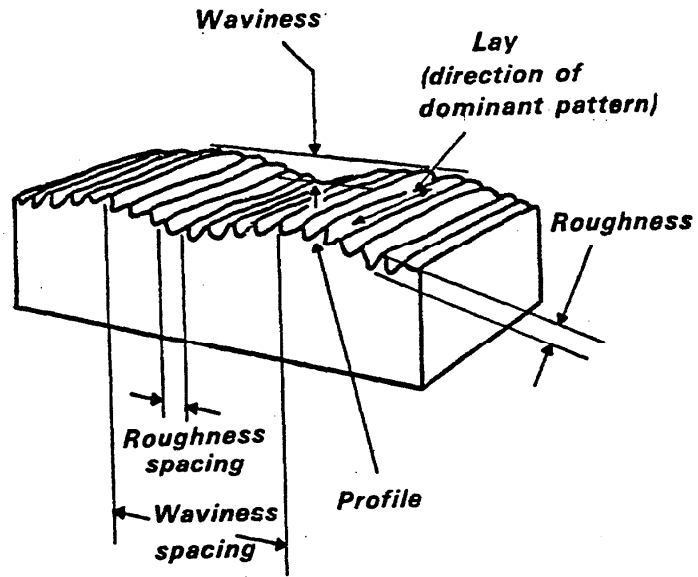
SECTION 2

GENERAL IDEAS ABOUT SURFACES

Participants in the tutorial received a copy of the ANSI Standard, ANSI/ASME B46.1-1985 [1] on Surface Texture and much of the material is taken from there. Figure 2-1 is taken from the British Standard 1134-1972, Assessment of Surface Texture [6] and it shows some key ideas in surface texture measurement. It is a schematic diagram of a surface that has been produced by some machining process, and you see here two orders of structure. The roughness with its typical roughness height and roughness spacing represents the more closely spaced peaks and valleys. Roughness is usually produced by the basic surface forming process. The waviness consists of the more widely spaced irregularities and is often produced by vibrations in the machine. The characteristic sizes of these two classes of structure are generally different.

"Lay" is the term used to indicate the direction of the dominant pattern of texture on the surface. On this surface, the lay is in the front-to-back direction. Surfaces produced by machining processes ordinarily have a strong lay pattern; that is, they are unidirectional.

Figure 2-2 lists the components of surface topography. The term "topography" itself represents all of the spatial structure of peaks and valleys that exist on a surface. Once again the roughness consists of the closely spaced irregularities and these may be cutting tool marks or may be produced by the grit of a grinding wheel. Roughness, therefore, has characteristic structure which can be related to those causes. The waviness consists of more widely spaced irregularities, which might be produced by vibration or chatter in the machine. Error of form consists of long-period or noncyclic deviations in the surface profile, and these could have been produced by errors in the machine ways or spindles, or by uneven wear in the machine. Finally, flaws are discrete and infrequent irregularities; these might include cracks, pits, and scratches. Please note at the bottom of the figure that by definition the roughness and waviness comprise the surface texture. Error of form is not considered



Surface characteristics and terminology

Figure 2-1

Components of Surface Topography

- **Roughness - Closely Spaced Irregularities**
(cutting tool marks, grit of grinding wheel)
- **Waviness - More Widely Spaced Irregularities**
(vibration & chatter)
- **Error of Form - Long Period or Non-cyclic Deviations**
(errors in ways or spindles, uneven wear)
- **Flaws - Discrete, Infrequent Irregularities**
(cracks, pits, scratches)

Roughness and Waviness Comprise the Surface Texture

Figure 2-2

part of surface texture and neither are flaws. So the ANSI Standard B46.1 only covers the two first topics, roughness and waviness. In standardization work, error of form is studied by the ASME/ANSI Committee B89 [2] and flaws are studied by the ANSI Committee on Surface Integrity [3].

We should add that the words surface roughness, surface texture, and surface topography, tend to get used interchangeably. In fact, this practice does not lead to a lot of confusion. Usually when we talk about texture, we mainly refer to the roughness itself. That quality has been the one of primary interest to engineers, although the specification of waviness poses important problems in a number of applications.

The term "surface finish" is not as carefully defined as the others. It generally refers to the overall description of the surface including the texture, the flaws, the materials, and any coatings applied. However, the term does not include errors of form. We generally prefer the terms "texture" and "roughness" to "finish" and will use those almost exclusively.

We will be discussing surface parameters a little bit later, but for starters we ask the question "What are you interested in when you measure surface roughness?" Figure 2-3 shows two quantities that are of primary importance here: a measure of surface height indicated by the roughness average parameter, R_a , and a measure of the spacings of the peaks and valleys of the surface roughness, indicated on this periodic surface profile by the wavelength parameter, D .

Figure 2-4 taken from ANSI B46.1 shows the ranges of surface roughness obtainable from various standard engineering production methods. These range from shaping, drilling, and electrical discharge machining which produce very rough surface finishes, on the order 250 μin (6.35 μm) or more, down to lapping and polishing which produce roughnesses of a few μin or so. The metric unit micrometer (μm) and the English microinch (μin) are both widely used in surface metrology.

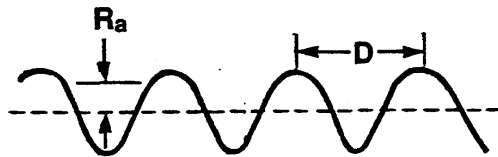


Figure 2-3

Two Key Surface Parameters

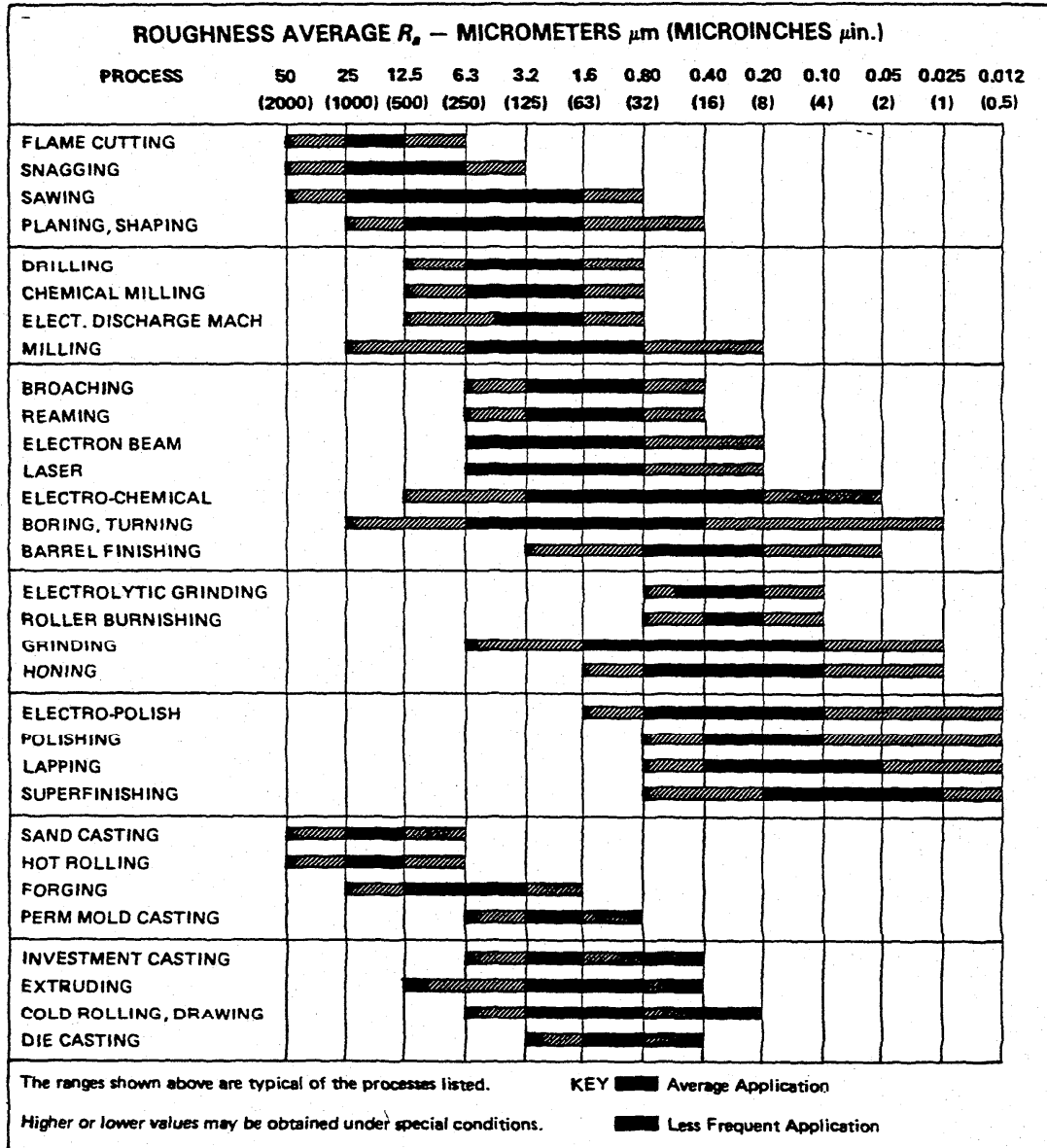


Figure 2-4
Surface Roughness Produced by Common Production Methods
(from ANSI B46.1-1985 [1])

$$1 \mu\text{in} = 0.0254 \mu\text{m} \text{ (exactly) ,}$$

$$1 \mu\text{m} = 40 \mu\text{in} \text{ (approximately) .}$$

Figure 2-5 shows some applications of roughness measurements. These include standard ones in the automotive and other metal working industries that often involve sliding components. Specified roughness heights for these kinds of applications are on the order of fractions of a micrometer.

Another interesting application is in shipbuilding, specifically ship hull surfaces and propellers. The surface roughness of these components should be on the order of several micrometers for hydraulically smooth surfaces [44] on high-speed ships, but the degradation of the marine environment is such that surfaces with roughness heights on the order of several hundred micrometers are not uncommon on ships that have been in service for considerable periods [45].

A slightly more unusual application is in the area of wind tunnels. Experiments in high-performance wind tunnels require that the models be aerodynamically smooth, or else the experiments might not be valid. For such an application, the smoothness of the model should be on the order of $0.1 \mu\text{m}$ or better [46].

In the optical and x-ray fields, basically the smoother the components are, the better. It is not uncommon for surfaces of optical and x-ray components to have roughnesses less than a nanometer.

Finally, in the area of surface science, the presence of steps on a surface can contribute in an important way to the chemical reactions that can take place on it. So in a sense, the presence of steps is a roughness parameter at the molecular level.

The surface finishing process does not come free. There is a cost for various finishing processes. Figure 2-6 [6] shows relationships between production time and resulting surface texture for several finishing

APPLICATIONS INCLUDE:

AUTOMOTIVE & OTHER METALWORKING INDUSTRIES
(Roughness Heights \approx Fractions of a μm)

SHIPBUILDING: HULL SURFACES & PROPELLERS
(Several μm -Several Hundred μm)

WIND TUNNEL MODELS
($\sim 0.1 \mu\text{m}$)

OPTICAL & X-RAY COMPONENTS
($< 1 \text{ nm}$)

SURFACE SCIENCE
(Presence of Steps, Crystal Structure)

Figure 2-5

Typical relationship of surface texture to production time

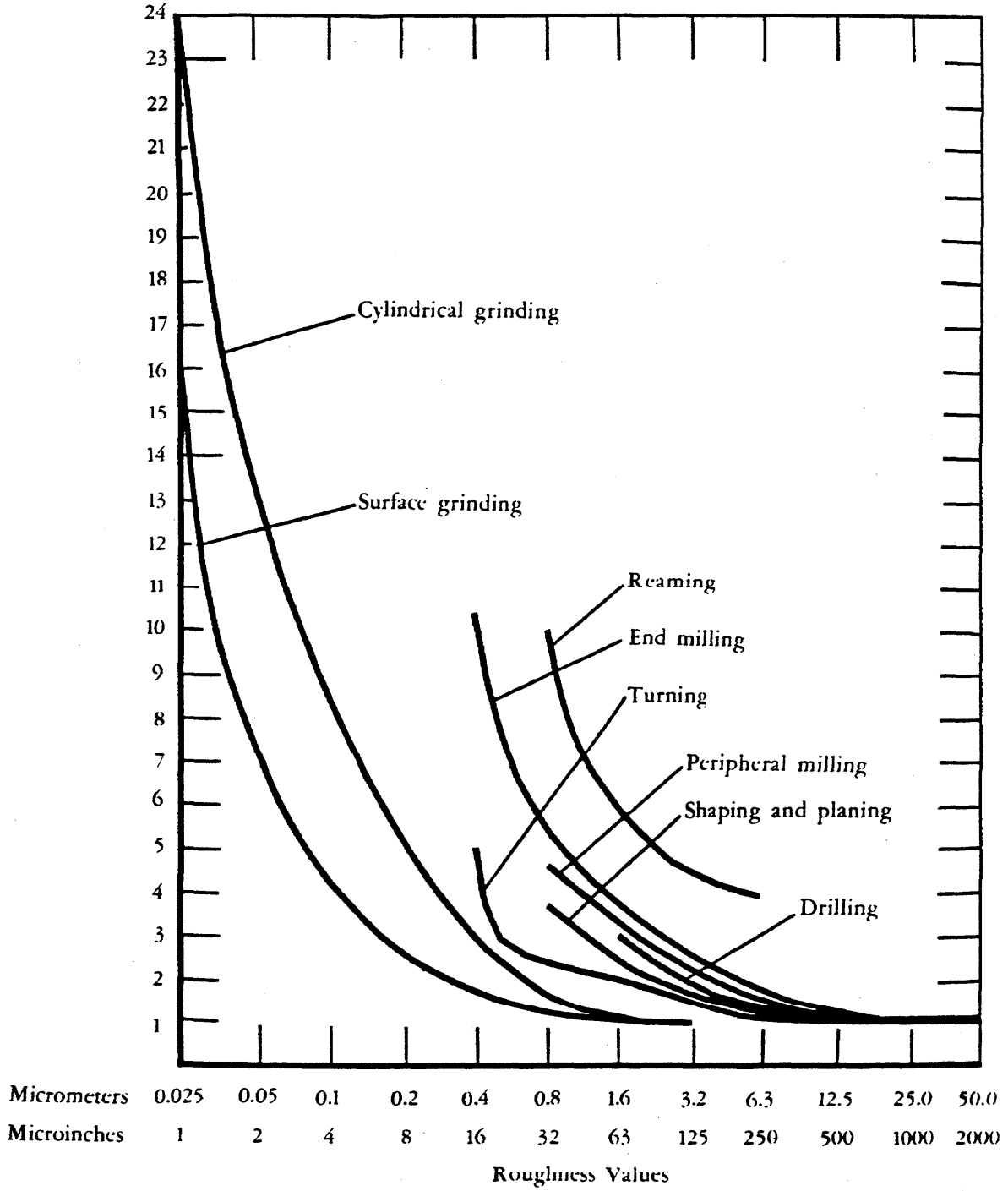


Figure 2-6
 (from BS1134-1972 [6])

processes. The finish is expressed as the roughness average (R_a) to be discussed later. You can see that for all these processes, the costs rise very rapidly as you try to decrease the surface roughness below certain values. Therefore, designers should take into account the fact that overfinishing a component can be costly. We note here that the units along the y-axis are arbitrary and that the chart should not be used to make cost comparisons between the different processes.

Surface topographic techniques may be divided into three major classes [17]: profiling techniques, area techniques, and microscopy. We highlight profiling and area techniques in Fig. 2-7.

With a profiling technique, knowledge of the surface is developed by careful probing of the surface with a high resolution probe. The surface height information consists of a profile of height vs. distance along the surface. Some examples of a profiling technique are the stylus technique, to be discussed in detail, several types of optical profiling, scanning tunneling microscopy (STM), and the fringe-field capacitance technique.

With an area technique, one probes a finite area of the surface and the measured quantities represent some statistical average of the peaks and valleys in that area. Examples of an area technique include optical scattering, ultrasonic scattering, and the areal capacitance probe. It should be noted that profiling techniques by and large take more operator time than area techniques because of the large amount of data required. Area techniques have greater potential for automated manufacturing because with a single measurement, you can possibly derive a parameter that monitors the surface condition.

On the other hand, profiling techniques tend to be accurate, whereas with area techniques, you have to relate the measured quantities to the actual properties of the surface. This usually involves a considerable modeling effort. In summary, profiling techniques tend to be more accurate, area techniques tend to be fast.

Surface Texture Techniques

<u>Profiling</u>	<u>Area</u>
Produce Point by Point Surface Height Information	Produce Area Average Properties
Accurate	Fast
Examples:	Examples:
Stylus Optical Profiling (several types) Fringe-Field Capacitance Scanning Tunneling Microscopy	Optical Scattering Areal Capacitance Ultrasonics

Figure 2-7

Various types of microscopy [20-41] may be considered as a third class of techniques to study surface topography. This includes conventional optical microscopy, scanning electron microscopy (SEM), transmission electron microscopy (TEM), and others. The contrast in the images can provide information about the heights of surface features such as the peaks and valleys. However, these techniques are usually qualitative because the contrast in the images depends on a number of factors in addition to height. When an individual microscopy technique directly yields quantitative surface height information, it may be classified as either a profiling or an area technique. Stereo electron microscopy [41], for example, may be considered to be a profiling technique.

REFERENCES

STANDARDS

1. American National Standard, ASME/ANSI B46.1-1985, Surface Texture (American Society of Mechanical Engineers, New York, 1985).
2. American National Standard, ANSI B89.1.1-1972, Measurement of Out of Roundness (American Society of Mechanical Engineers, New York, 1972), and others.
3. American National Standard, ANSI B211.1-1986, Surface Integrity (American National Standard Institute, New York, 1986).
4. ISO Standard, ISO 4287/1, Surface Roughness - Terminology - Part 1: Surface and Its Parameters (International Organization for Standardization, 1984), and others.
5. Deutsche Normen, DIN 4761-1978, Surface Character (Beuth Verlag GmbH, Berlin, 1978), and others.
6. British Standard, BS1134-1972, Method for the Assessment of Surface Texture, in 2 parts (British Standards Institution, London, 1972), and others.
7. Japanese Industrial Standard, JIS B0601-1976, Surface Roughness (Japanese Standards Association, Tokyo, 1976), and others.
8. French National Standard, E05-015-1984, Surface Texture of Products-Regulations: 1. General-Terminology-Definitions (AFNOR, Paris, 1984), and others.

9. SAE Standard J448a, "Surface Texture"; SAE Recommended Practice J449a, "Surface Texture Control"; and SAE Recommended Practice J911, Oct. 81, "Surface Texture Measurement of Cold Rolled Sheet Steels"; in 1983 SAE Handbook, Volume 1, Materials (Society of Automotive Engineers, Warrendale, PA).
10. ANSI Y14.36 - 1978, Surface Texture Symbols (American Society of Mechanical Engineers, New York, 1978).
11. ASTM Standard F1048, Test Method for Measuring the Effective Surface Roughness of Optical Components by Total Integrated Scattering (ASTM, Philadelphia, 1987).

REVIEWS

12. Rough Surfaces, T.R. Thomas, ed. (Longman Group Ltd., London, 1982).
13. Vorburger, T.V.; Teague, E.C. Optical Techniques for On-Line Measurement of Surface Topography, Opt. Eng. 3, 61 (1981).
14. Bennett, J.M.; Mattson, L. Introduction to Surface Roughness and Scattering, Report UU1P (Uppsala University, Uppsala, Sweden, 1988).
15. Young, R.D. The National Measurement System for Surface Finish, NBSIR 75-927 (U.S. Dept. of Commerce, Washington, DC, 1976).
16. Tabenkin, A. Function: The Key to Surface Finish Requirements, in Proc. of 4th Biennial International Manufacturing Technology Conference, Session 8 (NMTBA, McLean, VA, 1988).
17. Vorburger, T.V.; Hembree, G.G. Characterization of Surface Topography, in Methods of Surface Characterization, Vol.3 (Plenum Press, to be published).
18. Stedman, M. Basis for Comparing the Performance of Surface-Measuring Machines, Prec. Eng. 3, 149 (1987).
19. Vorburger, T.V. Measurements of Roughness of Very Smooth Surfaces, Annals of the CIRP 36/2, 503 (1987).

MICROSCOPY

20. Richardson, J.H. Optical Microscopy for the Materials Sciences (Marcel Dekker, Inc., New York, 1971).
21. Rabinowicz, E. Friction and Wear of Materials (John Wiley and Sons, New York, 1965).

22. Maracas, G.N.; Harris, G.L.; Lee, C.A.; McFarlane, R.A. On the Origin of Periodic Surface Structure of Laser-Annealed Semiconductors, *Appl. Phys. Lett.* 33, 453 (1978).
23. Kirk, C.P.; Nyssonen, D. Measuring Linewidths with an Optical Microscope, *Test and Measurement World* 6, 68 (January 1986).
24. Christie, A.O.; Evans, L.V.; Callow, M.E. A New Look at Marine Fouling, Part 4, *Shipping World and Shipbuilder*, 121 (January 1976).
25. Goldstein, J.I.; Newbury, D.E.; Echlin, P.; Joy, D.C.; Fiori, C.; Lifshin, E. Scanning Electron Microscopy and X-Ray Microanalysis (Plenum Press, New York, 1981).
26. Enger, R.C.; Case, S.K. Optical Elements with Ultrahigh Spatial-Frequency Surface Corrugations, *Appl. Opt.* 22, 3220 (1983).
27. Fractography and Materials Science, L.N. Gilbertson and R.D. Zipp, eds. (American Society for Testing and Materials, Philadelphia, 1981).
28. Kimizuka, M.; Hirata, K. Pattern Profile Control of Polysilicon Plasma Etching, *J. Vac. Sci. Technol.* B3, 16 (1985), and other articles in the same issue.
29. Ichinokawa, T.; Ishikawa, Y. Surface Analyses by Low Energy SEM in Ultra High Vacuum, *Ultramicroscopy* 15, 193 (1984).
30. Spence, J.C.H. Experimental High-Resolution Electron Microscopy (Oxford University Press, Oxford, 1981).
31. Rasigni, M.; Rasigni, G.; Palmari, J.P.; Llebaria, A. Study of Surface Roughness Using a Microdensitometer Analysis of Electron Micrographs of Surface Replicas: I. Surface Profiles, *J. Opt. Soc. Am.* 71, 1124 (1981).
32. Rasigni, G.; Varnier, F.; Rasigni, M.; Palmari, J.P.; Llebaria, A. Spectral-Density Function of the Surface Roughness for Polished Optical Surfaces, *J. Opt. Soc. Am.* 73, 1235 (1983), and references contained therein.
33. Field, M.; Kahles, J.F. Review of Surface Integrity of Machined Components, *CIRP Annals* 20 (2), 1 (1971).
34. Marks, L.D. Direct Imaging of Carbon-Covered and Clean Gold (110) Surfaces, *Phys. Rev. Lett.* 51, 1000 (1983).
35. Hojlund-Nielsen, P.E.; Cowley, J.M. Surface Imaging Using Diffracted Electrons, *Surface Sci.* 56, 340 (1976).

36. Osakabe, N.; Tanishiro, Y.; Yagi, K.; Honjo, G. Reflection Electron Microscopy of Clean and Gold Deposited (111) Silicon Surfaces, *Surface Sci.* 97, 393 (1980).
37. Osakabe, N.; Tanishiro, Y.; Yagi, K.; Honjo, G. Image Contrast of Dislocations and Atomic Steps on (111) Silicon Surface in Reflection Electron Microscopy, *Surface Sci.* 102, 424 (1981).
38. Osakabe, N.; Tanishiro, Y.; Yagi, K.; Honjo, G. Direct Observation of the Phase Transition Between the (7/7) and (1/1) Structures of Clean (111) Silicon Surfaces, *Surface Sci.* 109, 353 (1981).
39. Nankivell, J.F. The Theory of Electron Stereo Microscopy, *Optik* 20, 171 (1963).
40. Butler, D.W. A Stereo Electron Microscope Technique for Microtopographic Measurements, *Micron* 4, 410 (1973).
41. Hillman, W. Research and Development in the Field of Roughness Measuring, Part 3: Measuring Methods by Means of Scanning Electron Microscope, *Technisches Messen* 47, 273 (1980).

OTHERS

42. Abbott, E.J.; Firestone, F.A. Specifying Surface Quality, *J. Mech. Eng.* 55, 569 (1933).
43. Bennett, J.M. Comparison of Techniques for Measuring the Roughness of Optical Surfaces, *Opt. Eng.* 24, 380 (1985).
44. Schlichting, H. Boundary-Layer Theory, seventh edition (McGraw-Hill Book Company, New York, 1979), Chap. 21.
45. Townsin, R.L.; Byrne, D.; Svensen, T.E.; Milne, A. Estimating the Technical and Economic Penalties of Hull and Propeller Roughness, presented at the Annual Meeting of the Society of Naval Architects and Marine Engineers, November 19-21, 1981, New York.
46. Teague, E.C.; Vorburger, T.V.; Scire, F.E.; Baker, S.M.; Jensen, S.W.; Trahan, C.; Gloss, B.B. Evaluation of Methods for Characterizing Surface Topography of Models for High Reynolds Number Wind Tunnels, in AIAA 12th Aerodynamic Testing Conference, Vol. CP-822 (Amer. Inst. of Aeronautics and Astronautics, New York, 1982).
47. Candela, G.A.; Chandler-Horowitz, D.; Novotny, D.B.; Vorburger, T.V.; Giaouque, C.H.W. Film Thickness and Refractive Index Standard Reference Material Calibrated by Ellipsometry and Profilometry, in Optical Testing and Metrology, Proc. SPIE 661, 402 (1986).
48. Ackroyd, P. Surface Performance and Cost, *Quality* 27/8, 18 (1988).

SECTION 3

THE STYLUS TECHNIQUE

GENERAL

We now discuss the stylus technique which is the most commonly used class of surface texture measurement instrument. Figure 3-1 shows a schematic diagram of a stylus instrument. The stylus traverses the surface peaks and valleys, and the vertical motion of the stylus is converted by the transducer into an electrical signal which may be analyzed by digital or analog techniques. In many kinds of modern instruments, the signal undergoes analog-to-digital conversion. The resulting digital profile is stored in a computer and can be analyzed subsequently for roughness or waviness parameters.

Figure 3-2 is a photo which shows a close-up of the drive mechanism of a stylus instrument, including the stylus, the reference flat directly above the stylus, and a supporting leg. This instrument is one that would ordinarily be used in a metrology lab, rather than on the shop floor.

TRANSDUCERS

Figure 3-3 shows a schematic diagram of a stylus transducer [1,5]. This one is called a linear variable differential transformer (LVDT). It has a sensitivity of approximately one angstrom or one-two-hundredth of a microinch. The stylus is fastened to a ferrite core, which is positioned between two coils that form part of an AC bridge. As the ferrite core moves up and down between the coils, the balance of the bridge is changed. The resulting output, after suitable demodulation and amplification, is a voltage signal that is proportional to the displacement of the stylus. The output of the LVDT, therefore, is directly proportional to surface height and hence yields the profile as the surface is scanned. Less expensive types of transducers use inductive or piezoelectric sensing similar to techniques of magnetic phonograph cartridges. Therefore, these

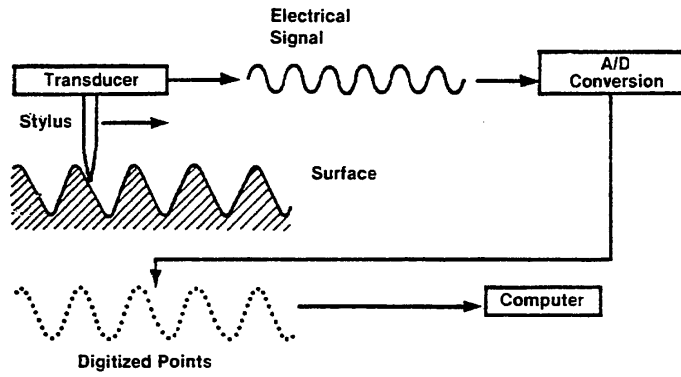


Figure 3-1
Schematic Diagram of Stylus Instrument

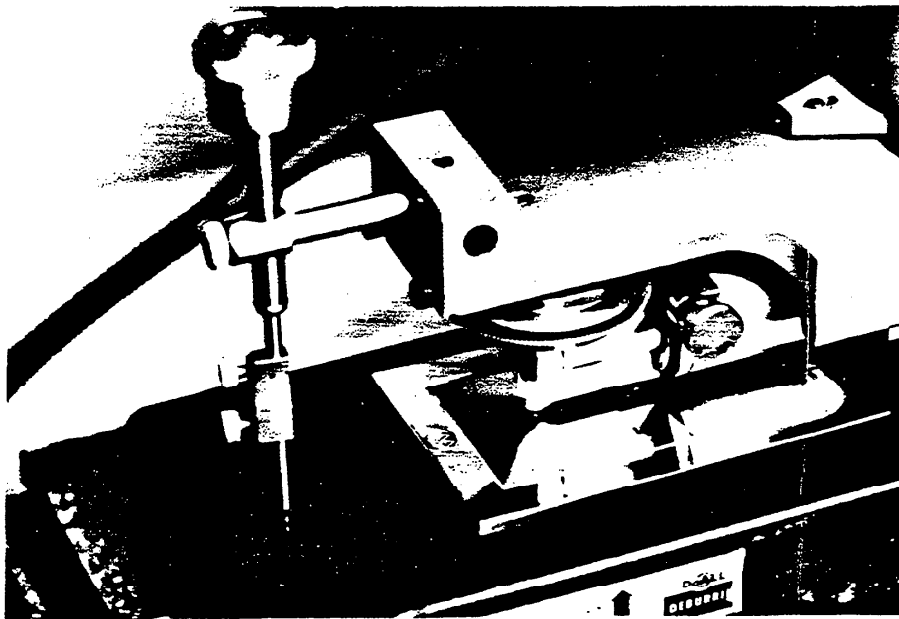


Figure 3-2
Photo of Stylus Drive Assembly

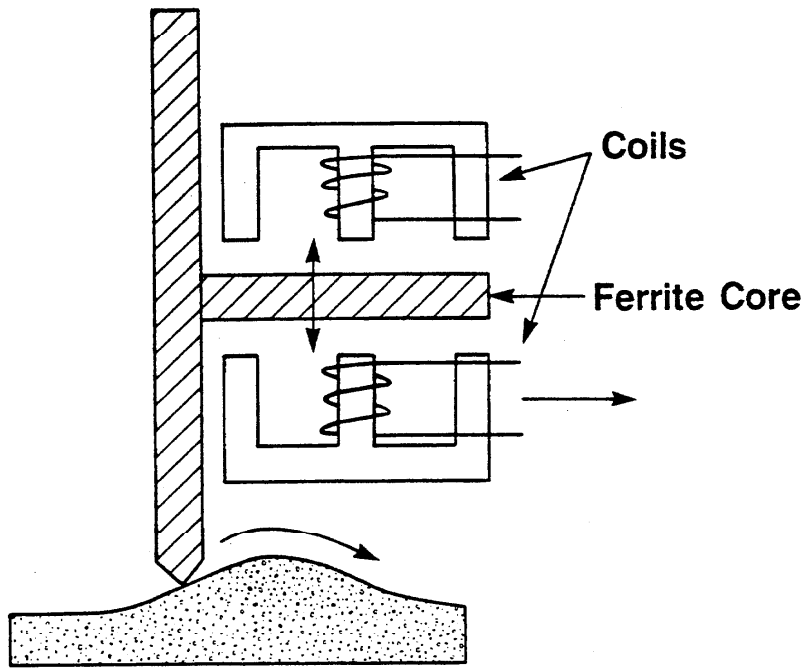


Figure 3-3
Schematic Diagram of LVDT Transducer

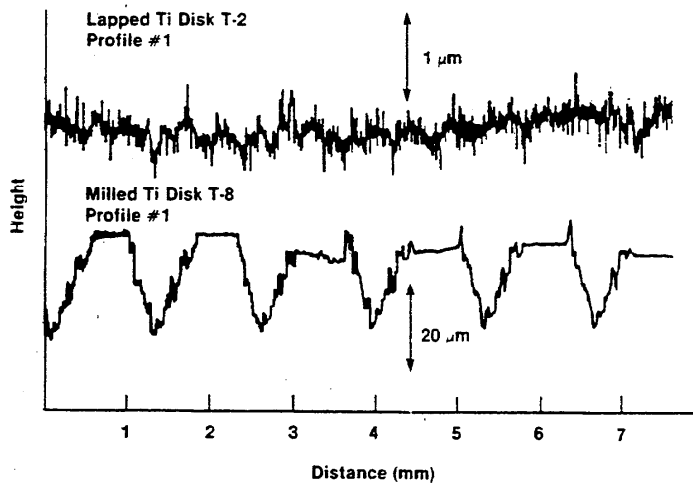


Figure 3-4
Typical Surface Profiles

are velocity- or motion-sensitive transducers. Those types of signals have to be mathematically integrated in order to yield surface profiles.

RESULTS

Figure 3-4 shows typical profiles (surface height vs. lateral distance) obtained with a stylus instrument for two different types of surfaces. These surfaces were used in an experiment on hydrodynamic drag that we participated in (see Sec. 7). The upper profile was taken from a titanium surface that had been lapped fairly smooth. The characteristic roughness structure is significantly less than 1 μm high. Compare that with the lower profile, measured on a surface that had been artificially roughened by ball end-milling to induce more hydrodynamic drag on the surface. This roughness structure is on a completely different scale from the other one.

Figure 3-5 is for another type of surface, one that can be used for calibration of stylus instruments. It shows a step whose height may be calibrated by an absolute technique, such as interferometry. The calibrated step height gives you a well-defined vertical scale for the stylus instrument. You can see how smooth this particular profile is. The step itself is only 200 nm high or 8 μin . This step can be used to calibrate the higher magnification ranges of stylus instruments.

The resolution limit of stylus instruments is approximately 0.1 nm as will be discussed in Sec. 5. Therefore, in principal, you can resolve structures which are less than 1 nm high with special stylus instruments.

KEY PROPERTIES

Figure 3-6 lists some of the properties of stylus instruments. As for their strengths, stylus instruments produce accurate surface profiles when used under proper conditions. The results are quantitative, i.e., from the profiles you can calculate any type of surface parameter or statistic

SiO₂/Si Step



Figure 3-5

PROPERTIES OF STYLUS INSTRUMENTS

STRENGTHS		DRAWBACKS	
ACCURATE	} VERTICAL HORIZONTAL	FRAGILE	POTENTIAL FOR SURFACE DAMAGE SLOW REQUIRES LEVELING 2-D
QUANTITATIVE			
RANGE			
RESOLUTION			

OTHER CONSIDERATIONS
CUTOFF
ESTABLISHING A REFERENCE LINE

Figure 3-6

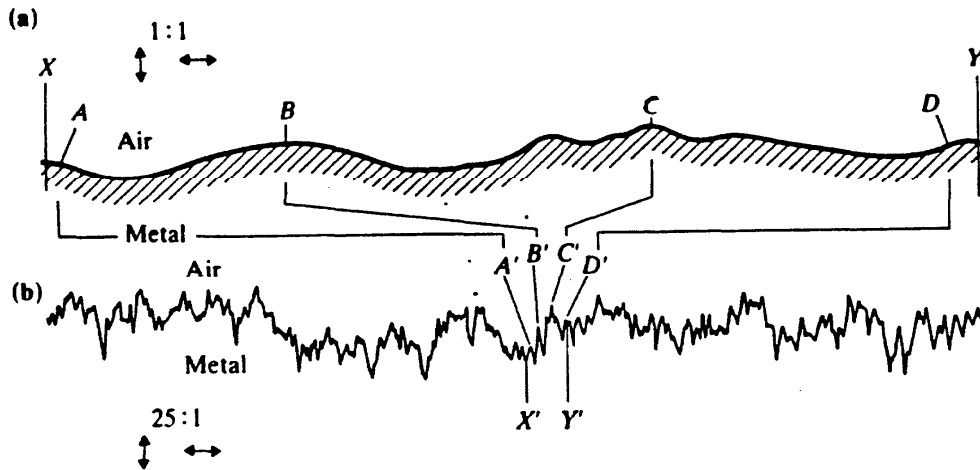


Figure 3-7
Distortion of Aspect Ratio in Surface Profiles
(from Reason [1])

that may be desired. Stylus instruments also have very good range and resolution, both in the vertical and the horizontal or lateral directions.

What are the drawbacks? The stylus itself is fragile and the sharp stylus also has the potential for damaging the surface as well. The instruments usually require leveling, so they can be difficult and slow to operate. In addition, they are two-dimensional instruments, so the surface profile is a vanishingly small fraction of the surface area.

Another characteristic that is important to note for stylus instruments, and other profiling instruments as well, is shown in Fig. 3-7. A typical profile obtained by a stylus instrument is shown at the bottom. This profile has a distorted aspect ratio [1], in order to condense the information in the recorded surface profile. The magnification is 200× in the horizontal direction and 5000× in the vertical direction. The aspect ratio of the profile is therefore distorted by a factor of 25 and can give a misleading picture to someone who is not used to reading surface profiles. If you plot this graph on an undistorted scale shown on top with both the vertical and lateral magnifications at 5000×, then you see how smooth the surface is. In particular, the surface slopes are much gentler than they ordinarily appear on a typical chart record.

In Fig. 3-8, we compare two types of stylus transducers: the LVDT in a surface profiling instrument and a magnetic phonograph cartridge. There are a number of differences between them. The latter is sensitive to the velocity of the stylus and not the displacement. Stylus force for a high quality stylus instrument is quite a bit less than that for the magnetic phonograph cartridge. The lateral velocity, therefore, is very much smaller because with a stylus force of 50 mg, say, you have to move at speeds of about 2 mm/sec or less to prevent bouncing of the stylus off the surface, a condition that would yield an erroneous profile. On the other hand, with a phonograph record rotating at 33 1/3 rpm, the velocity is typically 400 mm/sec. In addition, the sensitive frequency ranges are different.

COMPARISON OF STYLUS TECHNIQUES
(TYPICAL VALUES)

	<u>SURFACE TOPOGRAPHY</u>	<u>MAGNETIC PHONO CARTRIDGE*</u>
TRANSDUCER:	DISPLACEMENT	VELOCITY
FORCE:	50 mgm	1 gm
VELOCITY:	1 mm/sec	400 mm/sec
FREQUENCY RANGE:	0 - 300 Hz	20 Hz - 20 kHz
SPATIAL WAVELENGTH RANGE:	1 μm - 10 mm (50) / \ Stylus Low Size Cutoff	5 μm - 20 mm / \ Stylus Low Size Cutoff
STYLUS SIZE:	0.1 \times 1 μm (State of the Art)	5 \times 18 μm (Elliptical)
VERTICAL RESOLUTION:	0.1 nm (State of the Art)	1 nm @ 1kHz
MAX. DISPLACEMENT:	100 μm	50 μm

*S. Kelly, Wireless World (1969); B.I. Hallgren, J. Aud. Eng. Soc. (1975).

Figure 3-8

Stylus Instrument Parameters

- Bandwidth
Cutoff
Stylus Radius
- Reference Lines
Traverse Mechanisms
Filtering Roughness from
Waviness

Figure 3-9

However, when you combine the velocity and frequency to derive the spatial wavelength range of these instruments, you find that they are quite comparable. The spacings of structures that you sense along the grooves of a record with a magnetic phonograph cartridge are comparable to the structures that one normally measures in surface texture. Stylus sizes are rather comparable as well. A hemispherical stylus tip with a $10\ \mu\text{m}$ radius is standard in the U.S. for a surface topographic instrument; a $0.1\ \mu\text{m} \times 0.1\ \mu\text{m}$ tip size is the state of the art. By comparison, the $5\ \mu\text{m} \times 18\ \mu\text{m}$ tip is typical for an elliptical stylus in a phonograph cartridge. The vertical resolutions are also comparable for both devices, as well as the range or maximum displacement.

In Fig. 3-9, we list some important parameters of stylus instruments that need to be reckoned with. One crucial concept is the bandwidth of stylus measurements [14,31]. That is, over what spatial frequency range is your instrument sensitive? This is determined on the long wavelength side generally by an electronic cutoff (to be discussed in Sec. 4) or by the trace length of the instrument itself, if there is no electronic cutoff, or by the size of the component being measured. On the short wavelength side, the bandwidth might be limited by a low pass filter, but is usually limited by the stylus tip width itself.

A related question is the idea of the reference line. That is, with respect to what curve are the peaks and valleys of the surface measured? This question raises discussion about traverse mechanisms and about how you filter roughness from waviness, a topic similar to the question of bandwidth discussed above.

Figure 3-10, taken from the ANSI standard [32], shows you typical bandwidths for a stylus instrument. Stylus response is plotted vs. wavelength on the surface. The bandwidth is limited on the left hand side, generally by the stylus tip width, and on the right hand side by an electronic cutoff which has standard values that are selectable on the instrument itself.

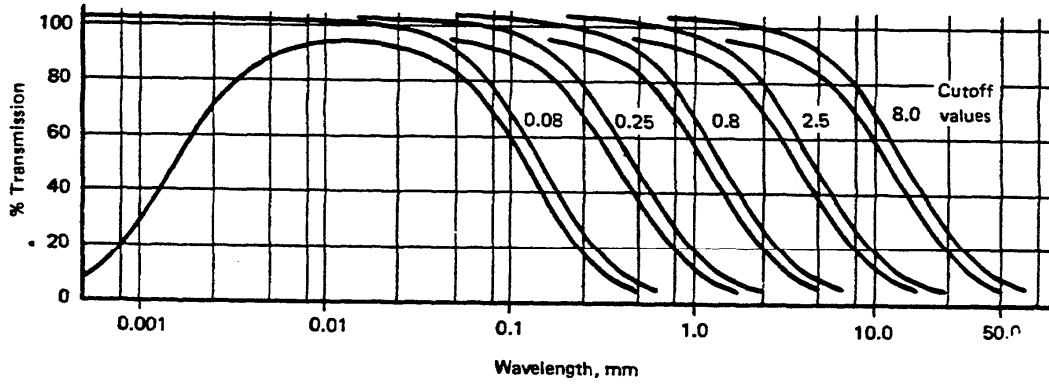
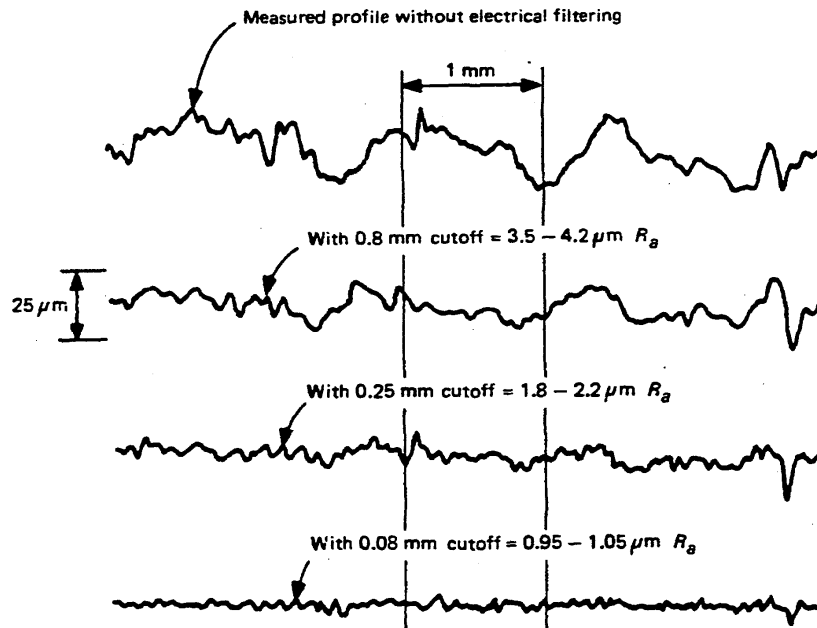


Figure 3-10
Wavelength Transmission Limits
(from ANSI B46.1-1985 [32])



GENERAL NOTE: Profiles are distorted by unequal vertical vs horizontal magnification.

Figure 3-11
Effects of Various Cutoff Values
(from ANSI B46.1-1985 [32])

Figure 3-11, also from the ANSI standard, shows results obtained for various cutoff filters. The profile on top has been measured without any high-pass electrical filtering whereas the others were taken with successively shorter cutoffs. The second curve from the top shows that with a 0.8 mm cutoff, some of the more widely spaced features are attenuated in the profile. At the bottom, however, you see only the finest features showing up on the surface profile. Therefore, as you reduce the cutoff, you emphasize shorter and shorter wavelengths on the surface.

Figure 3-12 from Tabenkin [29] shows how the cutoff that you use should depend on the finishing process for the surface you are trying to measure. For instance, the machining marks produced by planing tend to be widely spaced; therefore, you need longer cutoffs to measure them accurately. On the other hand, machining marks produced by polishing are rather closely spaced, and you can use a short cutoff to profile those marks accurately.

STYLUS TIPS

In the next series of figures, we show some work on measuring the tip width or radius of a stylus, which is almost synonymous with its quality. The method that we prefer is the razor blade trace because it is useful for all but the finest styli and can be done without removing the stylus from the instrument. However, this method was developed for an instrument with an LVDT or other type of direct profiling probe. It is probably not useful with a motion sensitive transducer. The technique [13,16] is shown in Fig. 3-13 and is quite easy. The stylus is stroked across a razor blade, which is clamped in the jaws of a vise. A new razor blade is very sharp. Its edge may be as small as 25 nm (1 μ in) across, and the apex angle is roughly 160°. Therefore, the resulting profile is characteristic of the stylus itself rather than the razor blade.

SELECTION OF CUTOFFS

Typical Finishing Process	Meter Cut-off (mm)				
	0.25	0.8	2.5	8.0	25.0
Milling		X	X	X	
Boring		X	X	X	
Turning		X	X		
Grinding	X	X	X		
Planing			X	X	X
Leaming		X	X		
Broaching		X	X		
Diamond Boring	X	X			
Diamond Turning	X	X			
Honing	X	X			
Lapping	X	X			
Superfinishing	X	X			
Buffing	X	X			
Polishing	X	X			
Shaping		X	X	X	
Electro-Discharge Machining	X	X			
Burnishing		X	X		
Drawing		X	X		
Extruding		X	X		
Moulding		X	X		
Electro-polishing		X	X		

Figure 3-12
(from Tabenkin, [29])

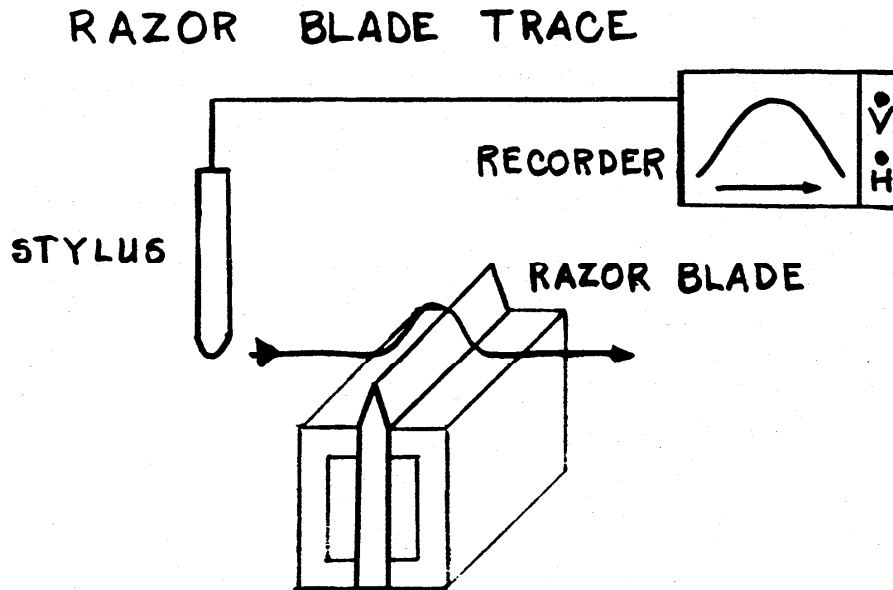


Figure 3-13

Figure 3-14 shows a scanning electron micrograph of the top of a razor blade looking down. You can see that the edge, the dark line here, is significantly smaller than $1\ \mu\text{m}$ across. This should be adequate for measuring the quality of all but the very finest styli.

The next series of photos shows several stylus tips and also three methods used to measure them. The stylus tip shown in Fig. 3-15 is interesting because this one was used in roughness calibrations for at least 12 years in our laboratory. Over that time, we made a number of stylus tip measurements and we were not able to measure any change in the stylus width. The shape was so stable that its degradation was unmeasurable. On the left, we show a scanning electron micrograph, in the middle is an optical micrograph, and on the right is the razor blade trace. You can see the resolution of the razor blade trace is rather comparable to that of the scanning electron micrograph, but the resolution on the optical micrograph is much worse. It should be noted that the distance scale on the right hand graph is slightly different from the one on the left. The stylus has a flat tip about $4\ \mu\text{m}$ across.

Styli are available with tip widths rated as small as $0.1\ \mu\text{m} \times 0.1\ \mu\text{m}$. These probably wear fast into shapes with tip dimensions on the order of $0.5 - 1\ \mu\text{m}$. The stylus in Fig. 3-16 is interesting because it is rather spherical. Its $1\ \mu\text{m}$ radius has been measured both by the SEM and by the razor blade technique. The final stylus (Fig. 3-17) has an odd shape, insofar as it is rather asymmetrical and looks somewhat weatherbeaten. The resolution of this stylus is significantly worse than the $1\ \mu\text{m}$ stylus and will give you quite a different profile of the surface than that one. We should add that the control of the stylus tip dimensions is a rather difficult problem for both manufacturers and users and for standards committees as well. We anticipate that standards in this area will be developing and changing in the future to meet the growing needs of surface measurement technology.

SEM OF RAZOR BLADE

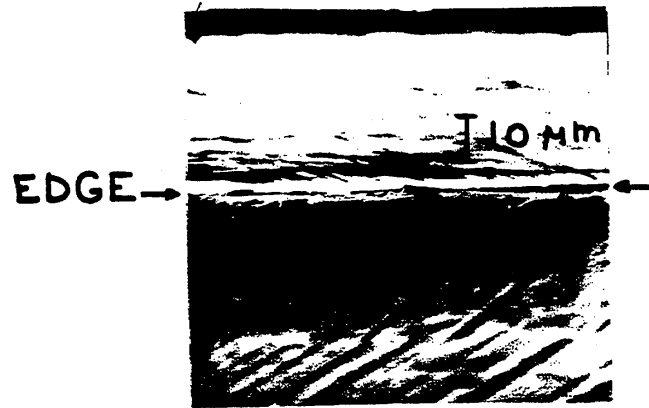


Figure 3-14

'2.5 μm' STYLUS

SEM

OPTICAL

RAZOR BLADE

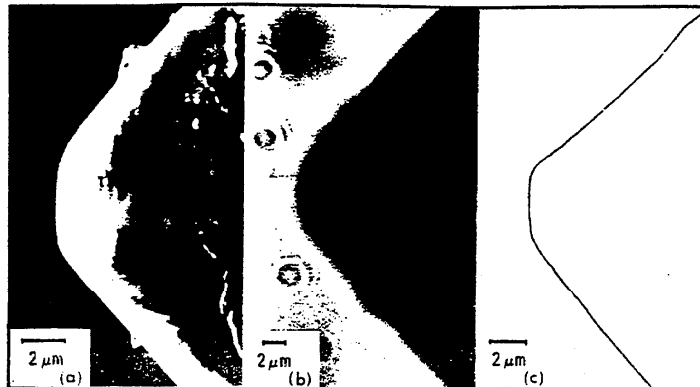


Figure 3-15

Comparison of Stylus Tip Profiles Obtained by Three Techniques

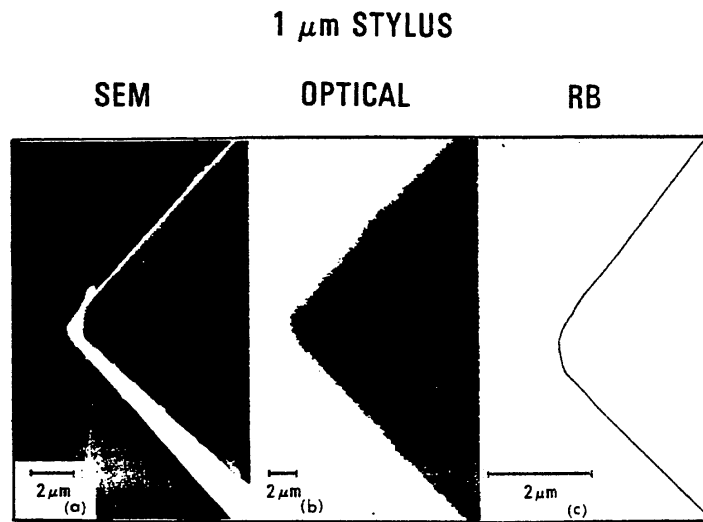


Figure 3-16
Stylus Tip Profiles

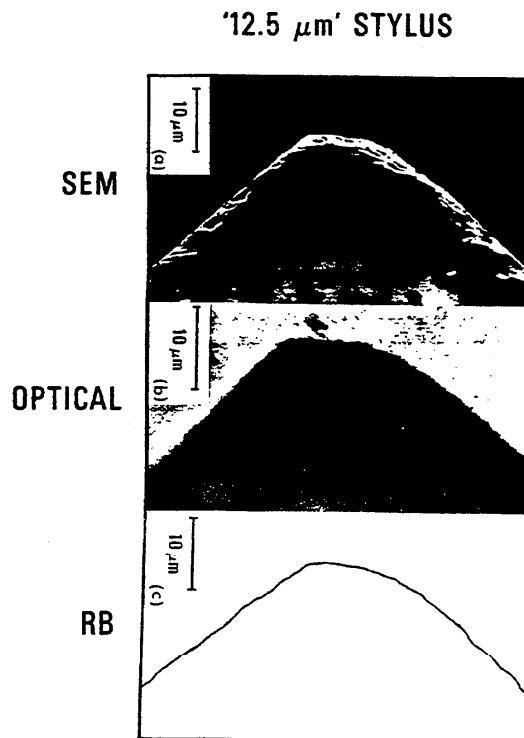


Figure 3-17
Stylus Tip Profiles

TRAVERSE MECHANISMS AND REFERENCE LINES

We now get into the subject of how you establish a reference line or curve. That is, with respect to what do you measure the peaks and valleys of the surface? This question leads us to discuss traverse mechanisms, and we show three design concepts in Fig. 3-18.

The left hand diagram shows the use of a skid. As the assembly carrying the stylus traverses across the surface, the skid serves as the reference because it is contacting the surface over a wide area of peaks. The stylus position is effectively measured with respect to that skid. This is a rather inexpensive design; all the same it is capable of producing profiles with high vertical resolution. However, the pitfall in using this technique is that you can produce a distorted picture of the surface profile, as we will discuss later. Another technique, which is more difficult to implement, is the use of a smooth reference datum. The motion of the carriage is constrained by sliding on the smooth reference, and the vertical motion of the stylus is measured with respect to the carriage. If not carefully designed, there is potential here for Abbe offset errors [33] and for errors due to out-of-straightness of the reference itself. A third solution, which avoids the problems connected with sliding across the reference, is the use of a flexure pivot. The stylus hangs from an assembly that rotates about the flexure pivot. The reference surface is given by a plane that is perpendicular to the axis of the pivot. This can produce very stable motion and very low mechanical noise on the order of 0.1 nm or less. The drawback here is the limit to which you can bend that flexure pivot. Therefore, the traverse lengths are generally short for this kind of device.

Figure 3-19 shows one of the pitfalls of using the skid [34]. A stylus instrument with a skid is traversing across a smooth surface which has a single bump. As the stylus traces over the bump, you have an accurate measurement of that feature, but as the skid slides over it, the profile shows an apparent depression in the surface due to the fact that the reference skid has moved up. Therefore, when using a skid under some

ESTABLISHING A REFERENCE LINE

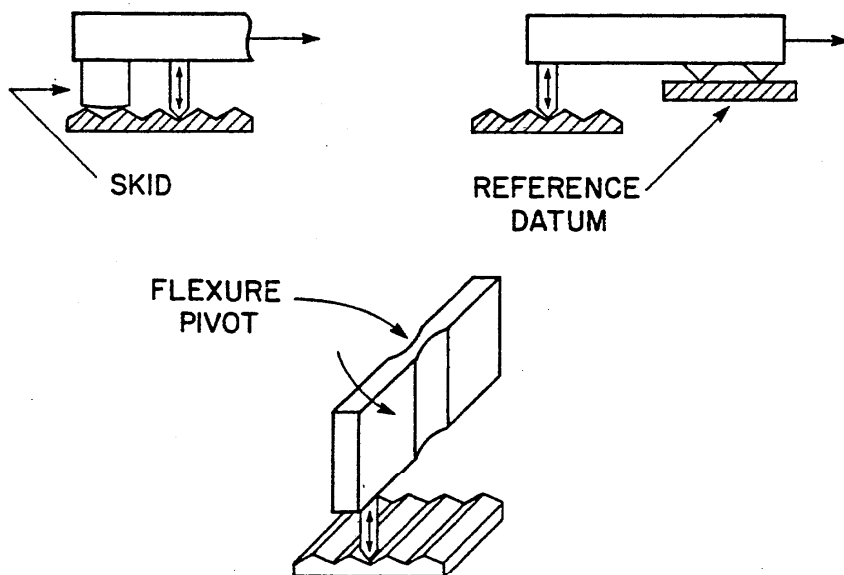


Figure 3-18

Pitfall of a Skid

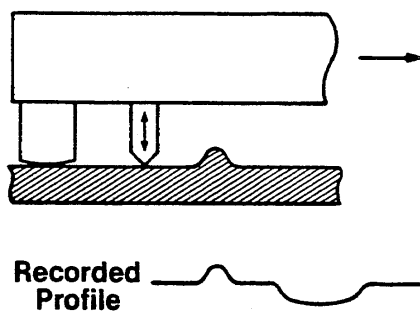


Figure 3-19

conditions, you can produce a profile with erroneous features that do not correspond to real features on the surface.

Once we have established a geometrical reference line, we may still have to distinguish between roughness and waviness by applying some kind of filter. Generally, an electrical filter is used. This subject will be discussed in Sec. 4. Alternatively, you can analyze the profile geometrically by dividing the profile into sampling lengths and drawing a best-line fit through each length [1]. In Fig. 3-20A, the roughness of the ground surface is measured with respect to that best-line fit over each length. The division of the profile into sampling lengths causes the features that have longer wavelengths than the sampling length to be deemphasized. The electrically filtered mean line also shown in Fig. 3-20B is the more standard approach and it yields a much smoother looking curve, but this approach leaves distortions of the surface profile. You can see the peaks of the electrical mean line do not line up exactly with the actual peaks of the surface. In Sec. 4, we will discuss new types of phase-corrected filters that are available in newer instruments. However, these are not yet standardized.

PITFALLS

We conclude this discussion on stylus instrument parameters by mentioning a few pitfalls of stylus instruments (Fig. 3-21) in addition to the distortion introduced by a skid.

With some types of instruments, the transducer may not be linear or the magnification settings may not be equal to the nominal values. With such an instrument, one pitfall is changing magnification after calibration. If you calibrate an instrument on one scale and then change the magnification to measure a surface very much smoother than your calibrating block, you run the risk of making an inaccurate measurement. In some cases, the linearity and the magnification settings are accurate enough so that this problem does not arise.

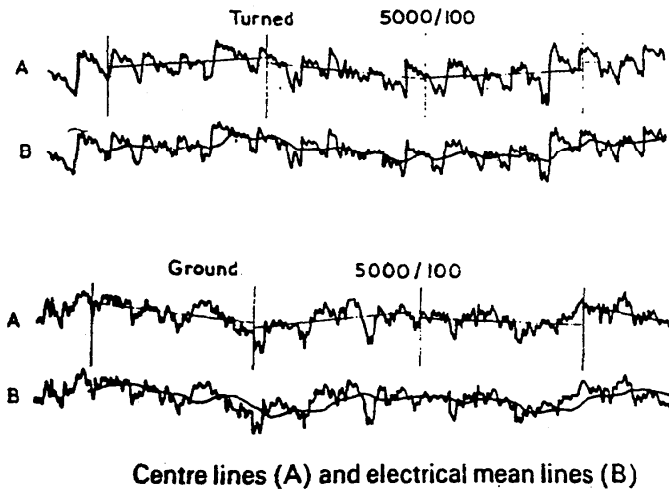


Figure 3-20

Pitfalls of Stylus Instruments

- Changing Magnification After Calibration
- Using a Defective Stylus
- Using the Wrong Cutoff

Figure 3-21

Another pitfall is using a defective stylus. So it is important that you perform quality checks on the styli periodically. Finally, using the wrong cutoff is a pitfall that you must take care to avoid. Figure 3-12 showed that the cutoff selection should depend on the type of manufacturing process that formed the surface.

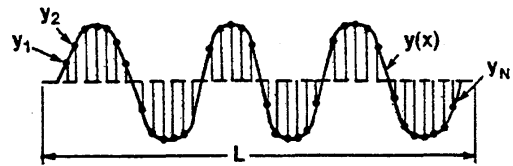
R_a AND R_q

We will discuss surface parameters in more detail in Sec. 4, but at this point we describe two important ones. These are the roughness average R_a and rms roughness R_q , whose definitions are shown in Fig. 3-22. If you have a surface profile with length L represented by the function $y(x)$ or by a set of digitized points y_1, y_2, \dots, y_N , then the roughness average R_a is basically the average deviation of that profile from the mean line. Geometrically, it is given by the total shaded area divided by the distance L ; analytically, it is given by the integral over 0 to L of the absolute value of $y(x)$; and digitally, it is the sum of the various y_i 's divided by the total number of them, N . The rms deviation of the profile from the mean line (R_q) is a similar parameter and is also described briefly in Fig. 3-22.

OTHER PROPERTIES

Linearity is a key factor in stylus instruments. Figure 3-23 shows a test that we did to see whether one of our LVDT transducers gives the same measurement of a surface feature, independent of where in its range you measure it. It shows a measurement of a step height taken at 4 different places in the range of the transducer: low, medium, high, and off scale. You can see that within the chart limits, which are the recommended limits for the range of the transducer, the spread in the values of the step height is only about 0.4%, so the linearity is approximately 0.4% in that range. However, as soon as you go beyond the maximum full scale reading, the calibration changes appreciably.

Surface Parameters



- R_a = Average Deviation of Profile $y(x)$ from the mean Line
 = Total Shaded Area / L

$$= \frac{1}{L} \int_0^L |y(x)| dx \cong \frac{1}{N} \sum |y_i|$$
- R_q = rms Deviation ...

$$\cong \sqrt{\frac{1}{N} \sum y_i^2}$$

Figure 3-22

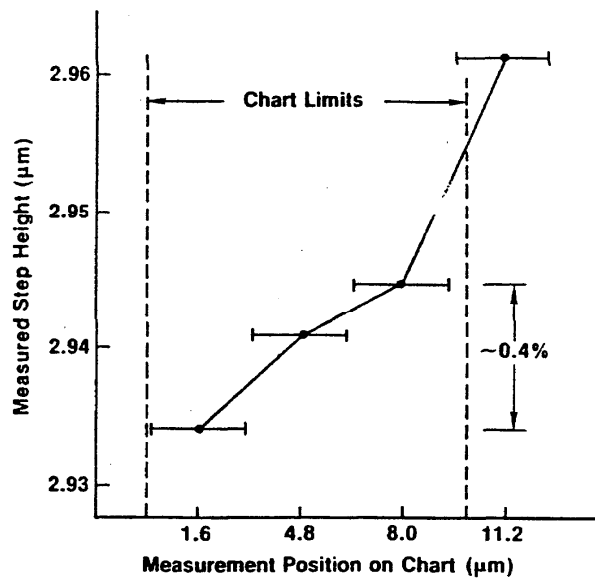


Figure 3-23

Results for Linearity Test of Stylus LVDT

Another interesting property of the stylus instrument is its velocity variation. Figure 3-24 shows an experiment on speed variation that Teague [16] performed using an interferometric measurement of stylus speed. The measured speed varied by about $\pm 2\%$ over the time of the measurement. The conclusion is that this stylus instrument was fairly accurate for measurement of lateral spacings of surface features. A variation in speed can introduce large distortions into the measured surface profile $y(x)$ if data are being measured on a highly sloped surface [37]. An example of this would be roughness profiles measured on the inclined sections of a ball.

DRAWING TERMINOLOGY

We come now to the subject of how you specify surface roughness on a drawing. The information here is taken from the ANSI Standard Y14.36 [30]. Figure 3-25 [29] contains a synopsis of the material in Y14.36. The symbol used for representing surface texture is given by $\sqrt{\quad}$. A number of surface properties can be represented with it. The allowed value of roughness average that is specified is shown above the V. It can be specified either as a maximum value, which may not be exceeded, or as a range of values shown here. The cutoff is specified inside the surface texture symbol and the lay of the surface may be represented there as well. You may also specify other parameters besides R_a . These include the waviness height and the maximum waviness width, as well as the maximum roughness spacing. In addition, the V can contain information about how the material should be removed. The circle indicates that material removal is prohibited. A specification with a line means that material removal is required. You can even specify an allowance for the depth of material removal to the left of the surface texture symbol.

Figure 3-26 shows seven ways for representing the surface lay. The two top ones are probably the most important, since they describe the orientation of the lay with respect to the line that represents the surface on the drawing. Figure 3-27 shows examples of how roughness can be specified on a typical drawing. You can see that about eight surfaces

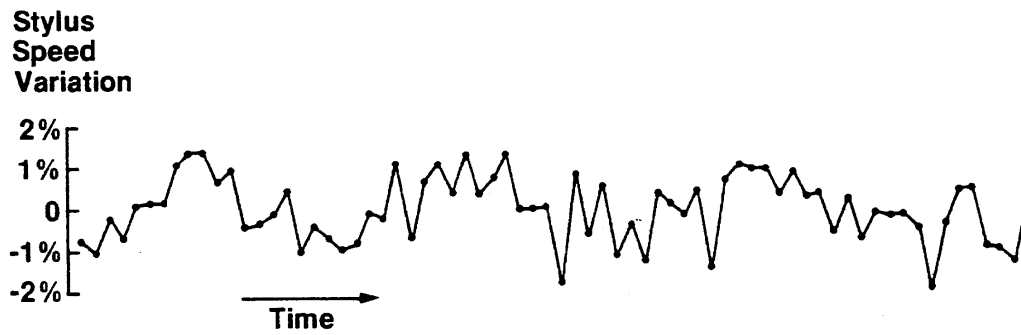
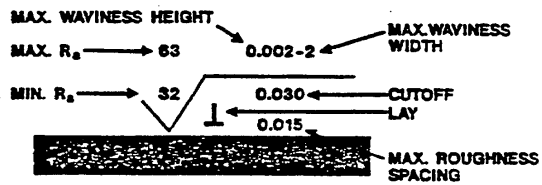


Figure 3-24

SURFACE TEXTURE SYMBOLS

PER ANSI Y14.36



- ✓ SURFACE MAY BE PRODUCED BY ANY METHOD
- ✓ MATERIAL REMOVAL BY MACHINING IS REQUIRED;
MATERIAL MUST BE PROVIDED FOR THAT PURPOSE
- 0.001 ✓ MATERIAL REMOVAL ALLOWANCE IN INCHES
(OR MILLIMETERS)
- ✓ MATERIAL REMOVAL PROHIBITED

Figure 3-25
(from Tabenkin [29])


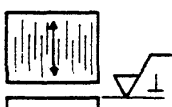


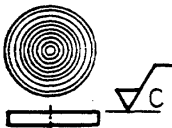
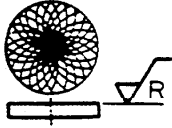
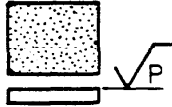
Lay Symbol	Meaning	Example Showing Direction of Tool Marks
—	Lay approximately parallel to the line representing the surface to which the symbol is applied.	
⊥	Lay approximately perpendicular to the line representing the surface to which the symbol is applied.	
X	Lay angular in both directions to line representing the surface to which the symbol is applied.	
M	Lay multidirectional.	
C	Lay approximately circular relative to the center of the surface to which the symbol is applied.	
R	Lay approximately radial relative to the center of the surface to which the symbol is applied.	
P ³	Lay particulate, non-directional, or protuberant.	

Figure 3-26
Lay Symbols
(from ANSI/ASME Y14.36 [30])

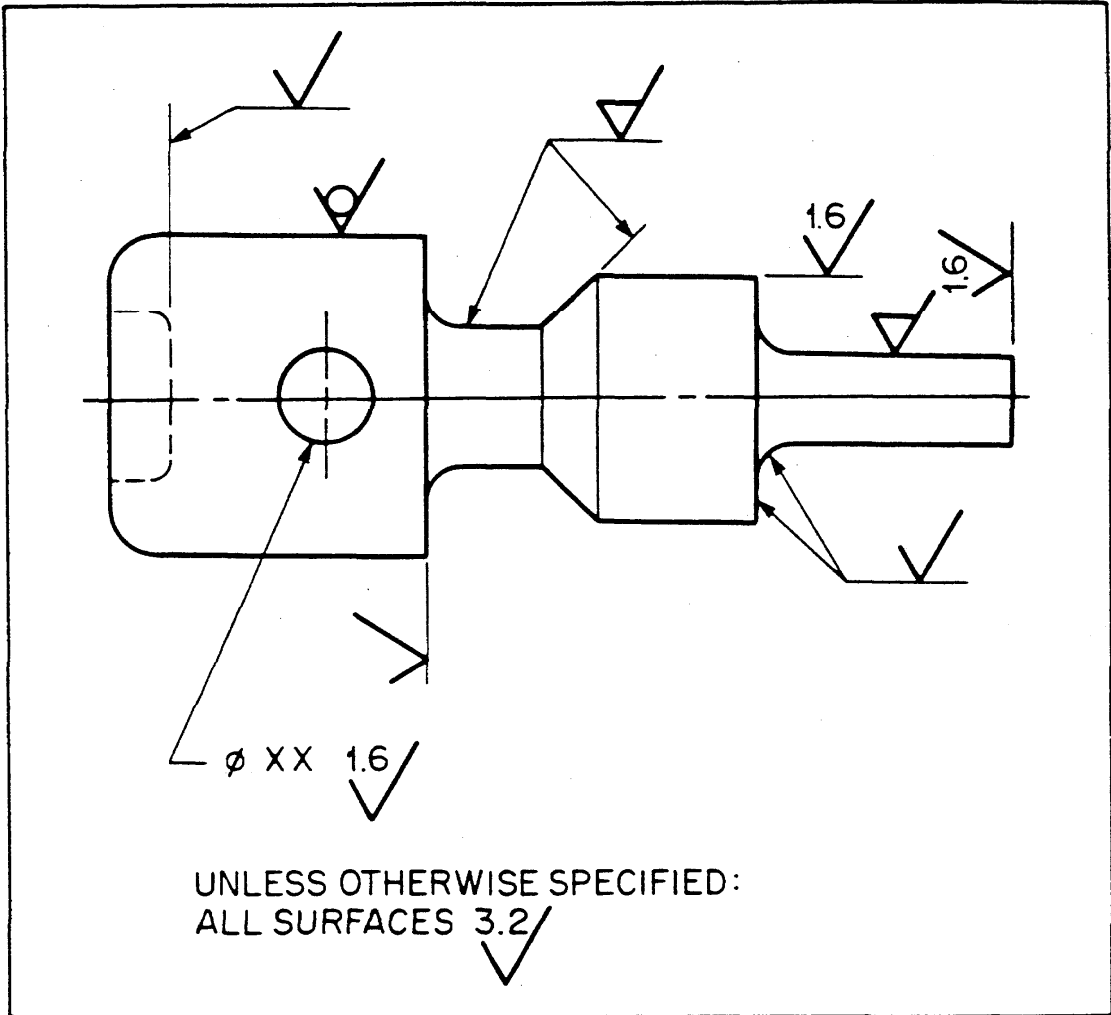


Fig. 2 APPLICATION OF SURFACE TEXTURE SYMBOLS

Figure 3-27
 (from ANSI/ASME Y14.36 (1978) [30])

are specified for roughness on this drawing. There is a general note at the bottom that if the surface texture symbol is shown for a surface, the surface roughness should be $3.2 \mu\text{m}$ or less, unless the roughness value itself is specified as well. In three cases, the roughness is specified more tightly as $1.6 \mu\text{m}$ maximum, and in one case shown here at the top, no material removal is allowed.

CALIBRATION

We come now to the subject of calibration of stylus instruments and, in particular, calibration specimens. There are three kinds of specimens that one might use to investigate the properties of stylus instruments. The top one shown here in Fig. 3-28 is a step height specimen which can be used to calibrate the gain of the stylus instrument. The middle profile represents precision reference specimens which are usually highly periodic, highly uniform surfaces where the roughness does not change significantly from place to place. When this type of specimen has a calibrated roughness value, it can be used to calibrate the gain of the instrument and its response dynamically. The bottom profile represents roughness comparison specimens or pilot specimens which may be used to test how the instrument measures real components. The pilot specimens may be used as check standards, since they should yield the same measured value of roughness from day-to-day. Therefore, you can use them, say, as a way of making sure that the roughness measuring instrument is giving consistent measurements from one day to the next for a line of components.

Figure 3-29 lists three important properties of precision roughness specimens for the calibration of instruments. It shows schematically the procedure of calibrating a stylus instrument wherein a calibrated roughness specimen is measured and the instrument is adjusted to give the correct value of R_a . A specimen used for this purpose should have low waviness and good uniformity, and the valleys should be significantly wider than the stylus tip size.

Roughness Specimens

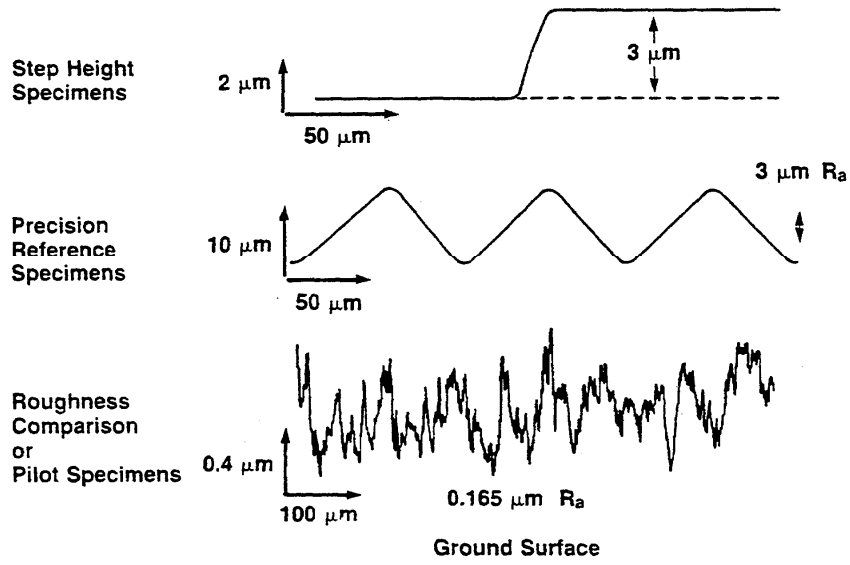


Figure 3-28

IMPORTANT PROPERTIES OF ROUGHNESS SPECIMENS: WAVINESS, UNIFORMITY, WIDTH OF VALLEYS

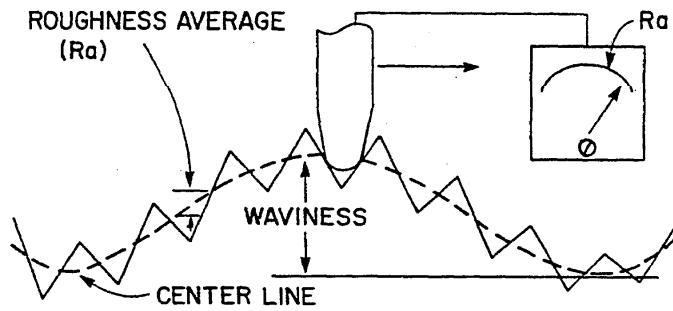


Figure 3-29

You want as small a waviness as possible because otherwise the surface would be difficult to level if you move it from one place to the next. Second, the surface roughness should be the same in different places; that is, it should have a high uniformity of roughness. Finally, the widths of the valleys are important because if you are using the measured R_a value on a precision reference specimen to check the gain of the instrument, then you do not want to have that R_a measurement be sensitive to the stylus on the instrument itself. You want the stylus to trace into the bottoms of the grooves in order to yield an accurate measurement of the surface profile and ensure that the calibration measurement is independent of the stylus itself. In some cases, roughness specimens have v-shaped grooves and this can be a disadvantage for calibration at a small roughness level.

Specimens that we have developed at NIST have sinusoidal profiles [7], so the valleys are fairly wide. Figure 3-30 shows three of these sinusoidal surfaces. SRM 2073, shown at the top, is available to the public now, and the other two should be available fairly soon. The top profile has a roughness pattern with a peak-to-valley (P-V) height of 10 μm , the next one has 3 μm P-V, and the bottom one has 1 μm P-V. They all have the same wavelength of 100 μm each. These specimens were produced by diamond-turning. They were machined in batches of about 36 in a facing operation, and the sinusoidal profile was generated by a numerically controlled tool [38]. Figure 3-31 is a schematic diagram of the process. NIST certifies both the roughness average R_a and the roughness wavelength for these specimens.

SOURCES OF UNCERTAINTY

There are a number of sources of uncertainty in roughness calibrations. First, there is the random uncertainty of the sample itself, i.e., the variations in R_a with position on the sample due to the fact that it is not completely uniform. Then you have sources of error that we classify as calibration errors. These, in turn, can be classified into systematic errors and random errors. We have so far identified three

**Stylus Profiles of the Three Roughness Areas
of a Prototype Specimen**

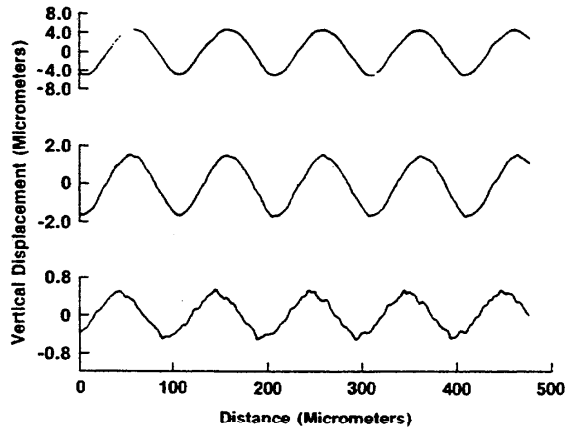


Figure 3-30

Diamond Lathe

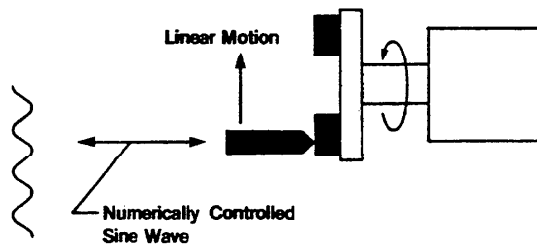


Figure 3-31

components of systematic errors, and three components of random errors. The first systematic component is the uncertainty in the measurement of the stylus width or radius. A stylus with a large radius fails to pick up some of the finer surface structure that may be detected by a fine stylus. Therefore, the measured R_a is smaller for a larger radius stylus. A second component of systematic error is instrumental noise which always tends to increase the measured R_a . Finally, there is the systematic error in the quoted value of the calibration step used to calibrate the gain of the stylus instrument. These are all considered systematic errors because they do not change from day to day.

The first source of random error is the uniformity of the calibration step height. Today I might measure the calibration step in one place and tomorrow measure it at a slightly different place where the step height is slightly different. If so, I am producing a variation in the calibration of the instrument from day to day due to the nonuniformity of the calibrating step. Second, there are the instrumental errors due to digitization, sampling, and nonlinearity that occurs when the instrument is calibrated. Third, the error due to transducer nonlinearity occurs again when the roughness specimen is measured. The magnitudes of these errors and the methods of adding them are described in Appendix A, taken from NIST calibration reports for step height and roughness measurements.

3-D PROFILING

Up till now, we have been discussing 2-D profiling. However, one can also perform 3-D surface mapping with stylus instruments [11,25]. Figure 3-32 shows a research instrument that was developed at NIST to do 3-D surface mapping. It uses a commercial LVDT transducer. The surface is translated under the transducer in a raster fashion to produce a map of the surface roughness. The displacement in two directions is accurately measured by laser interferometry. Such an instrument yields surface maps like the one in Fig. 3-33. This is an intensity map in which the bright regions are high points on the surface, and the dark regions are valleys.

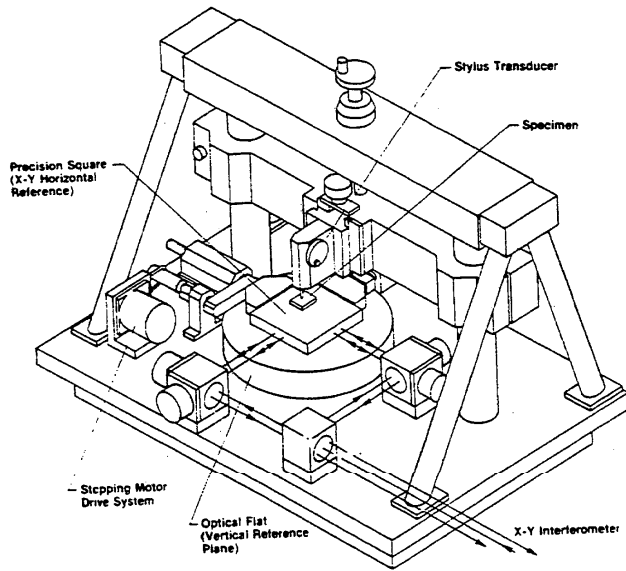


Figure 3-32

Three Dimensional Stylus Instrument
 (from Teague et al. [25])



Figure 3-33

Surface Map Obtained with 3-D Stylus Instrument
 (from Teague et al. [25])

The surface depicted here is a fairly smooth one with an R_a on the order of $0.15 \mu\text{m}$ or about $6 \mu\text{in.}$

Three-dimensional mapping offers the potential for much more complete information on surface roughness than two-dimensional profiles. However, the investment for these types of instruments is considerably higher than the cost for profiling instruments.

We conclude this section on stylus measurements by reviewing some of the characteristics of stylus instruments. Stylus instruments produce detailed quantitative profile outputs and their ratio of range-to-resolution in both the horizontal and the lateral directions is excellent. Therefore, the stylus instrument is a versatile surface measurement technique.

The stylus has potential for damaging the test surface. In ordinary use you only do two-dimensional profiling of the surface; 3-D mapping would require special operation. Stylus instruments are also difficult to adapt to curved surfaces unless you use a skid. However, counterexamples exist in the research literature. For example, Whitenton and Blau [36] have used the stylus technique to measure the wear volume and surface parameters of wear scars on balls.

REFERENCES

1. Reason, R.E. The Measurement of Surface Texture, in Modern Workshop Technology, Part 2 - Processes, H.W. Baker, ed., 3rd edition (Macmillan, London, 1970), Chap. 23.
2. Whitehouse, D.J. Stylus Techniques, in Characterization of Solid Surfaces, P.E. Kane and G.R. Larrabee, eds. (Plenum Press, New York, 1975), p. 49.
3. Bennett, J.M.; Dancy, J.H. Stylus Profiling Instrument for Measuring Statistical Properties of Smooth Optical Surfaces, Appl. Opt. 20, 1785 (1981).
4. Breitweiser, G. Surface Profile Measurements - A Survey of Applications in the Area of Vacuum Deposition, J. Vac. Sci. Technol. 11, 101 (1974).

5. Sec. 2, Ref. 19.
6. Namba, Y.; Tsuwa, H. Mechanism and Some Applications of Ultra-Fine Finishing, CIRP Annals 27 (1), 511 (1978).
7. Teague, E.C.; Scire, F.E.; Vorburger, T.V. Sinusoidal Profile Precision Roughness Specimens, Wear 83, 61 (1982).
8. Sayles, R.S.; Thomas, T.R. Surface Topography as a Nonstationary Random Process, Nature 271, 431 (1978).
9. Garratt, J.D. New Stylus Instrument with a Wide Dynamic Range for Use in Surface Metrology, Prec. Eng. 4, 145 (1982).
10. Reason, R.E. Surface Finish and Its Measurement, J. Inst. Prodn. Engrs. 23, 347 (1944).
11. Teague, E.C.; Young, R.D.; Scire, F.E.; Gilsinn, D.E. Para-Flex Stage for Microtopographic Mapping, Rev. Sci. Instrum. 59, 67 (1988).
12. Whitehouse, D.J. Theoretical Analysis of Stylus Integration, CIRP Annals 23 (1), 181 (1974).
13. Vorburger, T.V.; Teague, E.C.; Scire, F.E.; Rosberry, F.W. Measurements of Stylus Radii, Wear 57, 39 (1979).
14. Church, E.L.; Howells, M.R.; Vorburger, T.V. Spectral Analysis of the Finish of Diamond-Turned Mirror Surfaces, Proc. SPIE 315, 202 (1981).
15. Spragg, R.C. Accurate Calibration of Surface Texture and Roundness Measuring Instruments, Proc. Instn. Mech. Engrs. 182, 397 (1968).
16. Teague, E.C. Evaluation, Revision, and Application of the NBS Stylus/Computer System for the Measurement of Surface Roughness, NBS Tech. Note 902 (U.S. Dept. of Commerce, Washington, DC, 1976), and E.C. Teague (private communication).
17. Damir, M.N.H. Error in Measurement due to Stylus Kinematics, Wear 26, 219 (1973).
18. Ajioka, S. The Dynamic Response of Stylus, Bull. Japan Soc. of Prec. Eng. 1, 228 (1966).
19. McCool, J.I. Assessing the Effect of Stylus Tip Radius and Flight on Surface Topography Measurements, J. Tribology, Trans. ASME 106, 202 (1984).
20. Whitehouse, D.J. Some Ultimate Limits on the Measurement of Surfaces Using Stylus Techniques, Measurement & Control 8, 147 (1975).

21. Verrill, J.F. Use of the Talystep in Investigating Diffraction Grating Groove Profiles, *J. Phys. E.* 6, 1199 (1973).
22. Williamson, J.B.P. Microtopography of Surfaces, *Proc. Instn. Mech. Engrs.* 183, 21 (1967-68).
23. Sayles, R.S.; Thomas, T.R. Mapping a Small Area of a Surface, *J. Phys. E.* 9, 855 (1976).
24. Sayles, R.S.; Thomas, T.R.; Anderson, J.; Haslock, I.; Unsworth, A. Measurement of the Surface Microgeometry of Articular Cartilage, *J. Biomechanics* 12, 257 (1979).
25. Teague, E.C.; Scire, F.E.; Baker, S.M.; Jensen, S.W. Three-Dimensional Stylus Profilometry, *Wear* 83, 1 (1982).
26. Vorburger, T.V.; McLay, M.J.; Scire, F.E.; Gilsinn, D.E.; Giauque, C.H.W.; Teague, E.C. Surface Roughness Studies for Wind-Tunnel Models Used in High Reynolds Number Testing, *J. Aircraft* 23, 56 (1986).
27. Sayles, R.S.; Thomas, T.R. Measurements of the Statistical Microgeometry of Engineering Surfaces, *Trans. Am. Soc. Mech. Engrs., J. Lubric. Technol.* 101F, 409 (1979).
28. Gonzalez, R.C.; Wintz, P. Digital Image Processing (Addison-Wesley Publishing Company, Reading, MA, 1977), Chapt. 7.
29. Sec. 2, Ref. 16.
30. Sec. 2, Ref. 10.
31. Church, E.L.; Vorburger, T.V.; Wyant, J.C. Direct Comparison of Mechanical and Optical Measurements of the Finish of Precision Machined Optical Surfaces, *Opt. Eng.* 24, 388 (1985).
32. Sec. 2, Ref. 1.
33. Bryan, J.B. The Abbe Principle Revisited - An Updated Interpretation, *Prec. Eng.* 1, 129 (1979).
34. Scheffer, B. Comparaison de Differentes Normes Nationales (Regie Nationale des Usines Renault, Billancourt, 1969).
35. Lindsey, K.; Smith, S.T.; Robbie, C.J. "NPL Nanosurf 2": A Sub-Nanometre Accuracy Stylus-Based Surface Texture and Profile Measuring System with a Wide Range and Low Environmental Susceptibility, presented at the 4th International Precision Engineering Seminar, Cranfield, UK (May 1987).

36. Whittenton, E.P.; Blau, P.J. A Comparison of Methods for Determining Wear Volumes and Surface Parameters of Spherically Tipped Sliders, Wear 124, 291 (1988).
37. Whittenton, E.P. (private communication).
38. Clark, R.A. Production Techniques for the Preparation of Sinsuoidal Profile Surface Roughness Specimens in Production Aspects of Single Point Machined Optics, Proc. SPIE 508, 20 (1984).

SECTION 4

FILTERING AND PARAMETERS

INTRODUCTION

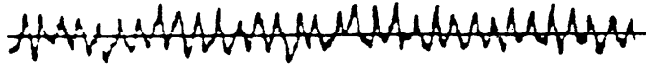
Surface texture plays an important part in the functional performance of many engineering components. In addition surface texture is often used as a fingerprint of the process, and the process is controlled based on information obtained from surface texture measurement [1]. Hence, characterization of surface texture has received considerable attention in recent years. One facet of this attention is the correct measurement of surface texture to obtain quantitative descriptors. In this section, the discussion is focused on mechanical and electrical filtering and their effects on numerical evaluation of surface profile parameters.

CONSTITUENTS OF SURFACE TEXTURE

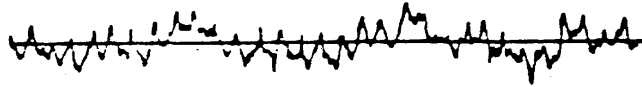
Surface texture is the fingerprint left on the workpiece by the manufacturing process. The texture is a combination of different wavelengths introduced by various aspects of the manufacturing process and is generally classified into different regions based on wavelength (Fig. 4-1).

The roughness irregularities produced by the tool feed marks and the deviations within these tool marks due to the rupture of metal is often referred to as primary texture [44]. Irregularities of longer wavelengths due to vibration, machine or work deflection, or inaccuracies in machine tools such as lack of straightness of the slideways or unbalance of the grinding wheel may be referred to as secondary texture (waviness and form error).

The measured profile is a combination of the primary and secondary texture. These distinctions are useful but they are arbitrary in nature and hence, vary with manufacturing processes. It has been shown, but not conclusively proven that the functional effects of form error, waviness



Primary Texture



Primary + Secondary Texture

Fig. 4-1

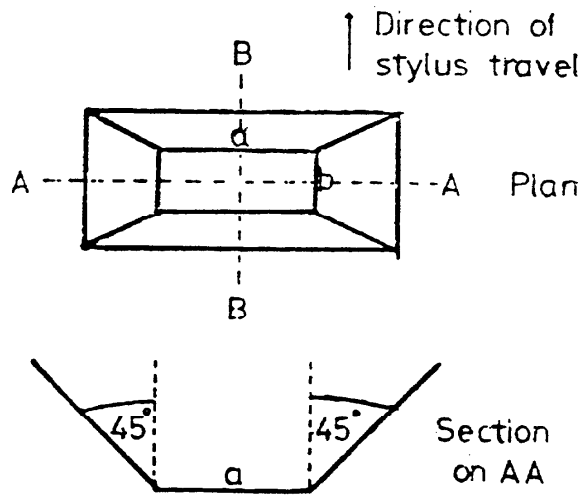
and roughness are different. Therefore, it has become an accepted practice to exclude waviness before roughness is numerically assessed.

MEASUREMENT OF SURFACE PROFILE

The most common technique for measuring surface profile makes use of a sharp diamond stylus. The stylus is drawn over an irregular surface at a constant speed to obtain the variation in surface height with horizontal displacement (Fig. 3-1). According to international standards, a stylus may have an included angle of 60° or 90° and a tip radius of curvature of 2, 5, or $10\ \mu\text{m}$ [2]. One type is a truncated pyramid, with a 90° included angle between opposite faces (Fig. 4-2). Its tip is a plateau whose dimensions are approximately $3\ \mu\text{m}$ in the direction of travel and $8\ \mu\text{m}$ in the other direction. It would seem that a profile containing many peaks and valleys with radius of curvature of $10\ \mu\text{m}$ or less and slopes steeper than 45° would be likely to be misrepresented by such a stylus. In the measurement of real surfaces, this problem does not arise because the slopes are usually around 10° (Fig. 3-7).

Variations in the tip radius of the stylus affect the shape of the traced profile. The tip radius of the stylus traces only an envelope of the actual profile. The resolution of the envelope profile depends on the actual contact between the stylus and the actual profile. As the stylus radius increases, contact is made with fewer points on the surface, and hence, the profile gets modified (Fig. 4-3). Increasing the stylus radius tends to reduce the measured value of average amplitude parameters like R_a [3]. However, the relative effect on R_a is not as great as on peak-to-valley parameters and others that are sensitive to the finest structures on the surface [43].

The stylus instruments can be used with two different datum attachments (Fig. 4-4). One is a fixed reference datum (a), which constrains the motion of the pick-up to a horizontal plane or a smooth curve. The transducer gives the instantaneous height difference between



a - 8 μ m, b - 3 μ m

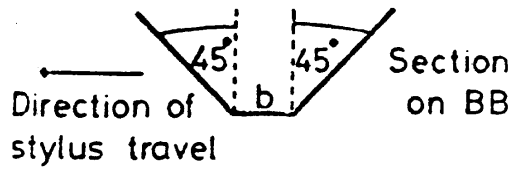


Fig. 4-2 Example of a Stylus Tip Shape

(from T.R. Thomas [37])

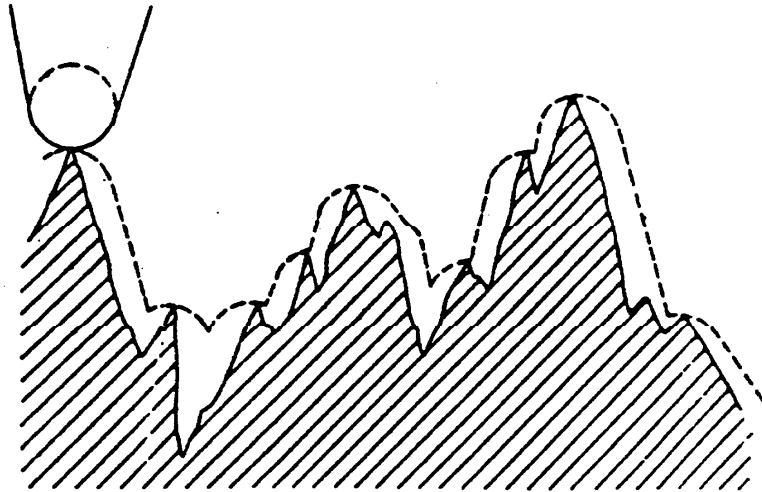
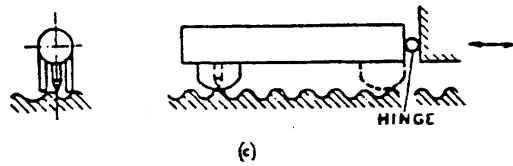
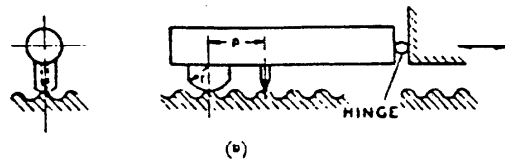
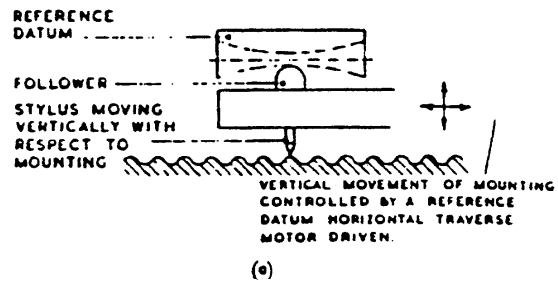


Fig. 4-3 Effect of Stylus Radius

(from Radhakrishnan [3])



- (a) TRUE DATUM
- (b) SURFACE DATUM, SINGLE SKID
- (c) SURFACE DATUM, MULTIPLE SKIDS

Fig. 4-4

(from Thomas [38])

the stylus and the motion of the pick-up assembly. This is the ideal way to measure the surface profile. Unfortunately, this method requires a leveling setup procedure by a skilled operator. In order to reduce the setup procedure, a skid may be used as a datum. The skid is a blunt foot having a large radius of curvature, and it is placed either besides or behind the stylus (b and c). The transducer thus senses the difference in level between the stylus and the skid. The skid provides the necessary datum and in so doing, it acts as a mechanical filter to attenuate the long spatial wavelengths of the surface. Comparison of Fig. 4-5a and b shows how the use of a skid can modify the measured surface profile. Figure 4-5c shows the profile path of the skid itself over the surface.

As a consequence of using the skid, the long wavelength information is lost. If those long wavelengths are functionally relevant, then the use of a skid should be avoided. In addition, the use of a skid on periodic surfaces or on surfaces with discrete peaks could result in distortion of the measured profile.

SEPARATION OF WAVINESS AND ROUGHNESS (FILTERING)

The numerical evaluation of roughness is always preceded by removal of waviness from the measured profile. This can be achieved in a surface texture measuring instrument by using an analog or digital filter [4-6]. In order to exclude waviness, a limiting wavelength has to be specified. This limiting wavelength is referred to as cutoff. The cutoff is given in μm or inch and the following values are available in many instruments, 0.08, 0.25, 0.8, 2.5, and 8 mm. The cutoff selected must be short enough to exclude irrelevant long wavelengths and at the same time long enough to ensure that enough texture has been included in the assessment to give meaningful results. Usually five cutoff lengths are used for assessment, and the overall traverse length is seven cutoff lengths (see Fig. 4-6) [2].

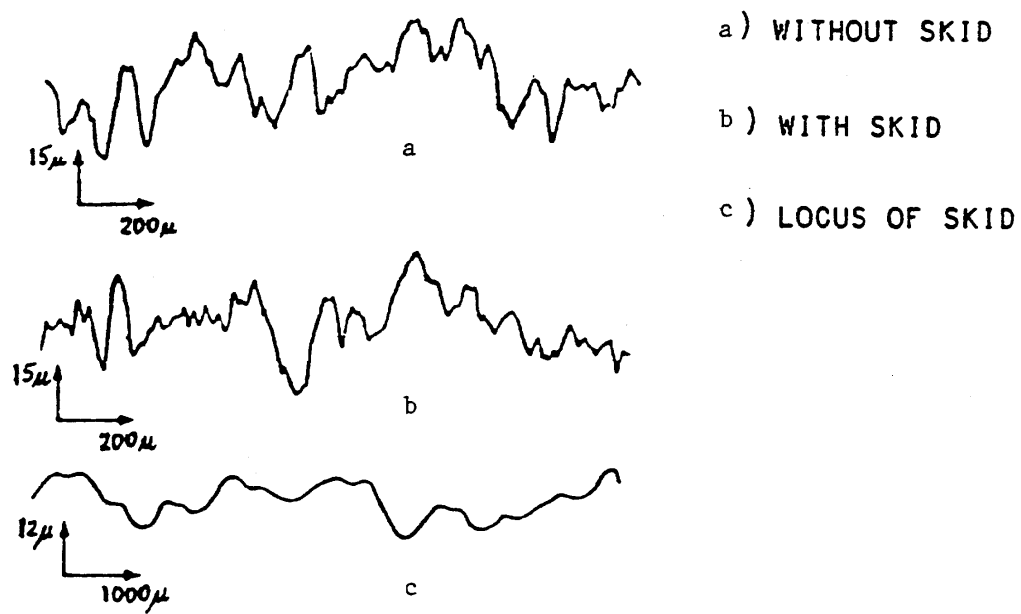


Fig. 4-5 Effect of Skid

(from Thomas [37])

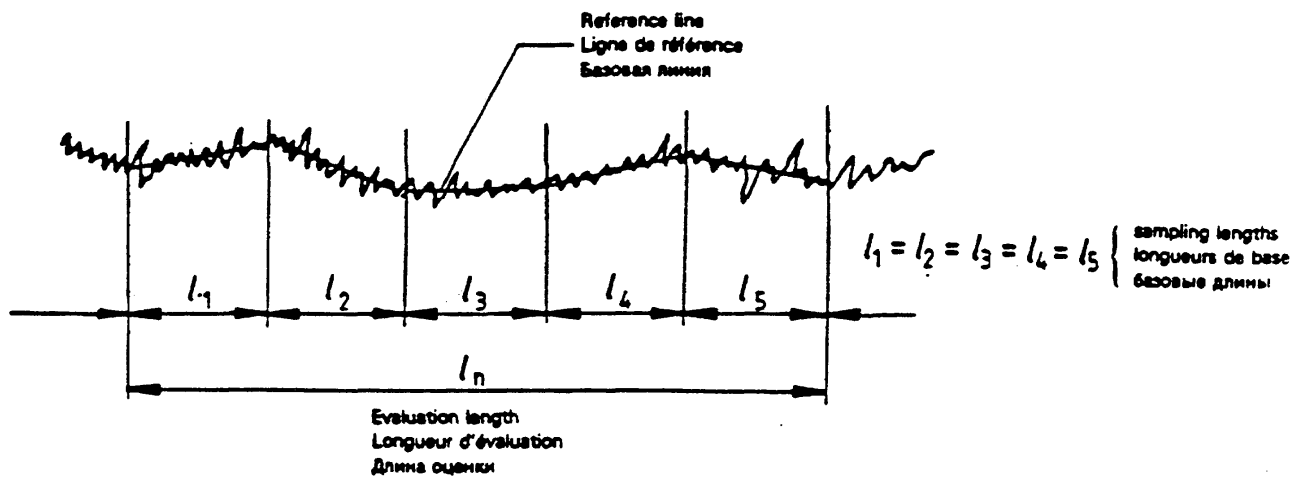


Fig. 4-6 Assessment of Surface Profile
(from ISO 4287/1 [2])

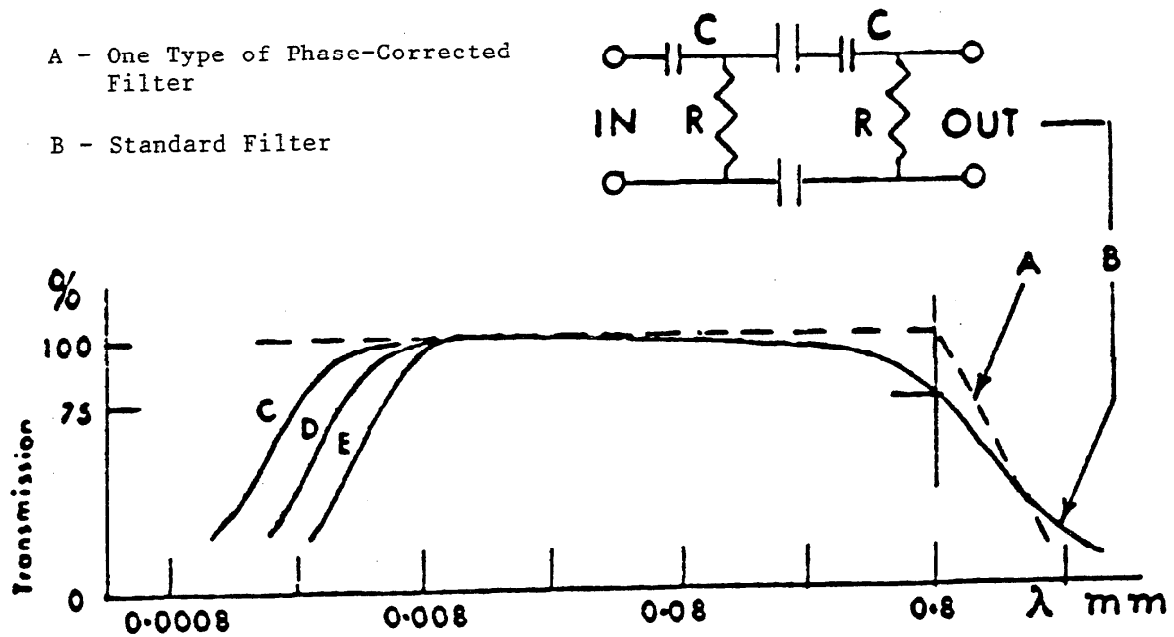


Fig. 4-7 Transmission Characteristics of a Standard 2RC Filter
(C, D, E, approximate $2\mu\text{m}$ stylus transmission for sinusoidal profiles with R_a values 0.3, 1.0, and $3.0\mu\text{m}$)
(from Reason [39])

Standard Filter

The transmission characteristics of a standard filter used in instruments are shown as curve B in Fig. 4-7. The signal emerging from the filter is often referred to as the filtered profile or modified profile. The modified profile is used for computing surface parameters like R_a and R_q . When the profile is passed through the standard 2RC filter, the components of surface texture get attenuated according to their wavelengths. Also these components get shifted in time (or phase) by different amounts [5]. The result of this relative shifting is that the filtered profile is a distorted version of the original profile. This distortion is referred to as phase distortion. Figure 4-7 also shows one type of phase-corrected filter (discussed below) that could be used instead. In addition, curves C, D, and E simulate the mechanical filtering action of the stylus at very short wavelengths.

The nature of this phase distortion is illustrated in Fig. 4-8. In general, it can be said that phase distortion has little effect on parameters such as the rms roughness, autocorrelation function, and power spectrum (to be discussed later). It affects parameters such as peak height values and their distributions, amplitude density curves, bearing areas, and first and second derivatives from which slopes and curvatures of crests are derived [40].

Figure 4-9 shows the mean line obtained with five different filtering techniques for both a repetitive triangular profile and a random profile [40]. Curves c correspond to the standard filter. The phase lags are apparent here for both types of profiles. The mean lines in a and b are straight lines defined over a chosen sampling length. Case a is a center line as defined in British Standard 1134 [40,42] and case b is a least-squares straight line. These approaches lead to discontinuities in the profiles. Curve b also illustrates how the resulting least-squares line for the repetitive profiles depends on the sampling length that is chosen. The rolling circle mean line (curve d) simulates the mechanical filtering action of a ball rolling on the surface. Lastly, the phase-corrected mean

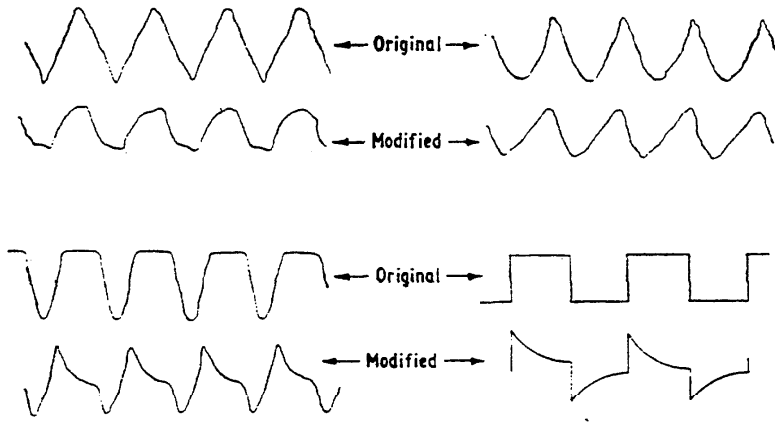


Fig. 4-8 Distortion produced by the standard filter of waveforms whose period is only slightly smaller than the cutoff.

(from Reason [40])

A REPETITIVE

B. RANDOM

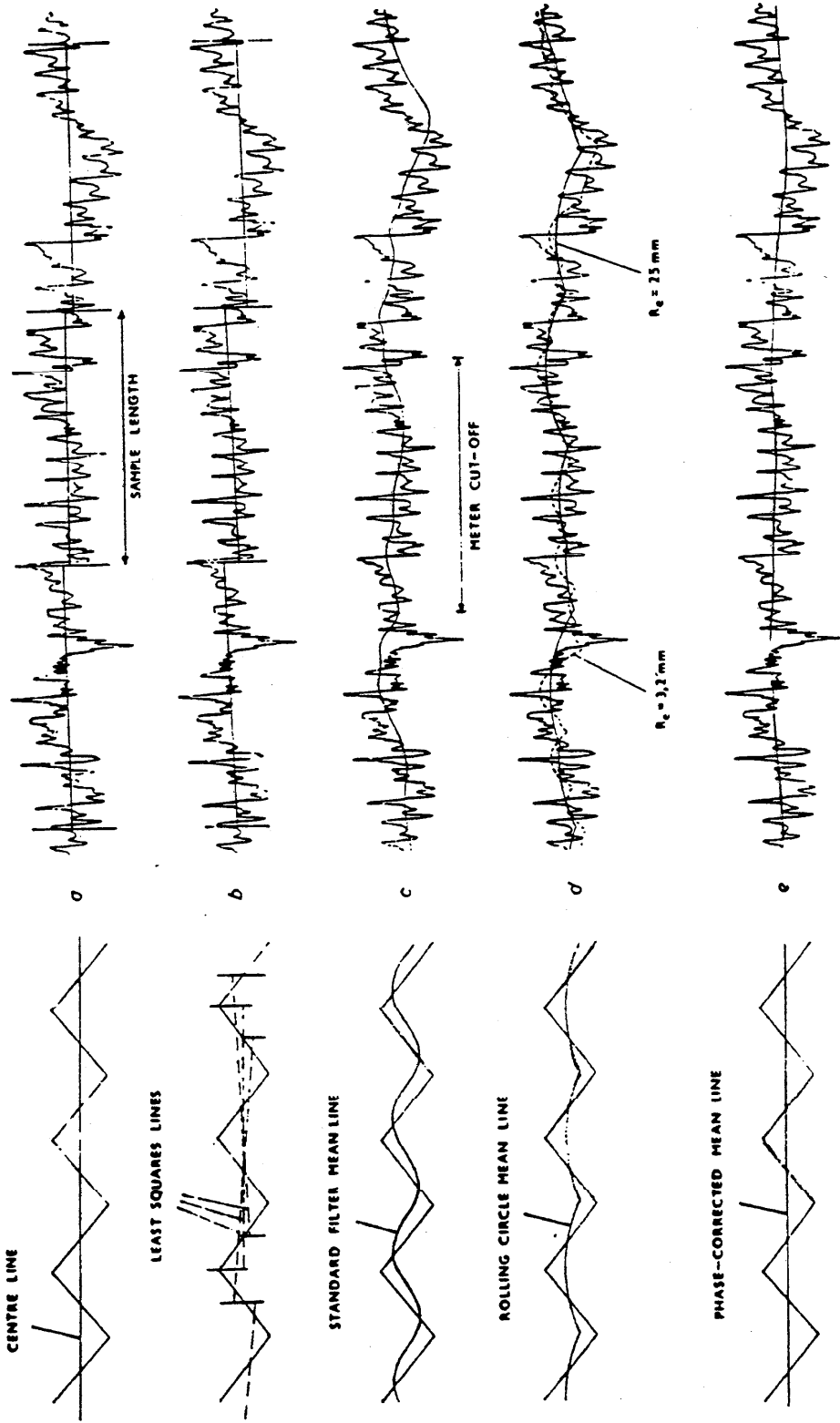


Fig. 4-9 Mean Line Obtained From Different Techniques
(from Reason [40])

line (curve e) is calculated as a weighted moving average of the profile points over a finite length.

Phase Corrected Digital Filters

In order to overcome the undesirable phase characteristics of the standard two-stage RC filter, a new class of filters has been developed [5], using digital techniques implemented on microcomputers. These filters have linear phase characteristics and they are generally referred to as phase-corrected filters in the context of surface profile analysis. Such a filter is generally implemented in the form of a recursive equation.

Furthermore, the developments in digital signal processing have led to the use of digital transform techniques for filtering surface profiles [7,8]. Figure 4-10 shows the general procedure using a Fast Fourier Transform (FFT).

ISO Phase-Corrected Filter (Proposed)

The International Organization for Standardization has been working on standardizing phase-corrected filters for surface profile processing. The transmission characteristic of the proposed ISO phase-corrected filter is shown in Fig. 4-11 [9]. Its attenuation near the cutoff is sharper than that of the standard 2RC filter. In addition, the nominal cutoff itself is defined differently. The cutoff is the 50% transmission point for the ISO filter, whereas it has been 75% for the standard 2RC filter. The main reason for the switch to the 50% transmission at the cutoff is to enable the use of a single filter to obtain both the roughness and waviness [9]. The ISO proposal is based on the constraint that the sum of the roughness and the waviness profiles should equal the original (unfiltered) profile. Therefore, if a filter that emphasizes long spatial wavelength (low-pass) is used first to obtain the waviness, then the waviness profile can be used as a mean line to obtain the roughness. This can be achieved by numerically subtracting the waviness from the unfiltered profile.

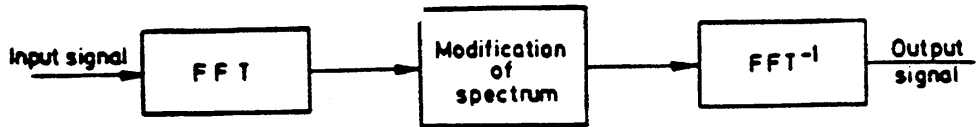


Fig. 4-10 Filtering of Surface Profiles Using FFT

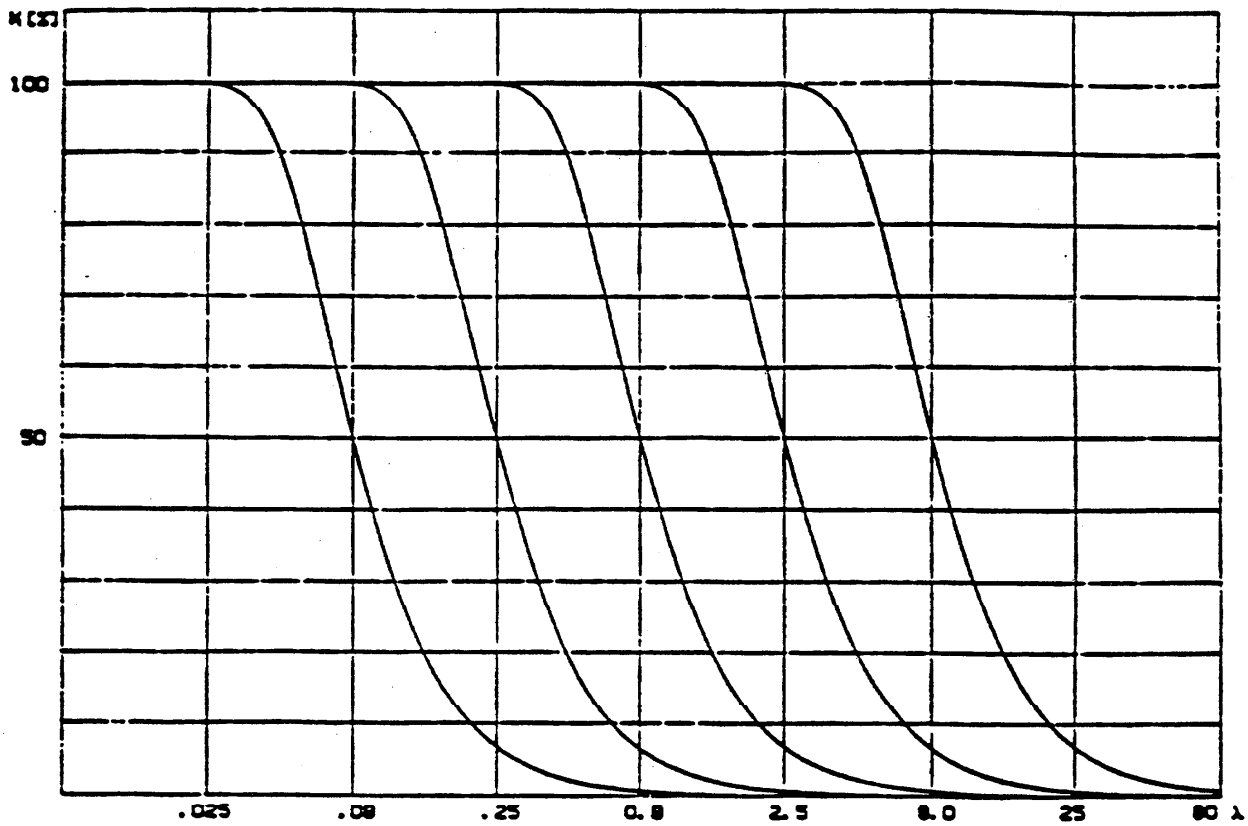


Fig. 4-11 Transmission Characteristics of Proposed ISO and Phase-Corrected Filter
(from ISO TC57 [9])

Figure 4-12 shows a comparison of the results (for a ground surface profile) obtained from the proposed ISO filter and the standard 2RC filter. The top curve is the unfiltered profile which shows a fine roughness pattern superimposed on a long-scale waviness pattern. Curve b shows the waviness profile obtained with the proposed low-pass ISO filter with cutoff (50%) of 0.8 mm. This may be contrasted with waviness curve c obtained with the standard 2RC filter. The proposed ISO filter has a sharper spectral cutoff than the standard one. Therefore, the ISO waviness profile has less contribution from short wavelength components and hence is smoother.

Likewise, curves d and e show that the roughness profile is defined better by the high-pass ISO filter than the standard one. Curves b and d, when added together, yield the total profile, curve a, by definition, whereas curves c and e do not.

The recommended method of realizing the proposed ISO filter is to calculate a moving average of the surface profile with a Gaussian weighting function. The weighting function $S(x)$ for the proposed filter is shown in Fig. 4-13 and given by

$$S(x) = (1/\alpha\lambda_c) e^{-\pi(x/\alpha\lambda_c)^2} \quad (1)$$

where,

x = position from the center of the weighting function,

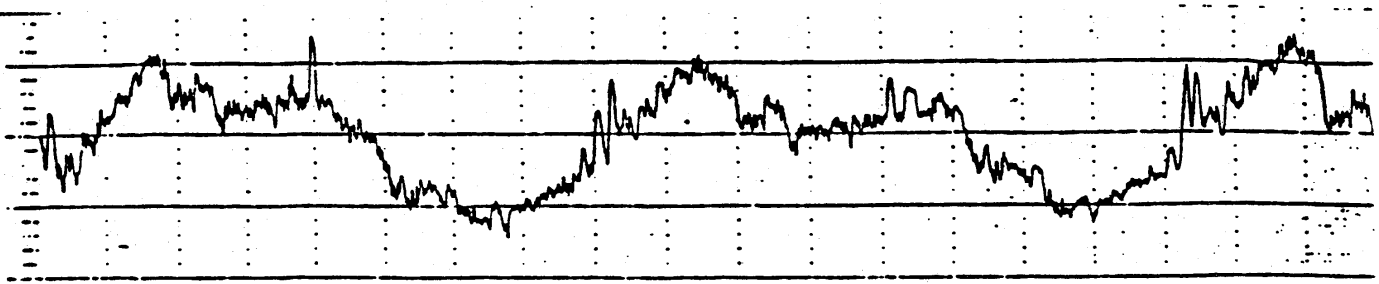
λ_c = nominal cutoff wavelength of the profile filter,

$$\alpha = \sqrt{\ln 2/\pi} = 0.4697 .$$

SURFACE TEXTURE PARAMETERS

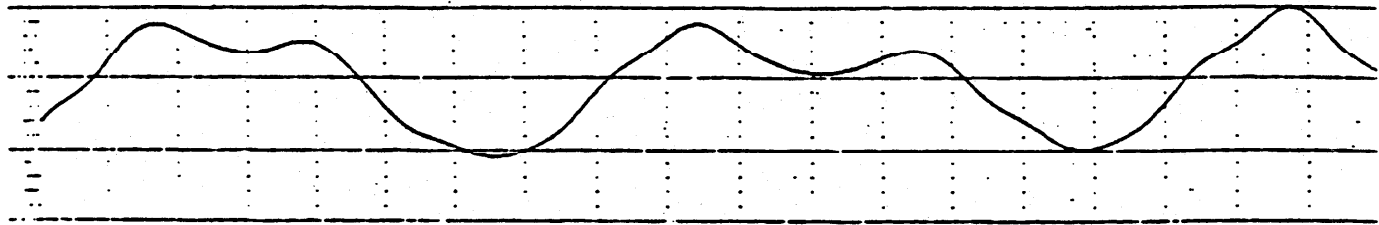
In general, surface topographies are highly complex owing to the fact that many surface finishing processes such as polishing and grinding are

(a) without filter



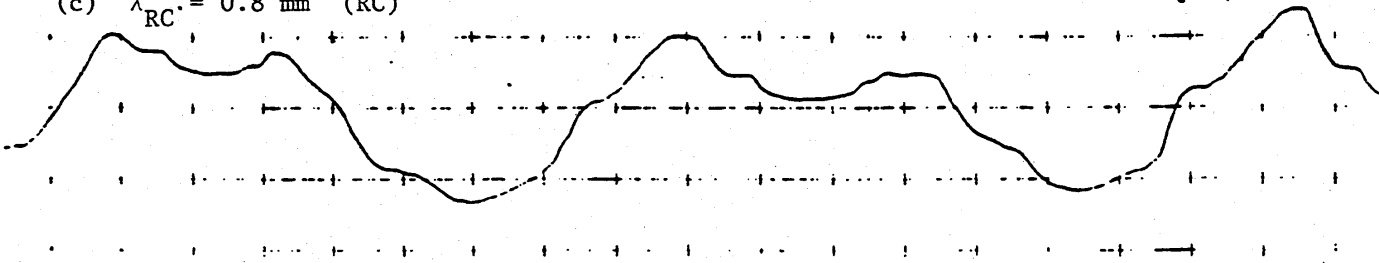
Waviness P-V Height = 3.4 μ m

(b) $\lambda_{50} = 0.8$ mm (ISO)

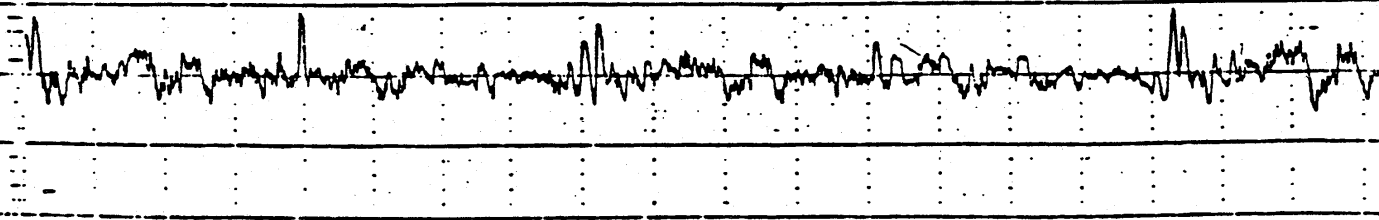


Waviness P-V Height = 4.0 μ m

(c) $\lambda_{RC} = 0.8$ mm (RC)



(d) $\lambda_{50} = 0.8$ mm (ISO)



(e) $\lambda_{RC} = 0.8$ mm (RC)

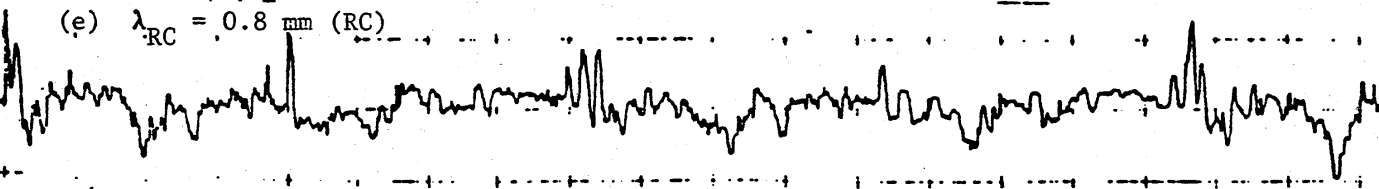


Fig. 4-12 Profile Diagrams of a Ground Aluminum Surface with Two Filtering Procedures (from G. Henzold [41])

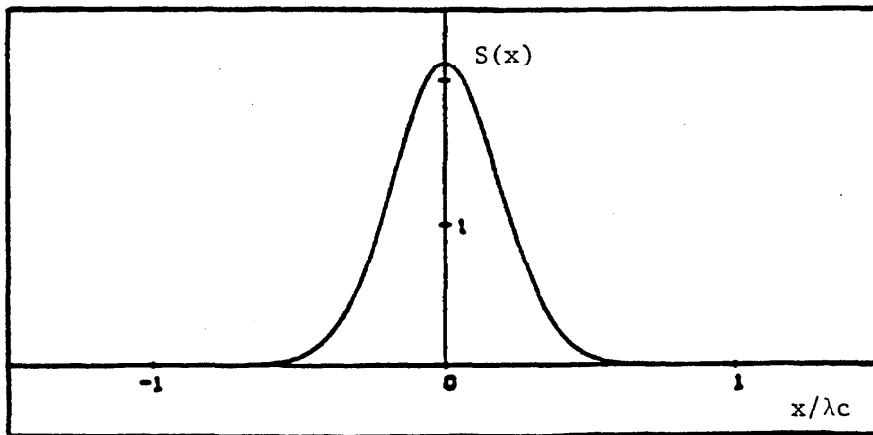


Fig. 4-13 Weighting Function of ISO (proposed) Filter [9]

statistical by nature. Characterization of such surfaces requires statistical descriptors. There are basically two kinds of descriptors: parameters such as rms roughness which attempt to quantify some aspect of the surface statistics with a single number, and surface statistical functions, such as the power spectral density. Many of these statistical parameters and functions have been developed previously to characterize random processes. In the following paragraphs, a few of these quantities are described.

There are a great variety of surface parameters, many of which have been developed to characterize the function of surfaces for particular applications [10-14]. In fact something like 50-100 parameters have been defined for industrial use and many of these appear in national standards as well [15]. Nevertheless, the confusing field of surface parameters may be classified adequately into four categories: height parameters, shape parameters, wavelength parameters, and combinations of these known as hybrid parameters.

Height Parameters

The most common statistical descriptors of surface height are the roughness average R_a and the rms roughness R_q . These are closely related, being given by the following formulas, shown in continuous and discrete form,

$$R_a = (1/L) \int_0^L |y(x)| dx = (1/N) \sum_{i=1}^N |y_i| , \quad (2)$$

$$R_q = \left[(1/L) \int_0^L y^2(x) dx \right]^{1/2} = \left[(1/N) \sum_{i=1}^N y_i^2 \right]^{1/2} , \quad (3)$$

The various terms in these formulas are shown in Fig. 3-22. R_a and R_q are both useful descriptors for the average height of surface profiles and

are used widely in general quality control. The rms roughness is commonly specified for the surfaces of optical components. In general, the lower the rms roughness of an optical component, the less stray light and the higher the quality of the component. R_a is used in the automotive and other metalworking industries to specify surface finish of many types of components ranging from cylinder bores to brake drums [16].

In general, these parameters are insensitive to wavelength and small changes in profile geometry. These parameters are also not intrinsic properties of the profile. Their value increases generally as the square root of the sampling length [17], and this behavior may be understood in terms of random walk methods for analyzing surface profiles.

In addition to these average height parameters, extreme height parameters have been defined for one application or another. Figure 4-14 gives a few of these extreme height parameters [6].

Wavelength Parameters

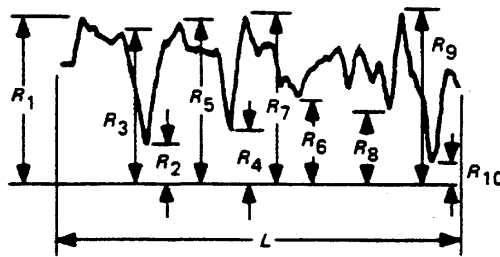
These are used to characterize the spacings of the peaks and valleys of the surface. The spacings or wavelengths are often characteristic of the process that formed the surface, such as the shot size for a blasted surface, the grit size of the grinding wheel or the feed of a tool. A typical wavelength parameter, recognized as standard by the International Organization for Standardization (ISO) [2], is the mean peak spacing S_m (Fig. 4-15), which may be defined for a surface profile as the average spacing between two successive negative going crossings of the mean line.

Shape Parameters

The periodic profiles in Fig. 4-16 all have the same R_a and wavelength but different shapes and hence may perform differently for different applications. In particular, profile (b) represents a good bearing surface, profile (a) a poor one. Because of its facets, profile (c) is best for use as a diffraction grating, whereas one of the other surfaces

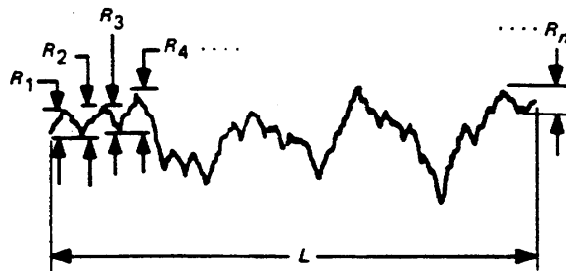


**MAXIMUM PEAK-TO-VALLEY
ROUGHNESS HEIGHT**



$$R_z = \frac{(R_1 + R_3 + R_5 + R_7 + R_9) - (R_2 + R_4 + R_6 + R_8 + R_{10})}{5}$$

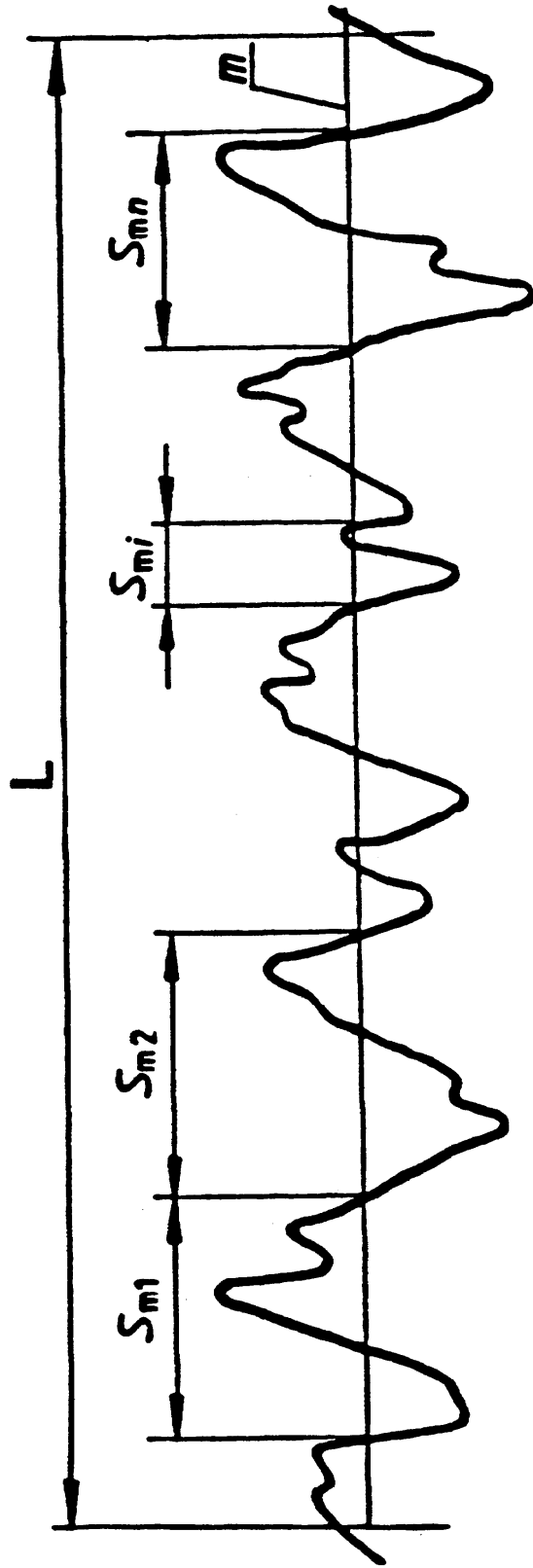
TEN-POINT HEIGHT



$$R = \frac{R_1 + R_2 + R_3 + \dots + R_n}{n}$$

**AVERAGE PEAK-TO-VALLEY
ROUGHNESS**

Fig. 4-14 Extreme Height Parameters
(from ANSI 46.1 [6])



$$S_m = \frac{1}{n} \sum_{i=1}^n S_{mi}$$

Fig. 4-15 Mean Peak Spacing Parameter
(from ISO 4287/1 [2])

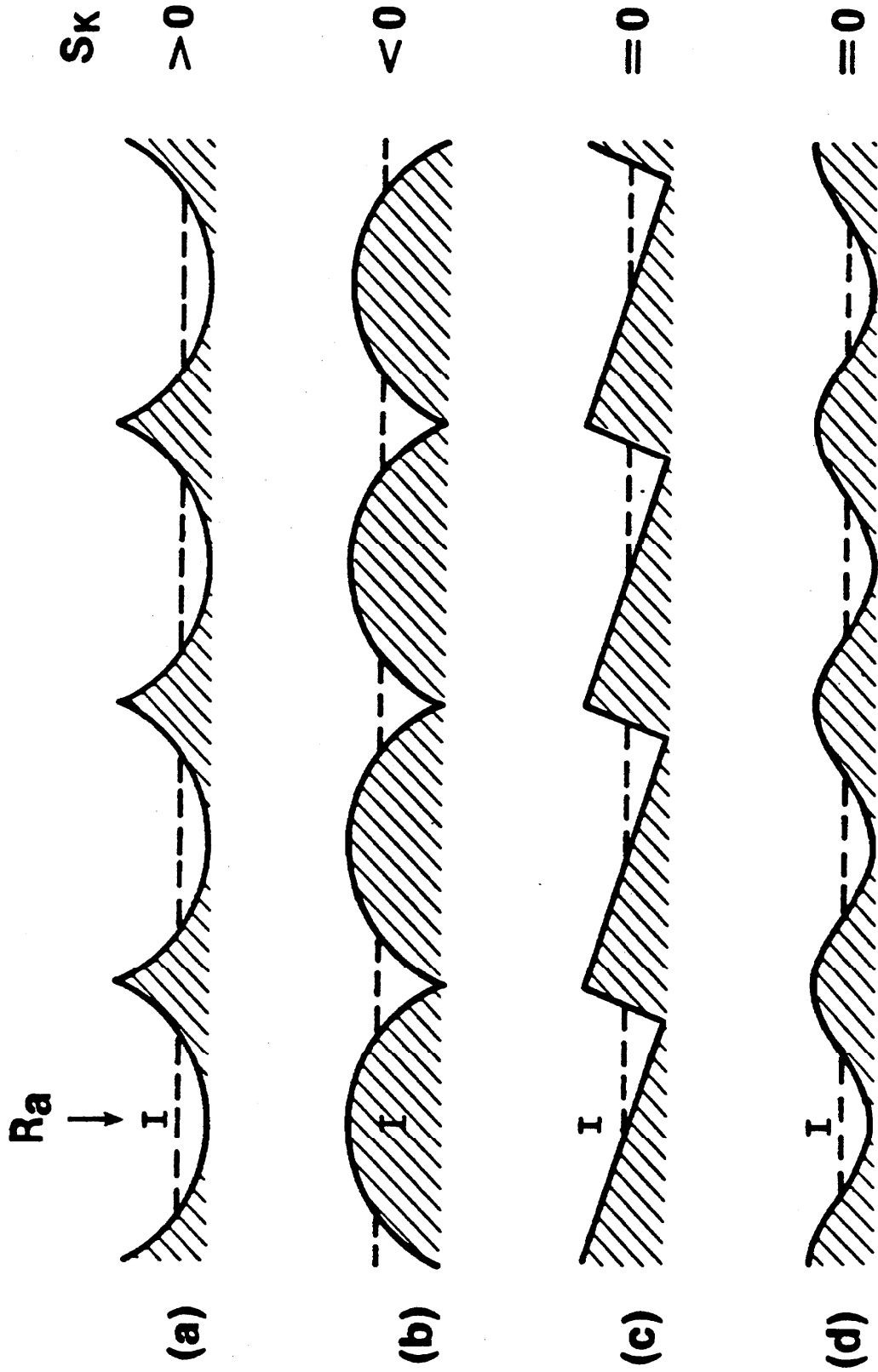


Fig. 4-16 Surface Profiles and Skew Parameter

may be most suitable for lubricated sliding. Shape parameters help to quantify the differences between these surfaces. The most important one, the skewness, R_{sk} or Sk , is a measure of the symmetry of the profile about the mean line. It is defined as

$$R_{sk} = \left(\frac{1}{R_q^3} \right) \frac{1}{N} \sum_{i=1}^N Y_i^3 . \quad (4)$$

According to this definition, the skewness of the profile (a) in Fig. 4-16 is positive, whereas its opposite number, profile (b), has negative skewness and the other profiles are symmetrical and have zero skewness.

Stout and coworkers [18] studied the evolution of skewness and a similar shape parameter known as kurtosis during a laboratory simulation of the running-in period of automobiles. They characterized the values of skewness and kurtosis for surfaces that had reached a stable surface condition after running in. Therefore, in the case of cylinder bores, the skewness is a functional parameter whose value serves as an indicator of surface condition.

Hybrid Parameters

Slope and curvature are two examples of quantities that combine the concepts of height deviation and lateral displacement and hence are termed hybrid parameters. They may be defined analytically or digitally in all manner of ways [19]. Hybrid parameters of one kind or another have found usefulness in a number of areas of tribology such as theories dealing with elastic contact [20] and thermal conductance [21].

STATISTICAL FUNCTIONS

More complete statistical descriptions of the properties of surface profiles may be obtained from statistical functions such as those used in connection with random process theory and time series analysis [22,23].

Four important ones are the amplitude density function or height distribution, the bearing area curve, the autocorrelation function, and the power spectral density. The definitions and applications of these functions are described in several works [22-29]. As examples, we discuss the power spectral density and the autocorrelation function in detail.

Power Spectral Density

The power spectral density (PSD) decomposes the surface profile into its Fourier components or spatial frequencies (F). It is given analytically by

$$\text{PSD}(F) = \lim_{L \rightarrow \infty} \frac{1}{L} \left| \int_0^L y(x) e^{-i2\pi Fx} dx \right|^2. \quad (5)$$

or in digitized form by

$$\text{PSD}(F) = \text{PSD}(k/L) = \text{PSD}(k/N\Delta) = \frac{1}{N\Delta} \left| \sum_{j=1}^N \Delta y(j) e^{-i2\pi kj/N} \right|^2. \quad (6)$$

Δ is the lateral point spacing of the digitized data points, the total length of the profile L is equal to $N\Delta$, and the set of spatial frequencies (F) in the digitized PSD are given by k/L , where k is an integer that ranges from 1 to $N/2$. The spatial wavelength is the inverse of the spatial frequency. The calculation of the digital Fourier transform in Eq. (6) may be speeded up enormously by using Fast Fourier Transform (FFT) algorithms [30,31].

In Fig. 4-17 we see how the power spectral density is sensitive to the different characteristics of surfaces produced by different processes. In this figure, the x-axis is labelled inversely with surface wavelengths rather than directly with spatial frequencies. Curve a shows the PSD plotted for a highly sinusoidal surface, a prototype of ones available

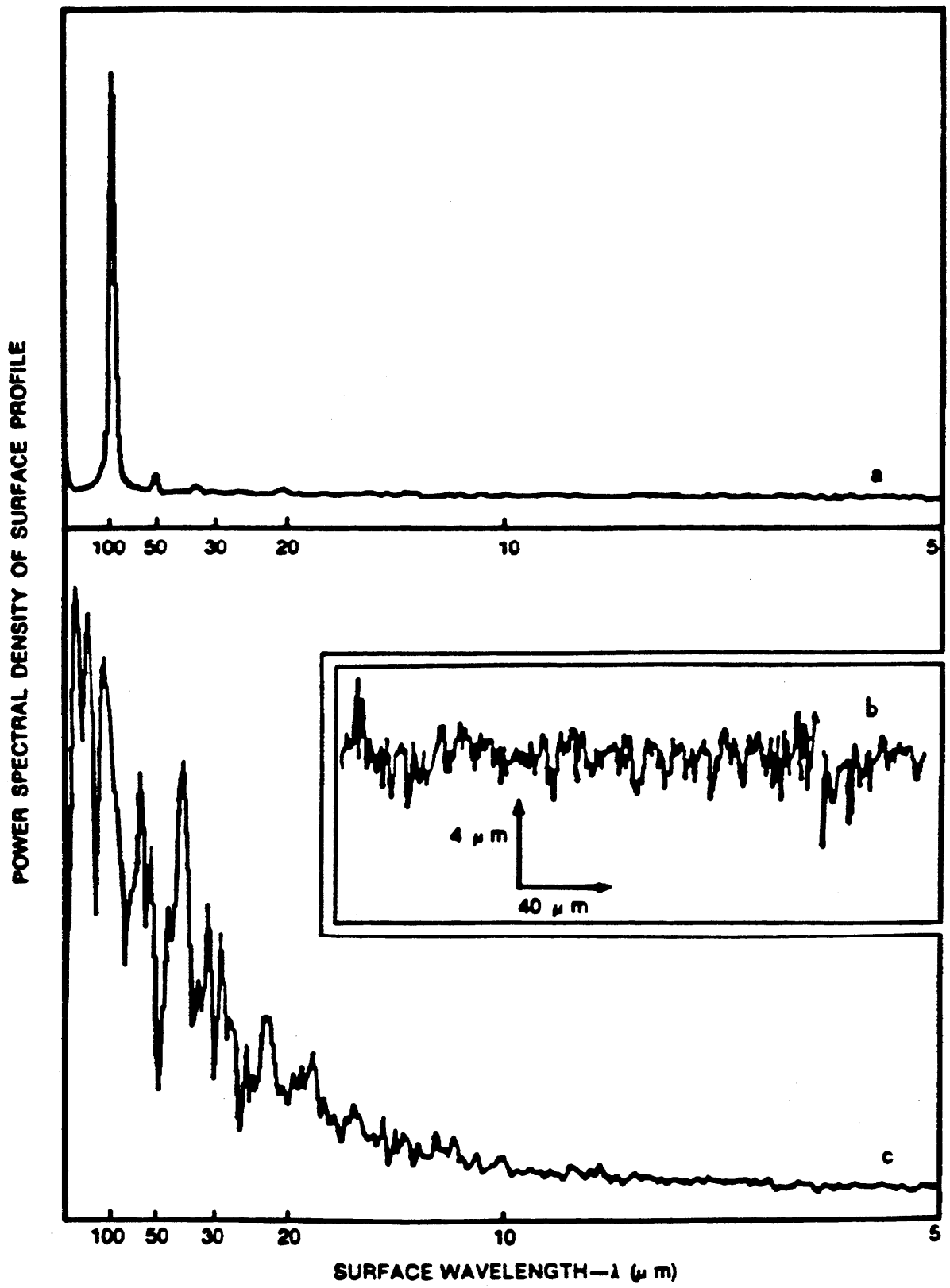


Fig. 4-17 Power Spectral Density Function

from NIST as standard reference materials [32,33]. The Fourier amplitude at the fundamental frequency of $0.01 \mu\text{m}^{-1}$ (wavelength = $100 \mu\text{m}$) is the dominant feature in the curve, but imperfections in the sinusoidal nature of the surface are also evident from the presence of higher harmonics in the spectrum. By contrast the PSD, curve c, for a more random surface, profile b, produced by grinding, has a fairly monotonic, albeit somewhat randomized, distribution with little evidence for periodic components.

The PSD for the ground surface points out a ubiquitous phenomenon for all but the most artificial of finished surfaces, that the power spectral density function generally increases with spatial wavelength up to wavelengths on the scale of the dimensions of the surface itself. This phenomenon results from random effects present in nearly all surface finishing processes [26] and may be described by statistical arguments analogous to those that describe the wandering of particles in Brownian motion [34]. The phenomenon was dramatically illustrated by Sayles and Thomas [34] who plotted the PSD's for a number of different surfaces ranging from lapped steel to the surface of the moon. In all cases, a generally monotonic increase of PSD with wavelength was observed. In Fig. 4-17, the reason why the PSD for the ground surface decreases suddenly near zero spatial frequency is that the measurement bandwidth itself was limited by the stylus trace length.

The above leads to a question of whether these statistical observations concerning the PSD break down for very small scale measurements where individual lattice steps can be recognized in the surface profile. How do the statistics change when the surface heights are quantized? Such a question may be answered with the recently developed technique of scanning tunneling microscopy.

Autocovariance and Autocorrelation

Another way to look at the information presented by the power spectral density is to take its Fourier transform to arrive at the autocovariance function

$$B(\tau) = \int_{-\infty}^{\infty} \text{PSD}(F) e^{i2\pi F\tau} dF \quad (7)$$

Alternatively, the autocovariance function may be calculated directly from the profile itself. That formula is given by

$$B(\tau) = \frac{1}{L} \int_0^L y(x)y(x+\tau) dx \quad (8)$$

where the quantities L and $y(x)$ have been defined previously.

The value of the autocovariance function at zero shift ($\tau=0$) is by definition equal to the rms roughness of the profile, provided that an appropriate mean line has been subtracted out of the profile to arrive at $y(x)$. When the autocovariance function is normalized by dividing by the zero shift value, the result is known as the autocorrelation function, $C(\tau)$.

$$C(\tau) = B(\tau)/R_q^2 = \int_0^L y(x)y(x+\tau)dx / \int_0^L y^2(x)dx \quad (9)$$

If we take into account the fact that the overlap between the shifted and unshifted profiles must decrease as the shift distance increases for a finite length profile and simultaneously use the digital formulation, the autocorrelation function may be described by

$$C_j = C(\tau) = \frac{1}{N-j} \sum_{i=1}^{N-j} y(i)y(i+j) / \sum_{i=1}^N y^2(i) \quad (10)$$

The autocovariance and autocorrelation functions are useful for visualizing the relative degrees of periodicity and randomness in surface

profiles. For example, Fig. 4-18 shows autocorrelation functions for a Ge and Si surface calculated from surface profiles measured by stylus. Both surfaces were produced by single-point diamond machining under similar conditions, but the periodicity imposed by the feed of the tool is much stronger on the Si surface; hence, its autocorrelation function is highly periodic. Because of its more random surface topography, the Ge surface exhibits a strongly decaying autocorrelation function with only a small amount of periodicity shown as a barely visible oscillation. From these studies, it is not clear what properties of the materials or cutting processes produced the differences.

Therefore, as measures of the lateral structure of surfaces, the PSD and the autocorrelation function seem to be useful in different ways. The PSD is useful for studying the strengths of various periodic components in the surface profile and for comparing these with the strength of the broad spectrum due to the random components. The autocorrelation function is useful for observing directly the lateral extent of the structures on the surface by studying the decay in the function near zero shift.

OTHER DESCRIPTORS

As stated before, scores of parameters and functions have been developed to quantify stylus profiles of surfaces, many of these for the fields of tribology, mechanical engineering, and optical engineering.

It is likely that in surface science too, other topographic parameters can be developed that correlate well with performance. For example, Blakely and Somorjai [35] and others [36] have correlated the ability of a surface to foster certain surface chemical reactions with the presence of lattice steps on the surface. These ideas could be quantified in terms of a step density parameter that might be defined as the fraction of surface atoms that are adjacent to lattice steps. It should be noted that step orientation is an important factor as well, so such a step density parameter might become further refined as a vector quantity. Such a parameter could conceivably be correlated with surface reactivity for

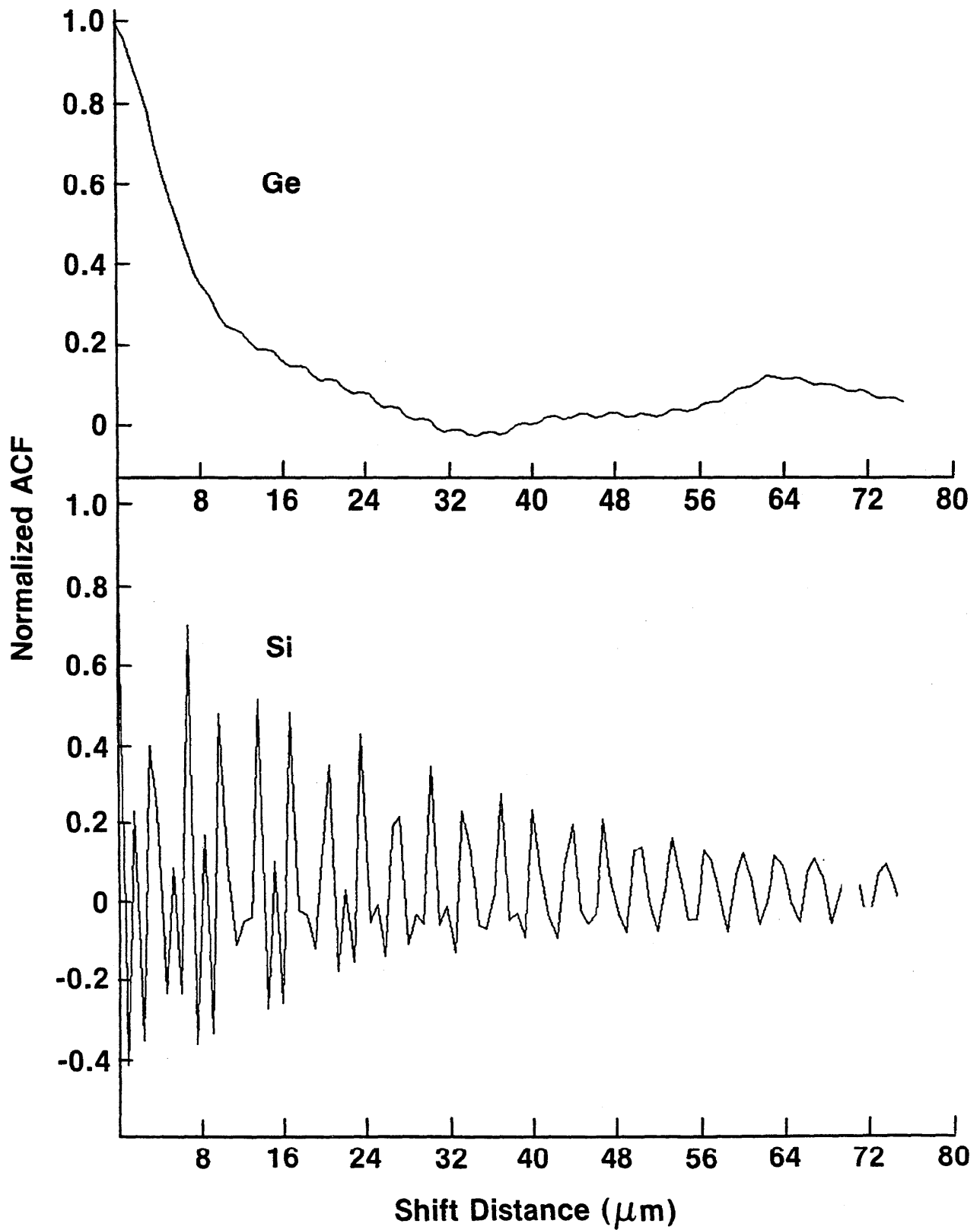


Fig. 4-18 Autocorrelation Function for Two Machined Surfaces
(The surfaces were supplied by E.L. Church.)

certain chemical processes. Other surface science phenomena that depend on roughness include surface plasmon coupling and surface enhanced Raman scattering. Specific topographic parameters could be discovered to correlate with these processes as well.

REFERENCES

1. Whitehouse, D.J. Surface - A Link between Manufacturing and Function, Proc. Inst. Mech. Engrs. 192 (19), 179 (1978).
2. Sec. 2, Ref. 4.
3. Radhakrishnan, V. Does the Stylus Radius Affect Surface Roughness Measurement, Tribology International 10, 101 (April 1977).
4. Whitehouse, D.J. Survey of Reference Lines in the Assessment of Surface Texture, CIRP Annals 21/2, 267 (1972).
5. Whitehouse, D.J. Improved Type of Wave Filter for Use in Surface Finish Measurement, Proc. Inst. Mech. Engrs. 182, Part 3k, 306 (1967-68).
6. Sec. 2, Ref. 1.
7. Raja, J.; Radhakrishnan, V. Filtering of Surface Profiles Using Fast Fourier Transformation, Int. J. of Mach. Tool Des. and Res. 19 (3), 133 (1978).
8. Raja, J.; Radhakrishnan, V. Digital Filtering of Surface Profiles, Wear 57, 147 (1979).
9. ISO/TC57/SC1/WG1, The Standardization of the Metrological Characteristics of Phase Corrected Filters for Use in Digital Surface Measuring Instruments (unpublished draft).
10. Thomas, T.R. Characterization of Surface Roughness, Prec. Eng. 3, 47 (1981).
11. Vorburger, T.V.; Scire, F.E.; Teague, E.C. Hydrodynamic Drag Versus Roughness for Rotating Disks, Wear 83, 339 (1982).
12. Scheffer, B.; Thurel, C. Donnees de base de la Realisation d'un Calculateur R et W, Mecanique, Matériaux, Electricite, No. 286, P. 19 (October 1973).
13. Bielle, J. Functional Needs, Machining Conditions, and Economics of Surface Finishing (translated by T.V. Vorburger and V.B. Roy), Prec. Eng. 7, 31 (1985).

14. Vorburger, T.V.; Scire, F.E.; Teague, E.C. Surface Roughness Measurements of Circular Disks and Their Correlation with Hydrodynamic Drag, NBS Tech. Note 1151 (U.S. Dept. of Commerce, Washington, DC, 1982).
15. Whitehouse, D.J. The Parameter Rash, Is There a Cure?, Wear 83, 75 (1982).
16. Young, R.D. The National Measurement System for Surface Texture, NBSIR 75-927 (U.S. Dept. of Commerce, Washington, D.C., 1976).
17. Thomas, T.R.; Sayles, R.S. Some Problems in the Tribology of Rough Surfaces, Tribology Int. 11, 163 (1978).
18. Stout, K.J.; David, E.J. Surface Topography of Cylinder Bores - The Relationship Between Manufacture, Characterization, and Function, Wear 95, 111 (1984).
19. Chetwynd, D.G. Slope Measurement in Surface Texture Analysis, J. Mech. Eng. Sci. 20, 115 (1978).
20. Whitehouse, D.J.; Archard, J.F. The Properties of Random Surfaces of Significance in their Contact, Proc. Roy. Soc. Lond. A316, 97 (1970).
21. Sayles, R.S.; Thomas, T.R. Thermal Conductance of a Rough Elastic Contact, Applied Energy 2, 249 (1976).
22. Nayak, P.R. Random Process Model of Rough Surfaces, Trans. ASME., J. Lub. Technol. 93, 398 (1971).
23. Bendat, J.S.; Piersol, A.G. Random Data: Analysis and Measurement Procedures (Wiley-Interscience, New York, 1971).
24. Longuet-Higgins, M.S. The Statistical Analysis of a Random, Moving Surface, Trans. Roy. Soc. London 249A, 321 (1957).
25. Blackman, R.B.; Tukey, J.W. The Measurement of Power Spectra (Dover Publications, Inc., New York, 1959).
26. Sayles, R.S. Chap. 5 in Rough Surfaces, Sec. 2, Ref. 12.
27. Williamson, J.B.P. Chap. 1 in Rough Surfaces, Sec. 2, Ref. 12.
28. Elson, J.M.; Bennett, J.M. Relation Between the Angular Dependence of Scattering and the Statistical Properties of Optical Surfaces, J. Opt. Soc. Am. 69, 31 (1979).
29. Peklenik, J. New Developments in Surface Characterization and Measurements by Means of Random Process Analysis, Proc. Inst. Mech. Engrs. 182, Pt. 3k, 108 (1967-68).

30. Brigham, E.O. The Fast Fourier Transform (Prentice-Hall, Inc., Englewood Cliffs, NJ, 1974) Chap. 10.
31. Vorburger, T.V. FASTMENU: A Set of FORTRAN Programs for Analyzing Surface Texture, NBSIR 83-2703 (U.S. Dept. of Commerce, Washington, DC, 1983), Chapter 11.
32. Standard Reference Material 2073, Sinusoidal Roughness Block (available from the National Institute of Standards and Technology).
33. Teague, E.C.; Scire, F.E.; Vorburger, T.V. Sinusoidal Profile Precision Roughness Specimens, Wear 83, 61 (1982).
34. Sayles, R.S.; Thomas, T.R. Surface Topography as a Nonstationary Random Process, Nature 271, 431 (1978).
35. Blakely, D.W.; Somorjai, G.A. The Dehydrogenation and Hydrogenolysis of Cyclohexane and Cyclohexane of Stepper (Higher Miller Index) Platinum Surfaces, J. Catalysis 42, 181 (1976).
36. Wagner, H. in Solid Surface Physics, Springer Tracts in Modern Physics, Vol. 85, G. Holder, ed. (Springer-Verlag, Berlin, 1979) p. 151.
37. Thomas, T.R. Some Examples of the Versatility of Stylus Instruments, Mecanique, Matériaux, Electricite, No. 337, 17 (1978).
38. Thomas, G.G. Engineering Metrology (John Wiley and Sons, New York, 1974).
39. Reason, R.E. Progress in the Appraisal of Surface Topography During the First Half Century of Instrument Development, Wear 57, 1 (1979).
40. Reason, R.E. Workshop Requirements of Surface Measurement, Proc. Inst. Mech. Engrs. 182, Pt. 3k, 299 (1967-68).
41. Henzold, G. Roughness and Waviness Measurements Using Phase Correct Filters, (unpublished).
42. Sec. 2, Ref. 6.
43. Radhakrishnan, V. Effect of Stylus Radius on the Roughness Values Measured with Tracing Stylus Instruments, Wear 16, 325 (1970).
44. Ward, H.C. Chap. 4 in Rough Surfaces, Sec. 2, Ref. 12.

SECTION 5

A SURVEY OF PROFILING TECHNIQUES

In Section 2, we classified the surface texture techniques into profiling and area techniques. Until now we have been discussing only stylus profiling techniques. This section deals with other profiling techniques and the next one with area techniques.

FRINGE-FIELD CAPACITANCE

Figure 5-1 shows a schematic diagram of the recently developed fringe-field capacitance instrument for surface profiling. The instrument has been developed by Garbini et al. [1] at the University of Washington and may soon be commercially available. It uses a thin knife-edge conductor embedded in an insulator which scans over the surface. The insulator serves as the skid, and the capacitance between the knife-edge and the surface is sensitive to the peaks and valleys underneath the average plane of that skid. The instrument has been shown to yield quite accurate profiles for a number of surfaces upon which it has been tested. One of the disadvantages of the fringe field capacitance instrument is the use of the skid, a procedure that can result in a distorted profile, as we discussed before. One of the potential advantages is its potential for dimensional inspection, as well as surface inspection. Early studies with this instrument have shown a great potential for high speed measurement of both the dimension and roughness of hole bores.

OPTICAL SECTIONING

We now discuss optical profiling techniques which have the advantage that they are generally non-contacting. The class of optical techniques may be divided into three major subclasses: optical sectioning, interferometry, and focus detection.

Optical sectioning [2] is a useful method for quickly obtaining a surface profile. Figure 5-2 shows how it works. The surface is located

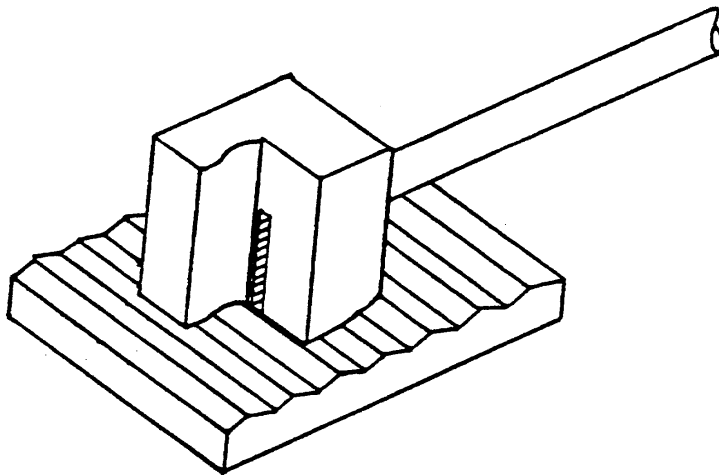


Figure 5-1
 Schematic of Fringe Field
 Capacitance Sensor
 (from Garbini et al. [1])

LIGHT SECTIONING MICROSCOPE

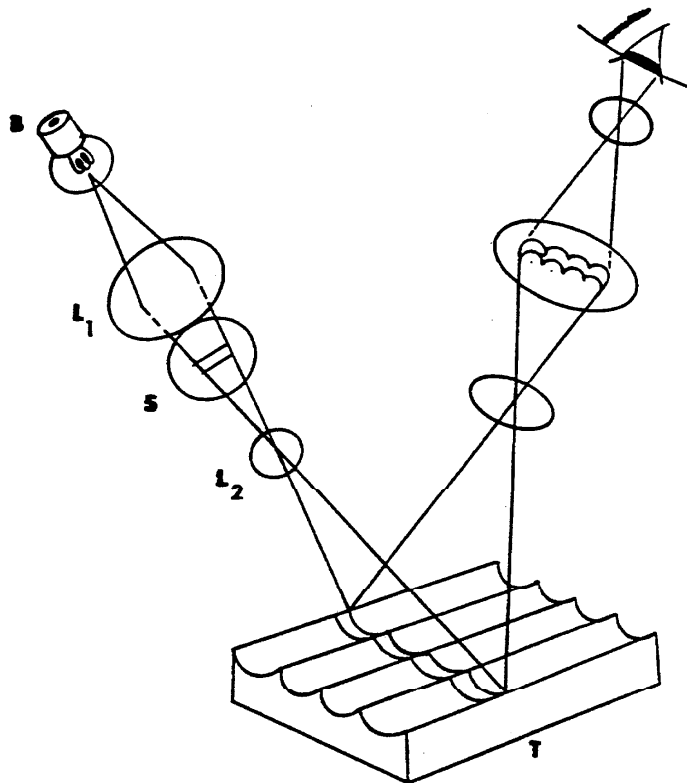


Figure 5-2
 Optical Sectioning

- Light Source** **B**
- Condenser Lens** **L₁**
- Slit** **S**
- Objective Lens** **L₂**
- Test Surface** **T**

under a special optical microscope which illuminates it with a thin line of light at an oblique angle of incidence, for example 45° . This essentially casts an illumination shadow on the surface texture. The resulting profile can then be inspected by means of an objective located in the opposite direction at 45° .

Optical sectioning is a convenient method for surface inspection. Because it is noncontacting, it can be used on soft materials. However, it has a small field of view so it yields short surface profiles generally less than 1 mm in length. Also, the optical sectioning technique has vertical resolution that is limited by the width of the beam on the surface. That width is limited by optical diffraction and it is very difficult to produce a beam width smaller than $1 \mu\text{m}$. Therefore, $1 \mu\text{m}$ is about the limit of resolution of optical sectioning.

INTERFEROMETRY

Interferometry has to do with forming an interference pattern between a reference beam and a measuring beam. However, there are a number of different configurations that interferometers can have and these differences are interesting. Figure 5-3 shows the basic Michelson, dual-beam interferometer. Actually, this is a modified version, called a Twyman-Green interferometer because it uses the focusing lenses (L_1 and L_2) to produce plane parallel wavefronts. A source of light from the bottom (A) is incident on a beam splitter (M). One part of the beam goes to a reference flat (R) and is reflected. The other component illuminates the surface to be measured (S) and also is reflected. Those two beams are recombined at the beam splitter, and if the path difference between them is not too large, the beams interfere and reveal a pattern of fringes at the screen [15]. The interference pattern consists of straight line fringes if there is a small degree of tilt between the measured surface and the reference surface and if both surfaces are perfectly smooth and flat. Undulation of the fringes is introduced by surface roughness or form deviations on either the reference or measuring surface. Assuming

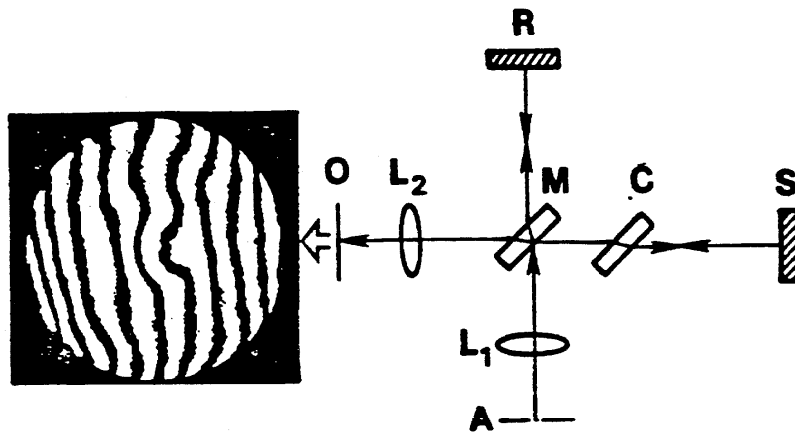


Figure 5-3
 Twyman-Green Interferometer
 (Photo by Wyant [15])

Multiple Beam Interferometer

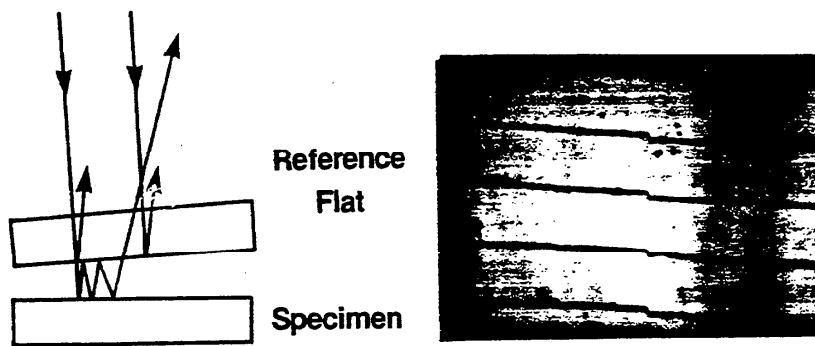


Figure 5-4

that the reference surface is perfectly smooth and flat, each fringe gives you a profile of the surface topography of the measured surface.

Figure 5-4 shows a Tolansky multiple-beam interferometer [12,13]. Now, the specimen and reference flat are both located in the focal plane of the objective of a microscope (not shown). The illumination is partially reflected from both the reference flat and the specimen and, once again, you have an interference pattern between the two reflected beams. This is recombined in the microscope to give you a pattern like the one shown on the right. An interesting feature of this interferometer is the use of multiple reflections between the specimen and the reference flat, if they are of high reflectivity. Multiple reflection produces very narrow fringes, and hence, improved height resolution. As you can see on the right, the width of the fringes themselves in relation to the basic fringe spacing is much sharper than that of the dual-beam interferometer.

The amount of tilt between the reference flat and the specimen determines the spacing of the fringes and that spacing calibrates the scale of the peaks and valleys that are measured on each individual fringe. The spacing between fringes is equivalent to a height difference of one-half of the optical wavelength, i.e., $\lambda/2$. The interferometric image here is of a small step approximately 25 nm (1 μ in) high [13]. A measurement of that height is determined by comparing the fringe shift at the step with the splitting of the fringes. The optical wavelength (λ) was the sodium yellow line with $\lambda = 589$ nm. Therefore, the height of the step is approximately 12 times smaller than $589/2$. Interferometry then is a sensitive technique for step height and roughness measurement, and it is intrinsically calibrated in terms of the wavelength of the optical light source.

RECENT INTERFEROMETERS

The two interferometers we have shown are traditional ones. We now discuss modern instruments that have been enhanced by electronic means. In particular, we discuss four types of instruments, all of which are

commercially available and which have interestingly different approaches to developing the interference.

The first was developed by Wyant and others [5]. A schematic diagram (Fig. 5-5) shows the test surface being inspected in an optical microscope that includes the usual microscopic elements. There is a light source and a set of lenses and apertures that bring the light down to an objective that illuminates the surface and collects the reflected light.

The output pattern falls on a photodiode detector array. The interference pattern is formed in the objective, shown in the detail on the right. A beam-splitter located just above the surface directs one component of the light to a smooth reference mirror above it and the other component to the surface. These reflected beams are then recombined at the beam-splitter and travel back up the microscope. The interference between those two beams causes the interference pattern in the detector array. However, the signal analysis is quite important here. The objective housing contains a piezo transducer that scans vertically and because of the interference produces a sinusoidal variation in the intensity as a function of time on each element of the photodiode array. Each time-varying signal is sampled in a way that yields a measurement of the optical phase variation over the surface of the reflected beam. The phase ϕ is directly related to surface height h by the formula

$$\phi = 4\pi h/\lambda \quad . \quad (1)$$

This configuration is called a Mirau interferometer. The surface profile or map is generated in the photodiode array, which can be either a linear array or an area array, respectively. Therefore, the instrument has the advantage that there is no physical movement to scan the surface to generate a surface profile. The only movement is the vertical movement of the piezo transducer over a total amplitude of approximately one-half wavelength of light. One disadvantage of this instrument is that the profiling accuracy is determined by the quality of the reference flat here.

SCHEMATIC DIAGRAM

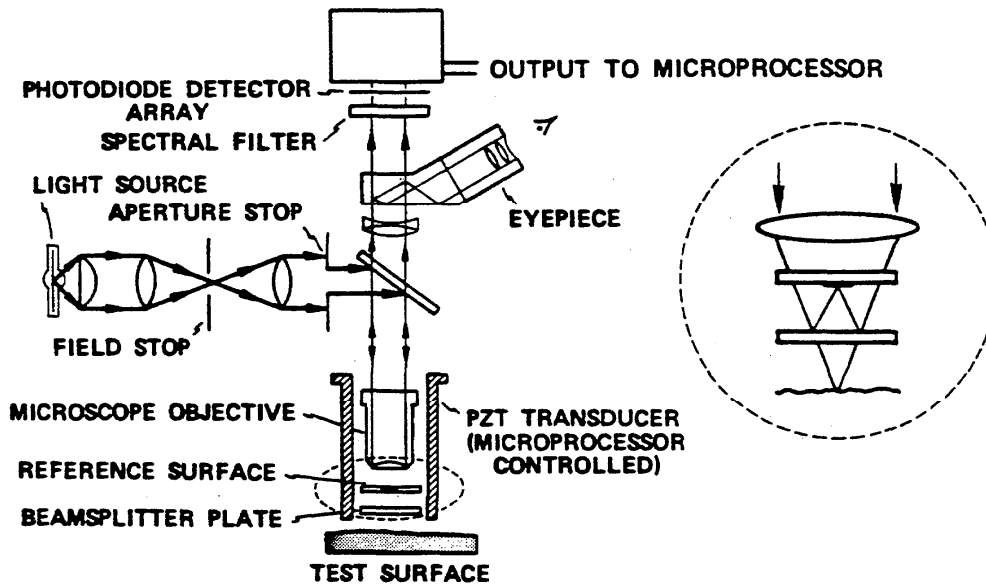


Figure 5-5

Schematic Diagram of Mirau Interferometric Microscope (from Wyant et al. [5])

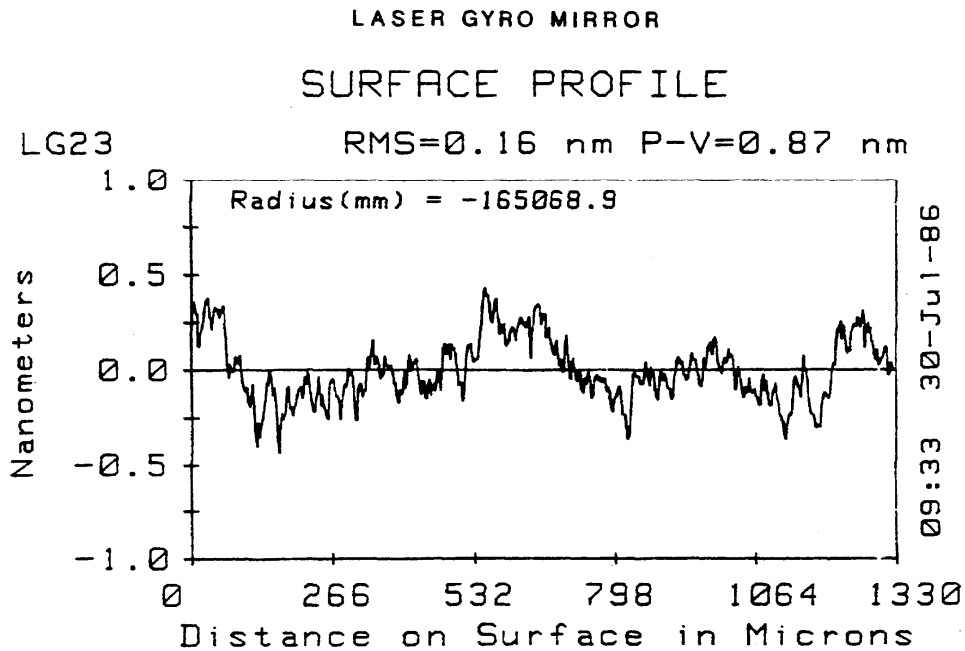


Figure 5-6

Surface Profile Obtained with Mirau Interferometric Microscope
(from Bennett [3])

Figure 5-6 shows a profile of a laser gyro mirror [3] taken by this interferometer. It is similar in resolution to other profiles that we will show, taken by similar interferometers. The scan length is approximately 1.3 mm. The vertical full scale is only ± 1 nm. So the profile is showing us subnanometer high structures on the surface. The rms roughness is measured to be 0.16 nm. In this case, that result is obtained after the shape of the reference flat has been removed by careful preanalysis. The ultimate vertical resolution of the instrument is therefore quite good. The lateral resolution is probably about $2 \mu\text{m}$ as evidenced by the lateral spacings of the structures in the profile.

Figure 5-7 is a schematic diagram of another instrument which takes quite a different approach [7,8]. The instrument uses laser heterodyne interferometry to record the surface profile, and that process takes place back in the electronics (not shown). What we emphasize here is, once again, a detail of the interference process taking place near the surface. In this case, there is no flat reference mirror, only the measured specimen shown on the top. The incident beam is split by a Wollaston prism, is focused through the objective, and illuminates the surface in two places. At the surface, the beam on the right is the reference beam, the beam on the left is the scanning beam. The surface is scanned by rotation about the axis shown, so the reference beam stays in one place on the interferometer axis and the scanning beam traces a circular path on the surface. This constrained motion helps to produce an extremely high resolution profile in the vertical direction as shown by Fig. 5-8. This is a circular profile, the two ends of which are at the same place on the surface. What you see is an overlay of three successive traces as well as one that indicates the noise of the instrument when the surface is not rotated. Full scale is ± 0.5 nm. The rms roughness calculated from the three overlaid traces shown is 0.60 nm, and the noise profile has an rms noise in the picometer range. This graph shows the kind of precision that optical interferometry is capable of. You should also note the excellent reproducibility of the three profiles.

Interferometer Detail

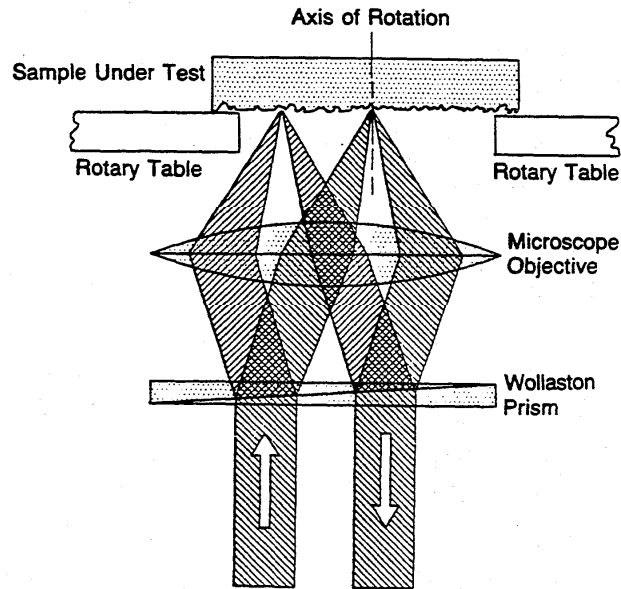


Figure 5-7

Schematic Diagram for Heterodyne Profiler (from Smythe [7])

UNCOATED ZERODUR SUBSTRATE/3

Overlay of 4 runs
RMS 0.60 angstroms
P-V 5.41

20 Feb 1987 11:32:20

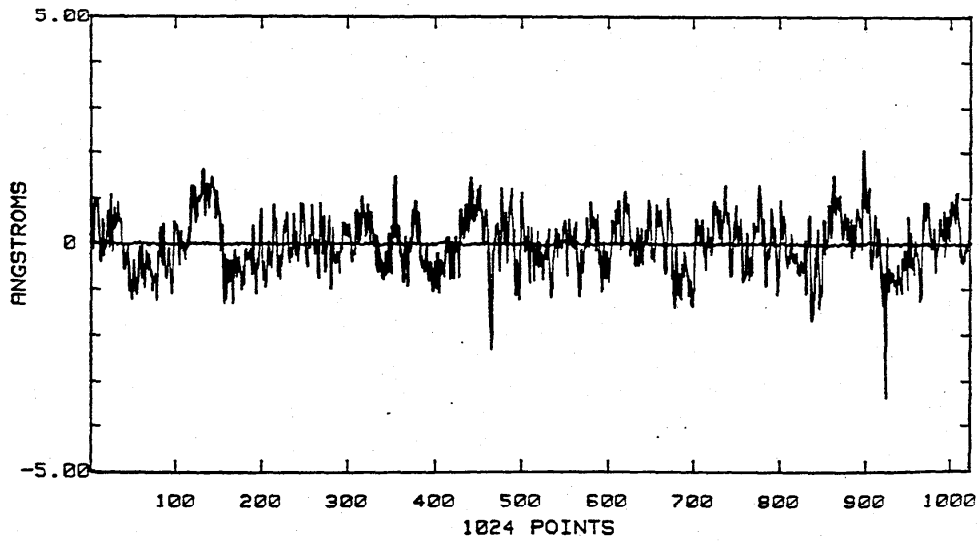


Figure 5-8

Surface Profile Obtained with Heterodyne Profiler (from Smythe [7])

The disadvantage of this instrument is that it is constrained to a circular profile with a certain length determined by the characteristics of the objective and the Wollaston prism. In this case, the trace length is approximately 1 mm.

The third interferometer (Fig. 5-9) was developed at NPL in England [6]. Once again, we show the detail of the interference taking place near the surface. This interferometer uses a birefringent lens that produces two concentric spots whose focal positions are dependent upon their initial polarization. One spot is focused on the surface, the other spot is defocused and is slightly larger. The outer spot essentially serves as the reference, with respect to which the peaks and valleys illuminated by the other spot are measured. Therefore, the instrument is essentially using the larger spot as an optical skid. Once again, you avoid the use a reference mirror. The reference is the average height of the outer spot. The advantage of this instrument is its great stability, and the lack of need for a reference mirror. In addition, the instrument can also scan over long distances. The disadvantage is that the range of measurable surface wavelengths is limited by the sizes of the two spots. In an early version of the instrument that range extended from about 1 μm , the size of the smaller spot, to about 10 μm , the size of the larger spot.

A fourth way to address the problems of scanning and of producing a reference is given in Fig. 5-10 [10]. It scans over a test specimen with a translating interferometric head that again contains a Wollaston prism that splits the source beam into two incident beams. The difference in phase between the two beams is proportional to the height difference between the two illuminated positions and that in turn is proportional to the slope of the surface in that location. As the beam is scanned over the surface, the profile is built up by integrating the successive differential height measurements. This interferometer once again has the advantage of not requiring a reference mirror. However, the disadvantage is that the integration of the differential height measurements produces accumulating statistical errors that can distort the measured profile. However, over the distance of approximately 1 mm, the rms noise of the

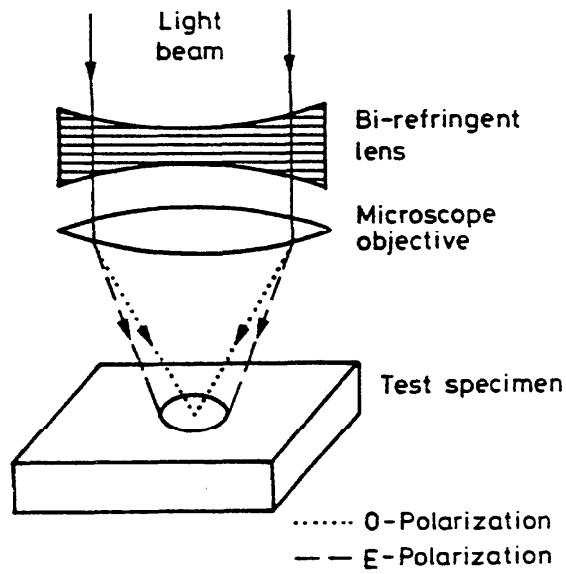


Figure 5-9
Schematic Diagram of Interferometric Profiler with Concentric Beams (from Downs [6])

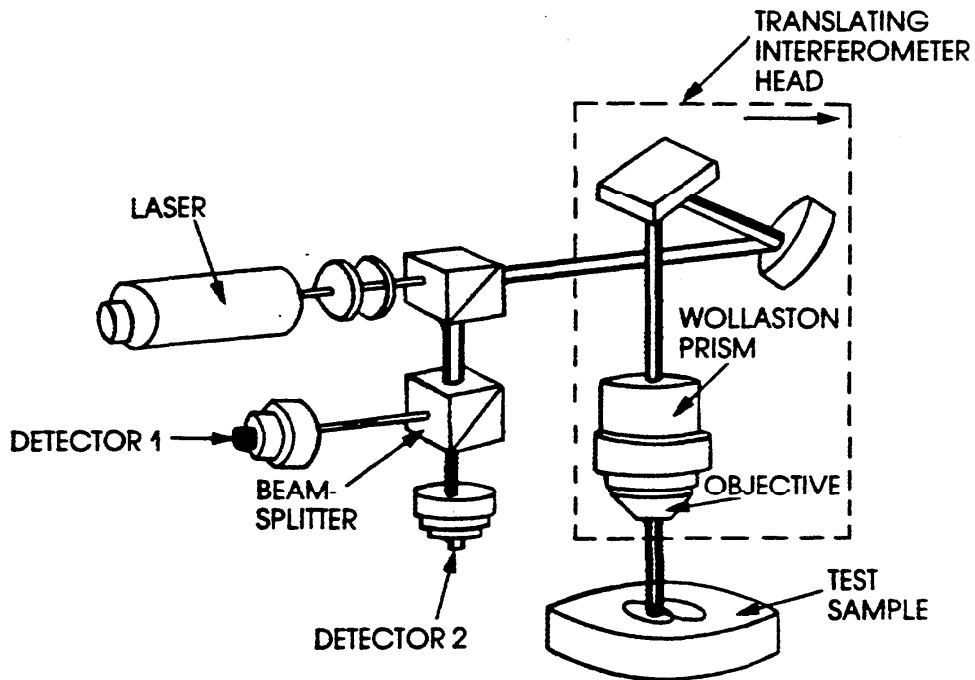


Figure 5-10
Schematic Diagram of Differential Interferometric Profiler (from Bristow [10])

instrument is quite good. In Fig. 5-11 you can see the profile resulting from a scan over a laser gyro mirror with a roughness of 0.175 nm. So the resolution over the length of 1 mm is comparable with the other instruments. In addition, there is no constraint on its ability to scan long distances. One concern is whether over the long scanning distances, the integration procedure may yield inaccuracies in the profiling. Initial studies over long trace lengths [10] suggest that the accuracy of the long trace profiler is comparable to stylus instruments.

Once again, note the characteristic structure of the profile of Fig. 5-11. Compare that to what you can get with a high resolution stylus instrument on a similar laser gyro mirror (Fig. 5-12). Although the latter profile looks like noise, it actually shows the surface at much better resolution and hence picks up much finer detail. The measured rms roughness is about 0.28 nm. Therefore, it seems that the lateral resolution of a high quality stylus is better than that achievable by the optical profiling instruments.

We can illustrate this with some data that Church et al. [11] took several years ago. Fig. 5-13 shows a profile of a highly periodic piece of diamond-machined silicon, measured by an optical interferometer and a stylus instrument. The stylus profile shows finer structure than the optical profile. This is further illustrated by taking the power spectral density of the surface profiles (Fig. 5-14). The fundamental periodicity of the silicon surface is approximately $3.4 \mu\text{m}$ and that spacing is Fourier transformed into the peak at a spatial frequency of $\sim 0.3 \mu\text{m}^{-1}$, shown clearly for both the stylus profile and the optical profile. However, the peak for the first harmonic at $\sim 0.6 \mu\text{m}^{-1}$ is considerably smaller for the optical profile than for the stylus profile. Therefore, the power spectrum information bears out the observations drawn from the profiles themselves.

The moderate lateral resolution of optical profiling instruments has been improved in recent work. Figure 5-15 is a profile taken from another profiling interferometer, similar to the Mirau system but with a Linnik

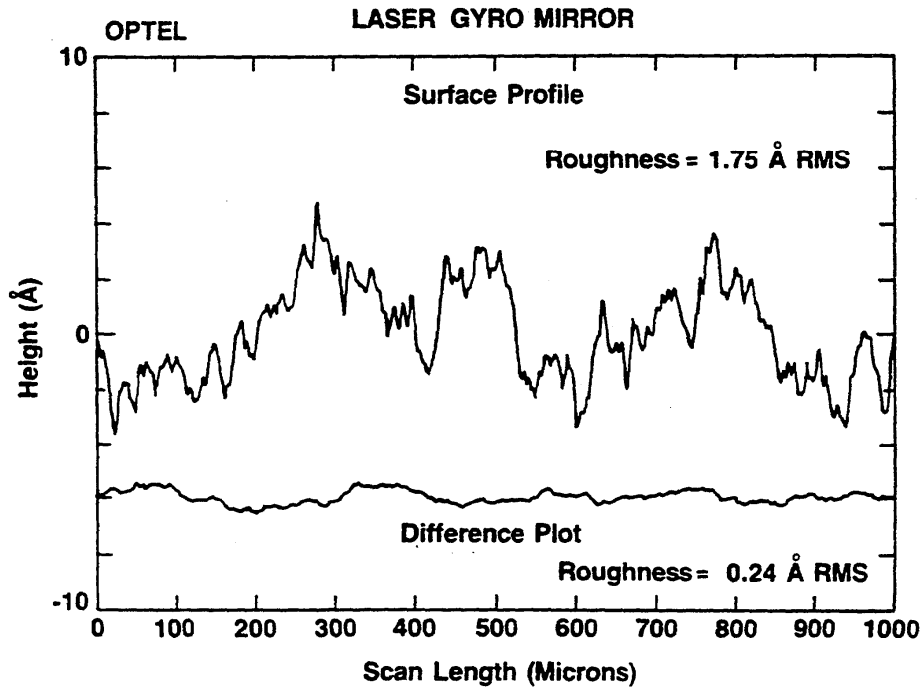


Figure 5-11
 Surface Profile Obtained with Differential Interferometric Profiler
 (from Bennett et al. [3])

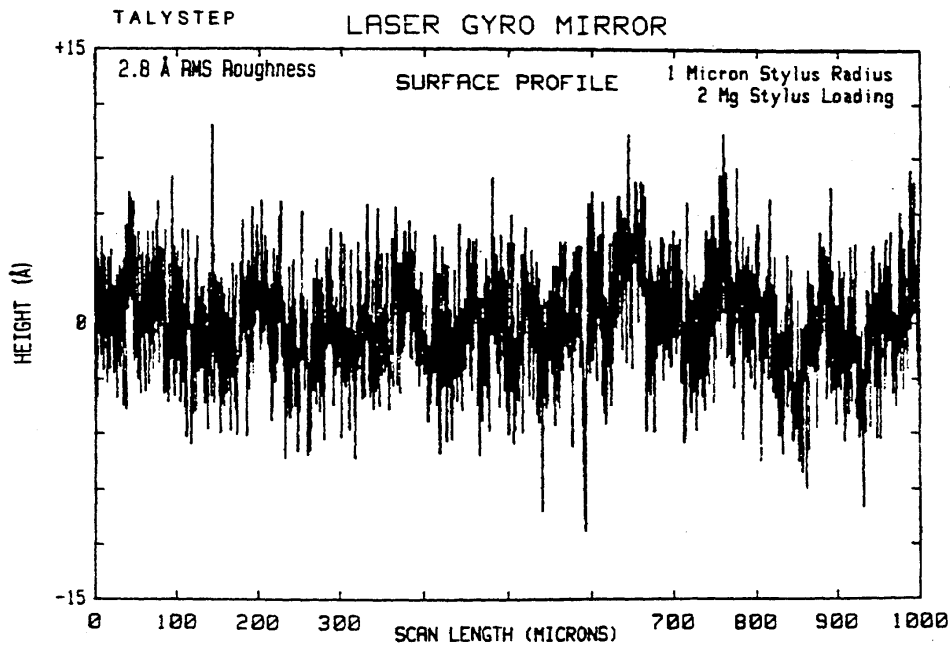


Figure 5-12
 Surface Profile Obtained with Stylus Instrument (from Bennett et al. [3])

Profiles of Machined Si

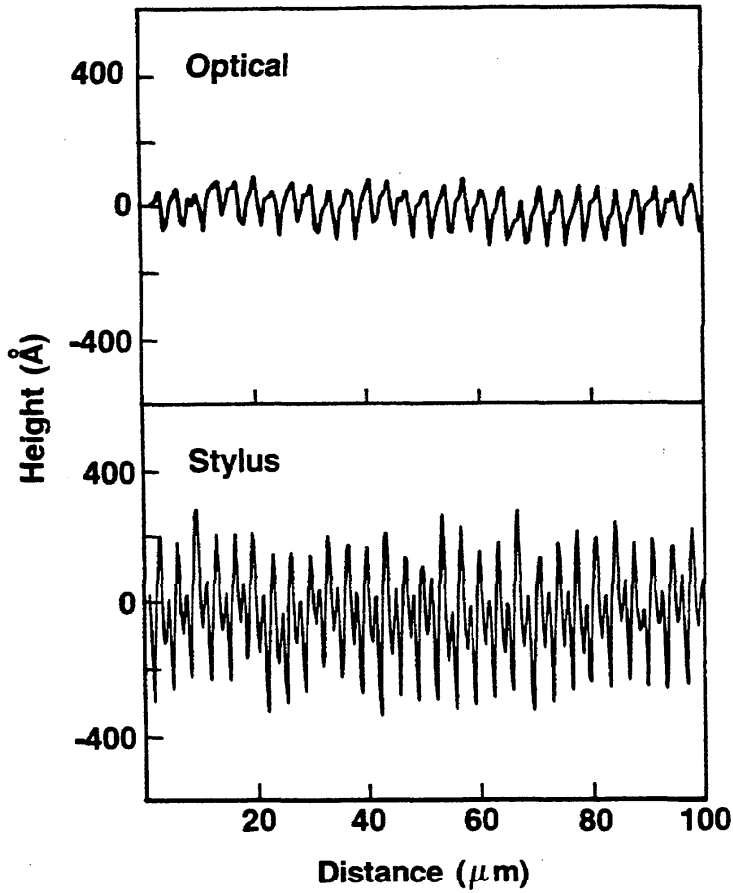


Figure 5-13
(from Church et al. [11])

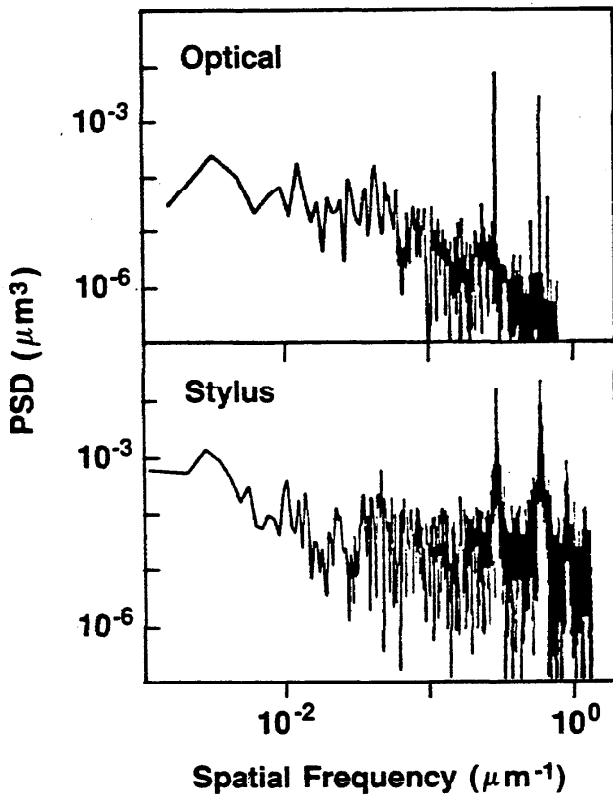


Figure 5-14
(from Church et al. [11])
Power Spectral Density Functions for
Machined Si Profiles

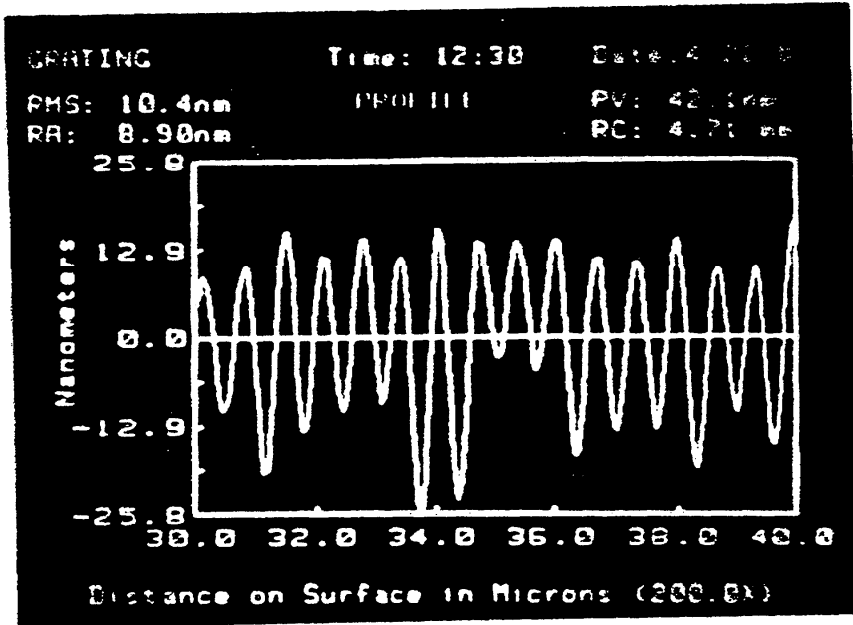


Figure 5-15

High Resolution Surface Profile Obtained with Linnik type profiling Microscope
(from Wyant et al.)

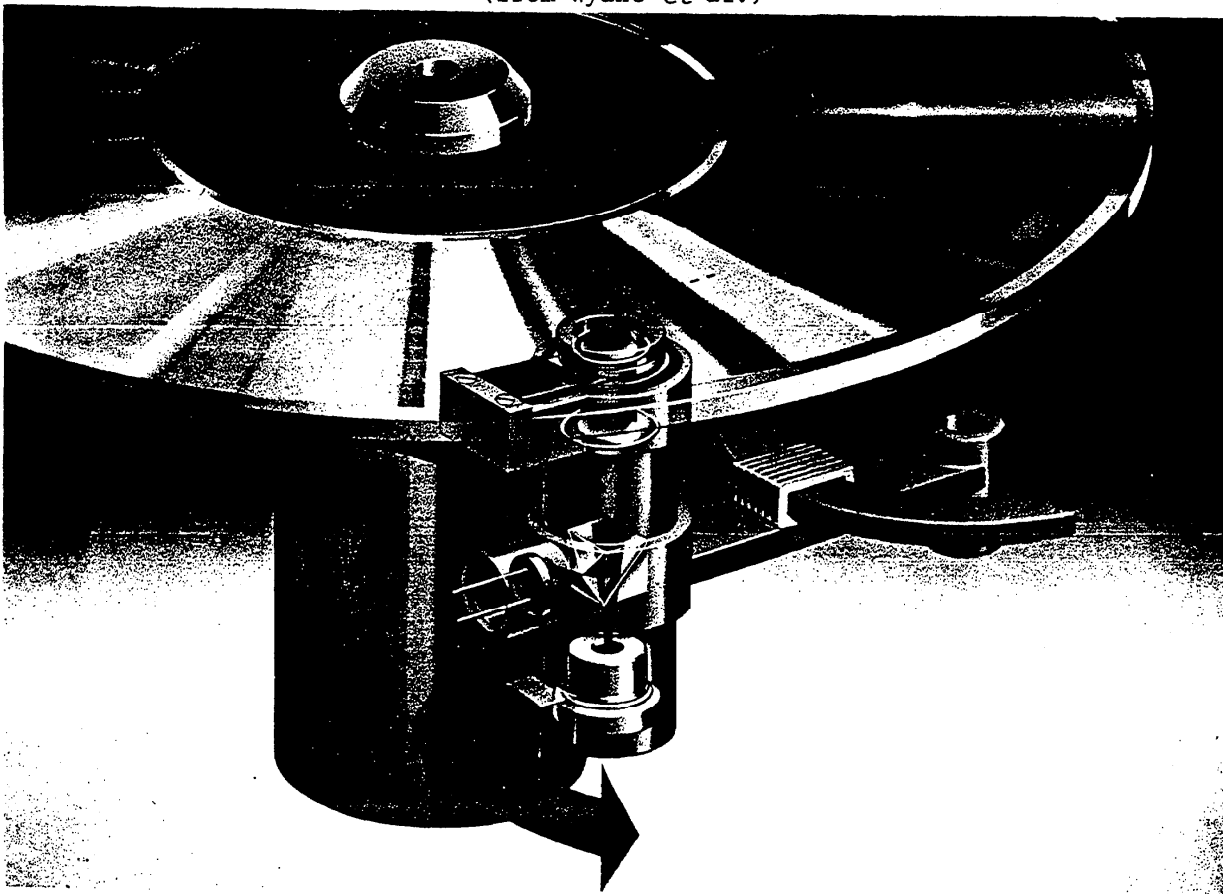


Figure 5-16
Schematic Diagram of Optical Focusing Instrument (from R. Brodmann)

head having matched high-power objectives. This is a profile of a diffraction grating with a period of $1 \mu\text{m}$. This optical profiler was able to resolve that periodicity. However, the lateral resolution of a stylus instrument can be made as small as $0.1 \mu\text{m}$, whereas that of optical interferometers is limited to about $0.5 - 1 \mu\text{m}$.

FOCUS DETECTION

We turn now to a type of optical instrument that relies on detection of the focus position of an optical spot to measure surface profile. These types of instruments have a long history, but nowadays are based on compact-disk technology. As shown in Fig. 5-16, the scanning head of the compact disk player focuses the light onto the surface of the disk itself. The degree of focus depends on the vertical position of the disk with respect to the scanning optics. There have been several profilers constructed using this general approach [19-21]. One of them [21] is shown schematically in Fig. 5-17. The surface is shown at the bottom and the light reflected from the surface goes through the objective lens and is deflected to the focus detector. The relative amounts of light detected on this set of detectors is dependent on the position of the original spot. The noise level of this instrument is about 0.6 nm , so its resolution is not quite as good as the interferometers just discussed. However, the range of this instrument is large (up to 1 mm or so), whereas the range of profiling interferometers is often limited by the spacing between visible light fringes, which is approximately $0.3 \mu\text{m}$.

STM AND AFM

The scanning tunneling microscope (STM) [22,23] is an exciting development for both surface profiling and microscopy. STM is shown schematically in Fig. 5-18. A fine electron emitter tip is held very close to the surface whose topography is to be measured. The surface itself must be electrically conducting. When a voltage is applied between the two, electrical current flows across the vacuum barrier. The magnitude of that current is extremely sensitive to the distance of the

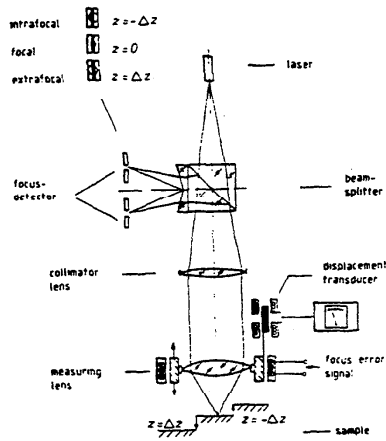


Figure 1 Dynamic focusing measuring principle: The focus error signal controls the lens movement and so maintains the focus on the surface.

Figure 5-17
(from Brodmann et al. [21])

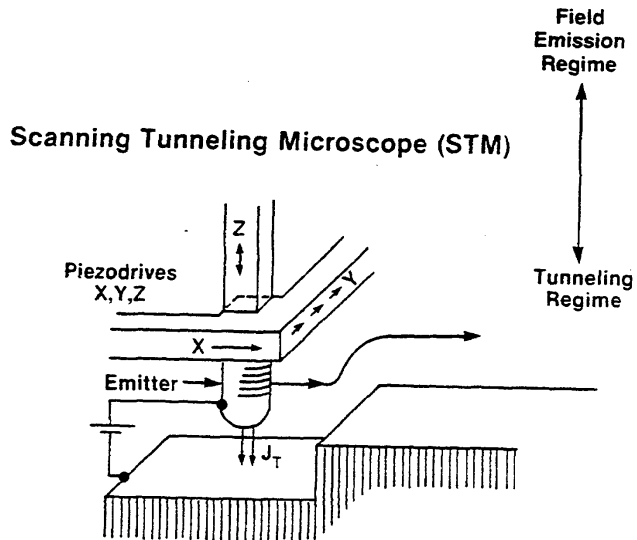


Figure 5-18

tip from the surface. When the tip is approximately 1 nm from the surface, the tunneling current changes by roughly 1 order of magnitude for each 0.1 nm change in the tip-to-surface distance. That tunneling current may be used as a feedback signal to keep the tip a constant distance away from the surface as you scan over it. The scanning is achieved by two piezo drives, x and y, which give the capability of mapping a small area by a raster approach. The topographic signal comes from the voltage applied to the z piezo drive to hold the emitter a constant distance from the surface during the scan.

The ideas of piezo scanning and current feedback were developed in the early 70's by R.D. Young and his group at the National Bureau of Standards [24,25]. Their surface scans were taken at distances of several hundred nm from the surface. Hence, the resolution of their surface profiles was somewhat moderate, ~100 nm. Later, Teague [26] made systematic observations of vacuum-tunneling phenomena by bringing two electrodes to within ~1 nm of each other. Finally, Binnig and Rohrer were able to reduce the mechanical noise of their system sufficiently so that they could perform surface scanning at very small tunneling distances. Under these conditions, they observed atomic resolution in their profile traces. An example of the atomic resolution is this raster map by Koehler et al. (Fig. 5-19) of a silicon (111) crystal surface, showing the individual atoms of the crystal. You can also see what look like adatoms in some places atop the basic crystal structure.

This instrument has become a valuable tool for surface scientists studying the crystal structure of surfaces [23,27-29], but it is also useful for engineers as well [30-32], particularly if you can accomplish long-range scanning. Fig. 5-20 [31,32] shows a scan of an optical grating which has a periodicity of 0.46 μm . This structure is observed clearly in the STM map and supports observations taken with a stylus instrument. The STM is capable of doing surface topographic mapping at higher resolution as well. Figure 5-21 is a map of a diamond-turned surface machined with a feed of 100 nm. The machining was done by Rohrer and others at the Los Alamos Scientific Laboratory. The STM is capable of picking out the

Si(111) 7x7 U. Koehler, J.E. Demuth, R.J. Hamers IBM Thomas J. Watson Research Center,
Yorktown Heights

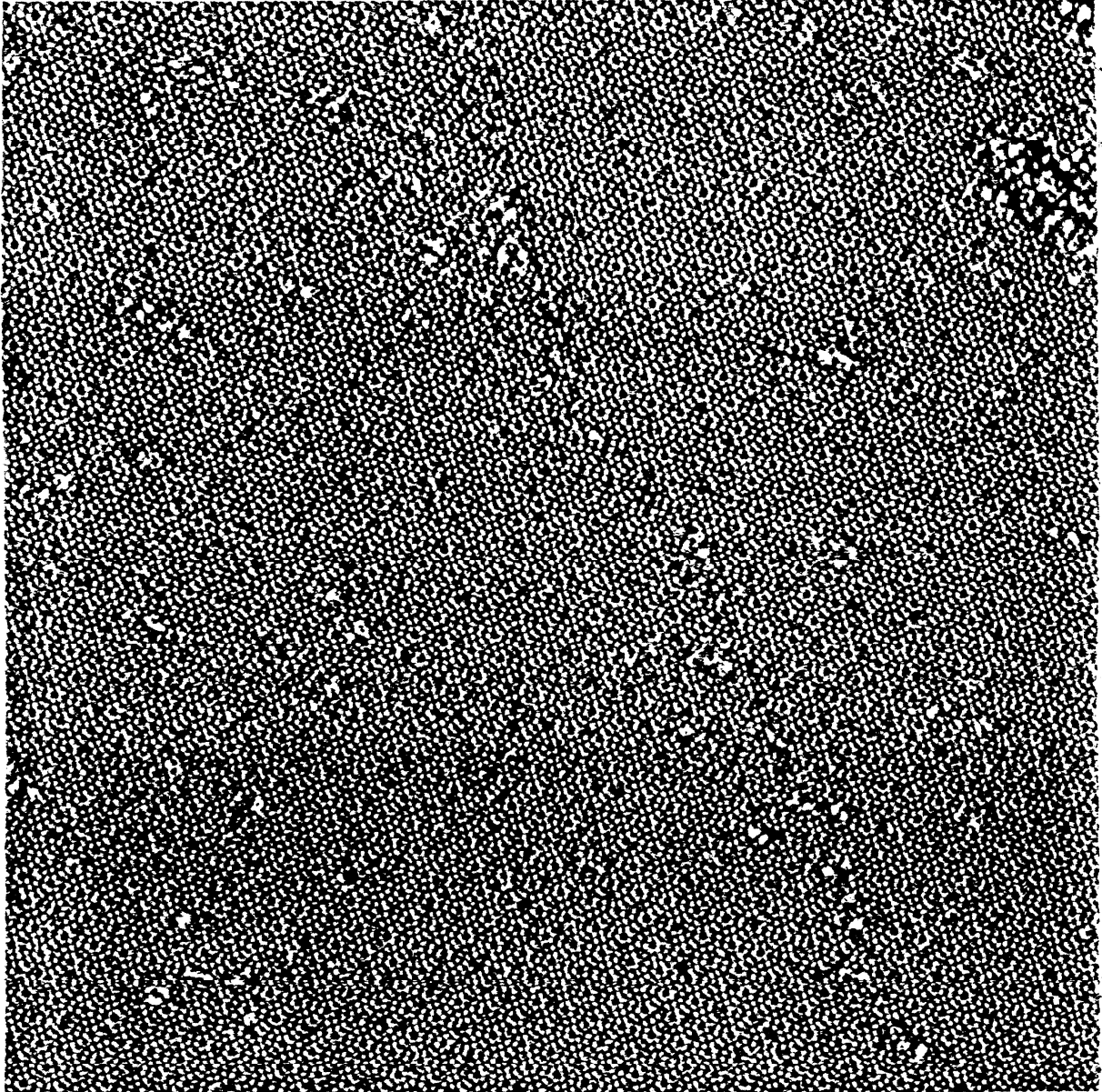


Figure 5-19
STM Map of Si(111) 7 x 7 Surface

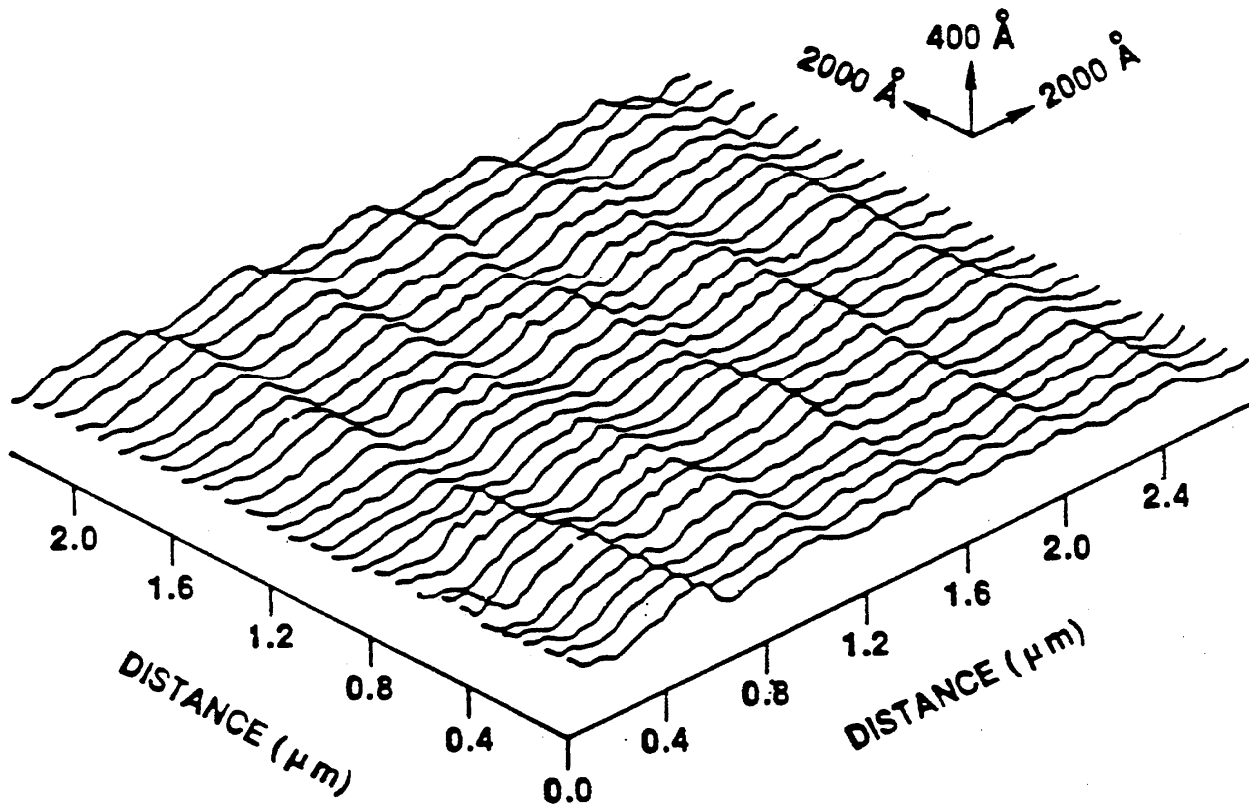


Figure 5-20

STM Map of Optical Grating (from Dragoset et al. [31,32])

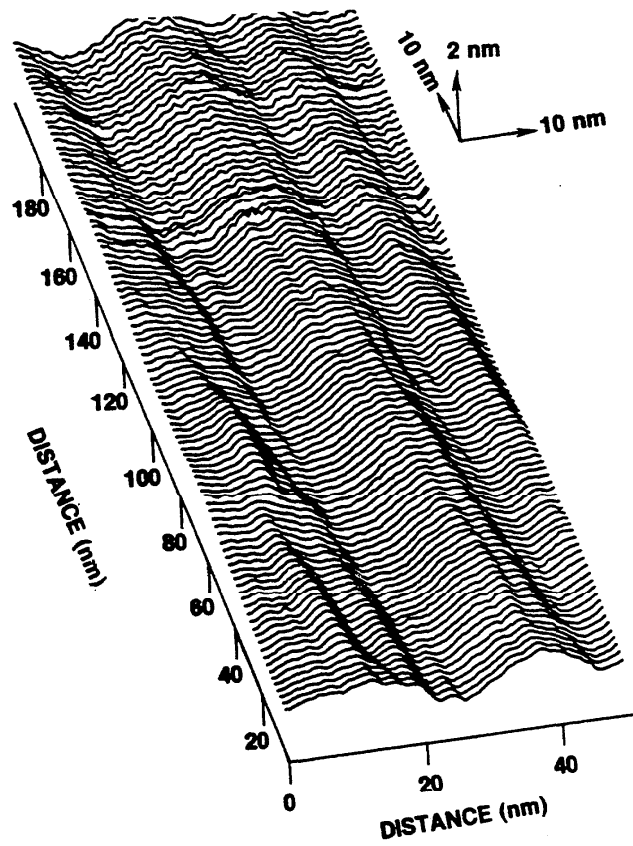


Figure 5-21
 STM Map of Diamond Turned Specimen
 (from Dragoset et al. [31,32])



Figure 5-22
 Ion Milled STM Tip (from Biegelsen et al. [35])

machined surface structures with spacings of ~ 100 nm, whereas the stylus instrument we used was not capable of observing those structures. In addition, you can see fine structure within the basic 100 nm grooves. So the STM has the potential of doing very high resolution scanning on surfaces important in areas of engineering such as tribology and optics. We fully expect that scanning tunneling microscopy will be developed to the point where it will be used for important problems in engineering.

The atomic resolution of the STM relies on the fact that the tunneling current must pass through a single atom or a small cluster of atoms in the emitter. When this capability was first discovered, it was considered to be somewhat magical, as were the recipes for producing tips that yielded atomic resolution. However, the fabrication of tunneling tips can be more systematic [35,36]. Figure 5-22 shows an example from the work of Biegelsen et al. [35]. This is a transmission electron microscopy (TEM) photo of a tungsten stylus produced by the ion-milling technique. The ion beam was incident at an angle of 45° from below and the shaft of the tungsten was rotated about its axis, yielding an ion-milled tip with a 90° apex angle. The tip is approximately 10 nm across, and serves as a suitable base above which individual atoms likely project to provide the atomic resolution during scanning.

One constraint in the STM is the required mechanical stability that is needed in order to allow for the high resolution of the probe. Another drawback is that it can be used only on conducting surfaces. This drawback may be avoided with a related technique known as the atomic force microscope, developed by Binnig et al. [33]. Several types of sensors are being studied for the atomic force microscope [37-39]. The original one, shown here on Fig. 5-23, has a scanning tip which is held in contact with the surface at extremely low contact forces of 5×10^{-8} N or less. It is fastened to a cantilever structure, whose deformation is measured by the STM behind it. As the surface is scanned, the variation in topography flexes the cantilever and this, in turn, is sensed by the STM. Surface

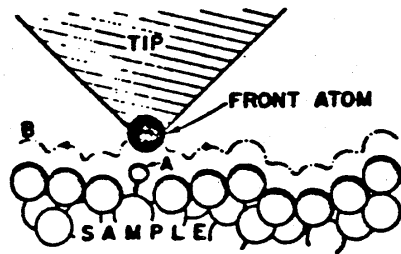


FIG. 1. Description of the principle operation of an STM as well as that of an AFM. The tip follows contour *B*, in one case to keep the tunneling current constant (STM) and in the other to maintain constant force between tip and sample (AFM, sample, and tip either insulating or conducting). The STM itself may probe forces when a periodic force on the adatom *A* varies its position in the gap and modulates the tunneling current in the STM. The force can come from an ac voltage on the tip, or from an externally applied magnetic field for adatoms with a magnetic moment.

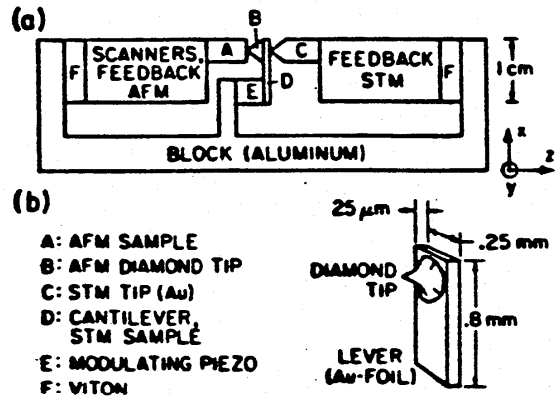


FIG. 2. Experimental setup. The lever is not to scale in (a). Its dimensions are given in (b). The STM and AFM piezoelectric drives are facing each other, sandwiching the diamond tip that is glued to the lever.

Figure 5-23

AFM Figures (from Binnig et al. [33])

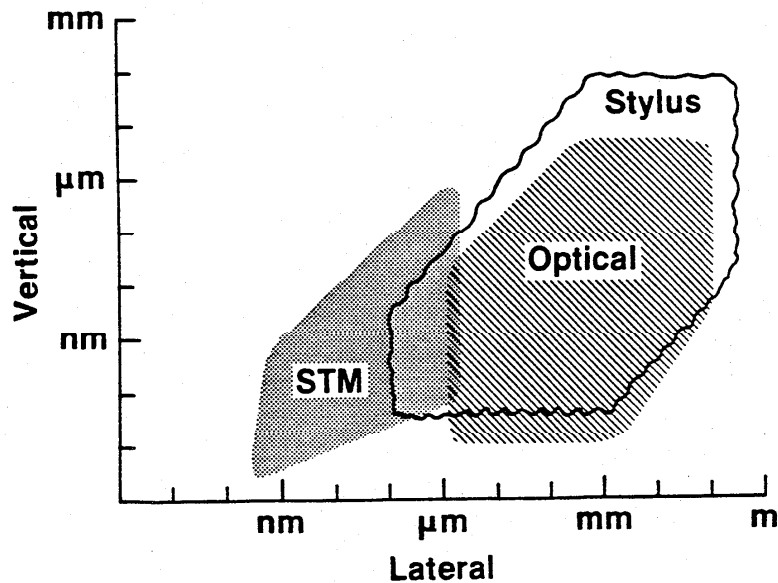


Figure 5-24

Range and Resolution of Three Techniques

maps with atomic resolution [40] have been recorded with AFM's as well as STM's.

Figure 5-24 [41] gives an overview of the range and resolution of three of the surface profiling techniques that we have been talking about. The graph is conceptually similar to ones developed by Stedman [42] and shows the vertical resolution, vertical range, lateral resolution, and lateral range of the stylus instrument, optical interferometers, and the scanning tunneling microscope. The chart was drawn up in 1987. The limits shown here are derived from typical instruments in each of the categories and may be exceeded by special purpose instruments. The chart shows several things. One is the versatility of the stylus instrument, which has the best ratio of range to resolution of the three, both in the lateral and in the vertical direction. The vertical resolution of the optical techniques is better than the stylus, but the lateral resolution is not as good. The STM has superb vertical and lateral resolution. Although the lateral range is presently somewhat modest, that condition will likely change as the engineering of STM's becomes more highly developed.

REFERENCES

FRINGE-FIELD CAPACITANCE

1. Garbini, J.L.; Jorgensen, J.E.; Downs, R.A.; Kow, S.P. Fringe-Field Capacitive Profilometry, *Surface Topography* 1, 99 (1988).

OPTICAL SECTIONING

2. Way, S. Description and Observation of Metal Surfaces, in Proc. Special Summer Conferences on Friction and Surface Finish (MIT, Boston, MA, 1940), p. 44.

OPTICAL INTERFEROMETRY

3. Bennett, J.M.; Bristow, T.C.; Arackellian, K.; Wyant, J.C. Surface Profiling with Optical and Mechanical Instruments, presented at the Optical Fabrication and Testing Workshop, Seattle, USA (Oct. 1986).

4. Dukes, J.N.; Gordon, G.B. A Two-Hundred-Foot Yardstick with Graduations Every Microinch, *Hewlett Packard Journal* 21 (12), 2 (1970).
5. Wyant, J.C.; Koliopoulos, C.L.; Bhushan, B.; George, O.E. An Optical Profilometer for Surface Characterization of Magnetic Media, *ASLE Trans.* 27, 101 (1984); and Bhushan, B.; Wyant, J.C.; Koliopoulos, C.L. Measurement of Surface Topography of Magnetic Tapes by Mirau Interferometry, *Appl. Opt.* 24, 1489 (1985).
6. Downs; M.J.; McGivern, W.H.; Ferguson, H.J. Optical System for Measuring the Profiles of Super-Smooth Surfaces, *Prec. Eng.* 7, 211 (1985).
7. Smythe, R.A. Heterodyne Profiler Moves from R & D to the Marketplace, *Laser Focus/Electro-Optics*, 92 (July 1987).
8. Sommargren, G.E. Optical Heterodyne Profilometry, *Appl. Opt.* 20, 610 (1981).
9. Bristow, T.C.; Arackellian, K. Surface Roughness Measurements Using a Nomarski Type Scanning Instrument, *Proc. SPIE* 749, 114 (1987).
10. Bristow, T.C. Surface Roughness Measurements over Long Scan Lengths, *Surface Topography* 1, 85 (1988).
11. Sec. 3, Ref. 31.
12. Tolansky, S. Multiple-Beam Interference Microscopy of Metals (Academic Press, London, 1970).
13. Feldman, A.; Vorburger, T. Comparison of Optical and Mechanical Methods of Thickness Measurement, in Integrated Circuit Metrology, *Proc. SPIE* 342, 92 (1982).
14. Blodgett, K.B.; Langmuir, I. Built-Up Films of Barium Stearate and Their Optical Properties, *Phys. Rev.* 51, 964 (1937).
15. Wyant, J.C. Precision Optical Testing, *Science* 206, 168 (Oct. 1979).
16. Guenther, K.H.; Wierer, P.G.; Bennett, J.M. Surface Roughness Measurements of Low-Scatter Mirrors and Roughness Standards, *Appl. Opt.* 23, 3820 (1984).
17. Eastman, J.M.; Zavislan, J.M. A New Optical Surface Microprofiling Instrument, *Proc. SPIE* 429, 56 (1983).
18. Wickramasinghe, H.K. Differential Laser Heterodyne Micrometrology, *Opt. Eng.* 24, 926 (1985); and See, C.W.; Vaez Iravani, M.; Wickramasinghe, H.K. Scanning Differential Phase Contrast Optical Microscope: Application to Surface Studies, *Appl. Opt.* 24, 2373 (1985).

OPTICAL FOCUS DETECTION

19. Simpson, J.A. Use of a Microscope as a Non-contacting Microdisplacement Device, *Rev. Sci. Instrum.* 42, 1378 (1971).
20. Kohno, T.; Ozawa, N.; Miyamoto, K.; Musha, T. Practical Non-Contact Surface Measuring Instrument with One Nanometre Resolution, *Prec. Eng.* 7, 231 (1985).
21. Brodmann, R.; Smilga, W. Evaluation of a Commercial Microtopography Sensor, *Proc. SPIE* 802, 165 (1987).

STM AND AFM

22. Binnig, G.; Rohrer, H. Scanning Tunneling Microscopy, *Helv. Physica Acta* 55, 726 (1982).
23. Golovchenko, J.A. The Tunneling Microscope: A New Look at the Atomic World, *Science* 232, 48 (1986).
24. Young, R.; Ward, J.; Scire, F. The Topografiner: An Instrument for Measuring Surface Microtopography, *Rev. Sci. Instrum.* 43, 999 (1972).
25. Young, R.; Ward, J.; Scire, F. Observation of Metal-Vacuum-Metal Tunneling, Field Emission, and the Transition Region, *Phys. Rev. Lett.* 27, 922 (1971).
26. Teague, E.C. Room Temperature Gold-Vacuum-Gold Tunneling Experiments, Ph.D. Thesis, North Texas State University, Denton, Texas, 1978; and Room Temperature Gold-Vacuum-Gold Tunneling Experiments, *J. Res. NBS* 91, 171 (1986).
27. Binnig, G.; Rohrer, H.; Gerber, Ch.; Weibel, E. Reconstruction on Si(111) Resolved in Real Space, *Phys. Rev. Lett.* 50, 120 (1983).
28. Park, S.; Quate, C.F. Tunneling Microscopy of Graphite in Air, *Appl. Phys. Lett.* 48, 112 (1986).
29. Feenstra, R.M.; Fein, A.P. Scanning Tunneling Microscopy of Cleaved Semiconductor Surfaces, *IBM J. Res. & Dev.* 30, 466 (1986).
30. Garcia, N.; Baro, A.M.; Miranda, R.; Rohrer, H.; Gerber, Ch.; Garcia Cantu, R.; Pena, J.L. Surface Roughness Standards, Obtained with the Scanning Tunneling Microscope Operated at Atmospheric Air Pressure, *Metrologia* 21, 135 (1985).

31. Dragoset, R.A.; Young, R.D.; Layer, H.P.; Mielczarek, S.R.; Teague, E.C.; Celotta, R.J. Scanning Tunneling Microscopy Applied to Optical Surfaces, *Opt. Lett.* 11, 560 (1986).
32. Dragoset, R.A.; Vorburger, T.V. Scanning Tunneling Microscopy (STM) of a Diamond-Turned Surface and a Grating Replica, *Proc. SPIE* 749, 54 (1987).
33. Binnig, G.; Quate, C.F.; Gerber, Ch. The Atomic Force Microscope, *Phys. Rev. Lett.* 56, 930 (1986).
34. Becker, R.S.; Golovchenko, J.A.; Swartzentruber, B.S. Atomic-Scale Surface Modifications Using a Tunneling Microscope, *Nature* 325, 419 (1987).
35. Biegelsen, D.K.; Ponce, F.A.; Tramontara, J.C.; Koch, S.M. Ion Milled Tips for Scanning Tunneling Microscopy, *Appl. Phys. Lett.* 50, 696 (1987).
36. Fink, H.W. Mono-Atomic Tips for Scanning Tunneling Microscopy, *IBM J. Res. Develop.* 30, 460 (1986).
37. Amer, N.M.; Meyer, G. A Novel Optical Approach to Atomic Force Microscopy, *Appl. Phys. Lett.* 53 (12), 1045 (1988).
38. Erlandsson, R.; McClelland, G.M.; Mate, C.M.; Chiang, S. Atomic Force Microscopy Using Optical Interferometry, *J. Vac. Sci. Tech. A.* 6 (2), 266 (1988).
39. Rugar, D.; Mamin, H.J.; Erlandsson, R.; Stern, J.E.; Terris, B.D. Force Microscope Using a Fiber-Optic Displacement Sensor, *Rev. Sci. Instrum.* 59, 2337 (1988).
40. Marti, O.; Drake, B.; Hansma, P.K. Atomic Force Microscopy of Liquid-Covered Surfaces: Atomic Resolution Images, *Appl. Phys. Lett.* 51, 484 (1987).

OTHERS

41. Sec. 2, Ref. 19.
42. Sec. 2, Ref. 18.

SECTION 6

AREA TECHNIQUES

Area techniques yield measurements that represent statistical averages of the surface peaks and valleys over a significant area of the measured surface. The techniques that we will discuss are optical scattering, ultrasonics, and areal capacitance. However, other area methods [27,28] have also been developed.

OPTICAL SCATTERING

When a light beam illuminates a surface as shown in Fig. 6-1, the scattering phenomena depend on the surface roughness. If the surface were quite smooth, you would have a single specular reflected beam that would be detected, say, by detector 3. As the surface roughness begins to increase, the specular beam diminishes in intensity and a diffuse angular distribution (AD) appears. The shape of the AD and the intensity of the specular beam are related to the surface roughness. There are other aspects about the scattered light pattern that are indicators of the roughness as well. If you have a laser light source, the pattern of scattered light contains fine structure known as speckle, and the contrast of the speckle pattern is characteristic of the roughness. In addition, the change of polarization properties of the light ($P_i \rightarrow P_f$) upon reflection is also a function of the roughness. We schematically represent the measurement of these scattering phenomena by the five detectors shown in Fig. 6-1. Our main focus here is the measurement of the AD.

Just as the intensity of the specular beam can be related to the surface roughness, so also can the amount of light scattered out of the specular beam. That is the basis for a technique known as total integrated scatter (TIS) which has been standardized by the ASTM for inspection of optical surfaces [1,17]. A schematic diagram is shown on Fig. 6-2. The surface is illuminated by a laser beam whose intensity can be measured. The laser beam passes through the hole in a hemisphere and

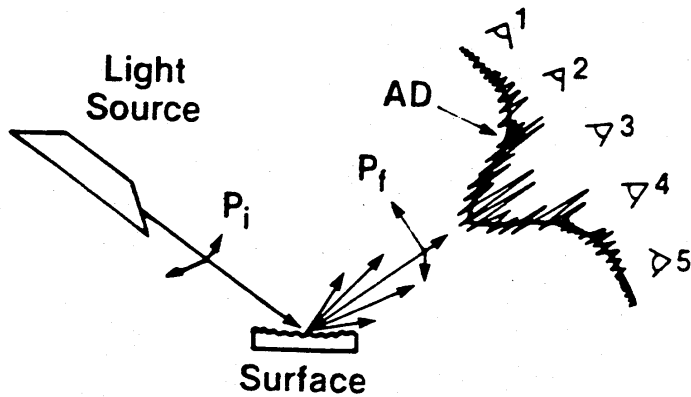


Figure 6-1
Schematic Diagram of Optical Scattering

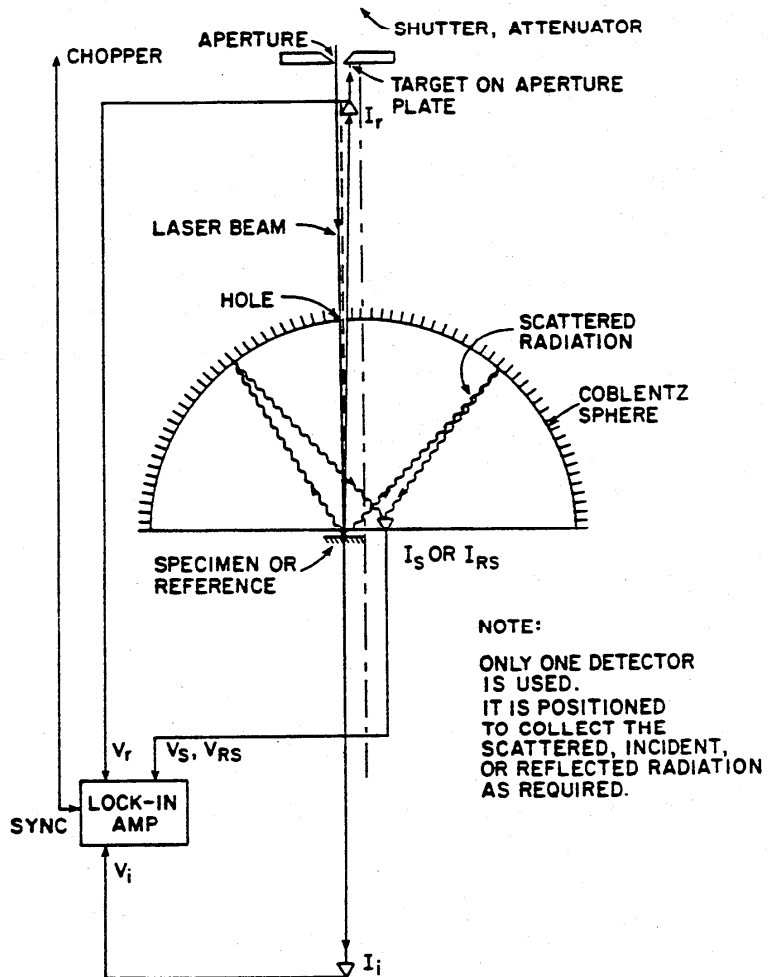


Figure 6-2
Schematic Diagram of TIS (from Detrio et al. [1])

scatters from the surface. The specularly reflected component passes back through the same hole and is not detected as scattered light. However, any radiation scattered out of the specular beam is focused by the collecting hemisphere onto the conjugate point to the surface where a detector measures the collected intensity of the scattered radiation. Within a spatial bandwidth [18] determined by the size of the hole and the angular span of the hemisphere, the amount of scattered radiation I_{scat} is related to the rms surface roughness (R_q) by the formula

$$I_{\text{scat}}/I_o = (4\pi R_q/\lambda)^2,$$

where I_o is the intensity of the specular beam, assuming the incident light beam is normal to the surface. This formula should be essentially correct for surfaces with rms roughness much less than the wavelength (λ) of the illuminating light beam.

The test method was adopted as a standard after a round-robin experiment involving eight optical laboratories to test the method's variability. Figure 6-3 shows the results for four surfaces polished to different degrees of smoothness. Along the horizontal scale is plotted the mean value of the rms roughness derived by the laboratories, and on the vertical scale are plotted the different measured values. The spread of values is on the order of $\pm 15\%$. That result is moderately good and shows the basis for standardizing the technique for testing optical surfaces by this approach. The accuracy of the technique likely declines as rms roughness increases above 10 nm.

Our group has been studying optical scattering to measure much rougher surfaces, such as those produced by grinding and lapping operations on engineering components. The theory of optical scattering from rough surfaces is more difficult in this roughness regime, and the rms roughness cannot be related to the total integrated scatter using the previous formula. The measurement system is called DALLAS [16] (detector array for laser light angular scattering), shown in Fig. 6-4. A laser beam

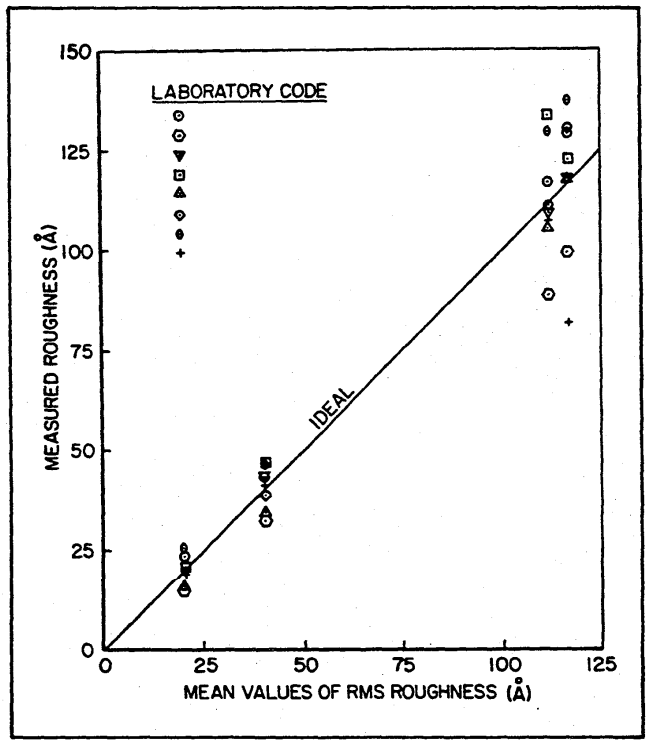


Figure 6-3
 Round Robin Results for TIS (from Detrio et al. [1])

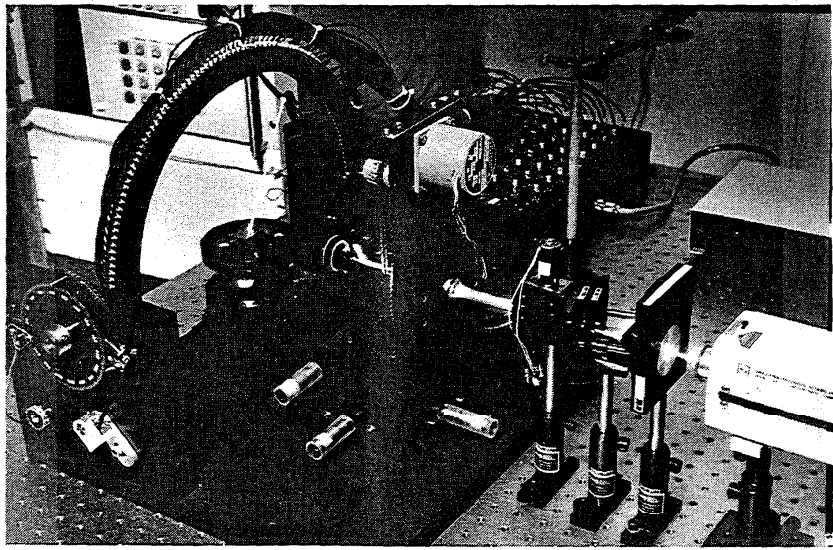


Figure 6-4
 Photo of DALLAS

traveling from the right is deflected by a mirror into a cantilevered tube to another mirror which deflects the beam down to the surface. The light scattering pattern, as we discussed previously, is characteristic of the roughness of the surface. That light scattering pattern is sampled by a set of lenses in the semicircular yoke. Each lens focuses the light down to one of the optical fibers strung along in black, that transmit the light to a bank of PIN silicon photodiodes with integral op-amps. The output voltages are scanned, digitized, and stored in a computer and yield plots of intensity as a function of angle in the yoke. In principle, the computer-controlled stepping motor allows you to detect nearly the entire hemisphere of scattered radiation.

The next several figures illustrate the phenomena by showing light scattering patterns from a set of periodic, sinusoidal surfaces [19]. Figure 6-5 illustrates the concept by showing a laser beam incident on such a surface and scattering into a set of discrete diffraction beams. Figure 6-6 shows a set of three such diffraction patterns, photographed on the wall of our laboratory, from three different sinusoidal surfaces. The one on the right was taken from a sinusoidal surface with $40\ \mu\text{m}$ wavelength and a $1\ \mu\text{m}$ R_a . The pattern in the middle was for a surface with the same R_a , but a longer wavelength of $100\ \mu\text{m}$, so the spots are closer together. The surface on the left again had the same R_a , but an $800\ \mu\text{m}$ wavelength. For this one, you cannot quite resolve the diffraction spots. Therefore, the spacing of the diffraction spots is related to the wavelength of the surface roughness. Figure 6-7 shows the conjugate experiment. On the right is the pattern from a sinusoidal surface with a wavelength or peak spacing of $100\ \mu\text{m}$ and an R_a of $3\ \mu\text{m}$. The middle pattern is for the same spacing, but the R_a is only $1\ \mu\text{m}$ so the intensities of the outlying spots are very weak. The pattern on the left is from a surface with an R_a of $0.3\ \mu\text{m}$, so it shows only a few diffraction spots. Therefore, as the surface gets smoother, the scattering produces fewer diffraction peaks, until finally we are left with only the specular beam, and the surface itself looks like a mirror.

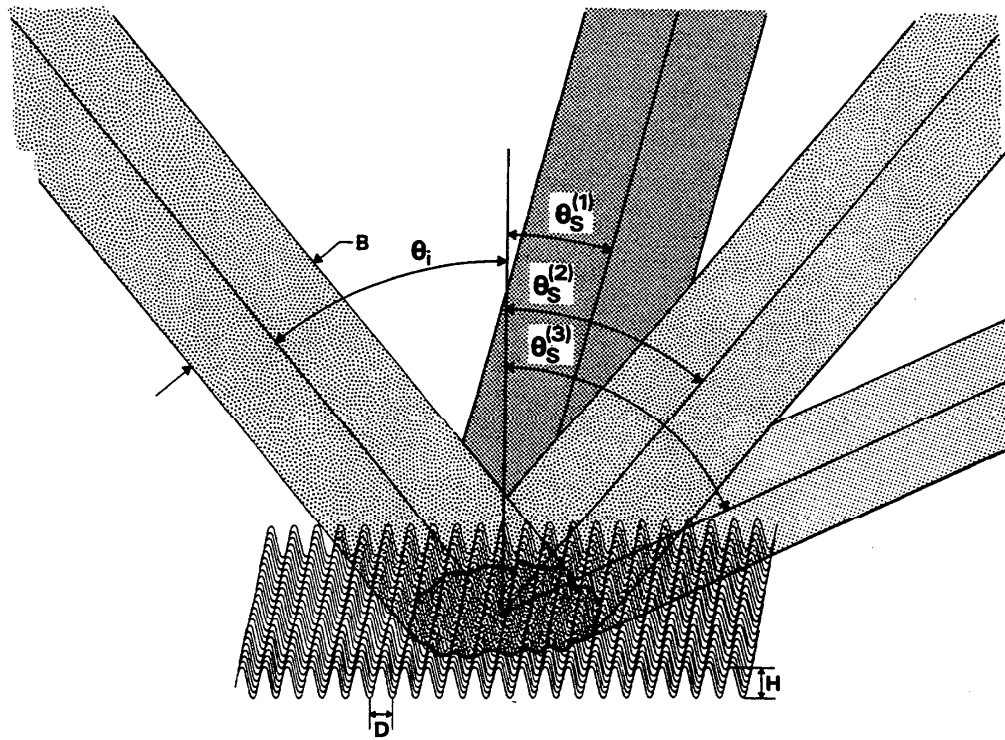


Figure 6-5
Optical Scattering from Sinusoidal Surface

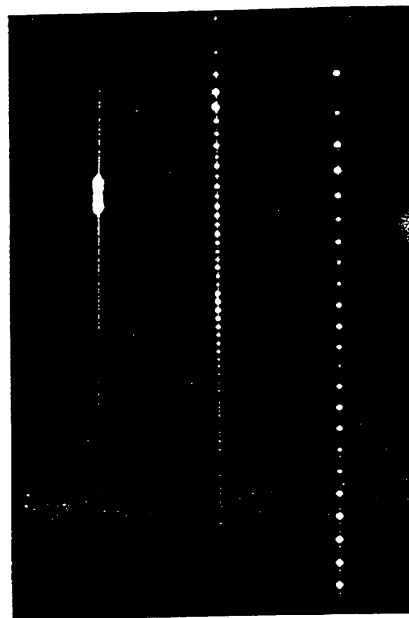


Figure 6-6
Optical Scattering Patterns from three Sinusoidal Surfaces

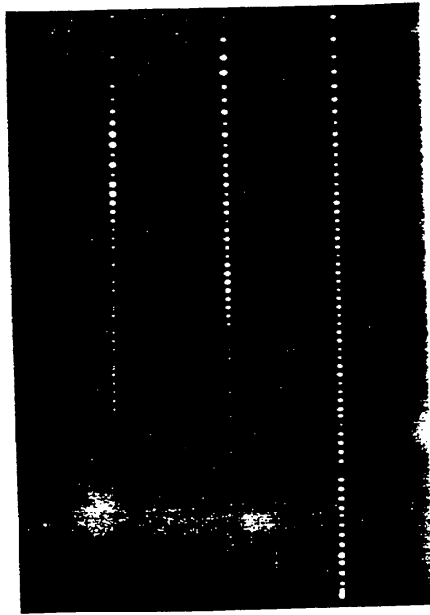


Figure 6-7
Optical Scattering Patterns from Three Sinusoidal Surfaces

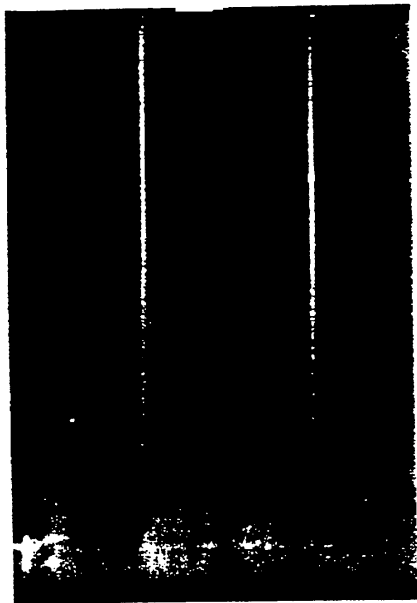


Figure 6-8
Optical Scattering Patterns from Hand-lapped Surfaces

Figure 6-8 shows scattering patterns for two hand-lapped surfaces. The one on the left had an R_a of $0.25 \mu\text{m}$ and shows quite a diffuse scattering pattern. The other is for an R_a of $0.12 \mu\text{m}$. Its scattering pattern is not quite as diffuse and there is a recognizable specular beam as well.

The DALLAS instrument has been used to measure both the sinusoidal and random surfaces, and we have done two types of experiments with these data. First, we have measured the surfaces with our stylus instruments and stored the digitized profile data. Then with these measured profiles, we have applied an optical scattering theory to predict the light scattering intensity pattern. That comparison between experiment and theory is excellent for both random surfaces and for sine waves. Second, we are also doing the more critical job of calculating the important roughness properties of the surface strictly from the light scattering pattern itself. This has been done successfully for our sinusoidal surfaces as shown by the results in Fig. 6-9 [20]. We have fitted the measured scattering distributions to theoretical distributions and calculated the values of the surface R_a and peak spacing that give us the best fit. The values we derived from optical scattering are shown on the right for six different surfaces with varying R_a and wavelength. You can see these results agree extremely well with those measured by a stylus on the left. So for a surface that is fairly easy to model, the periodic sine wave, we can demonstrate that the optical scattering predicts very accurately what the roughness is.

We are now pursuing these studies for realistic surfaces that have been produced by other processes. Figure 6-10 shows the light scattering intensity pattern for a hand-lapped surface [21]. It is a plot of intensity over 5 orders of magnitude vs. scattering angle in the yoke. The light beam was incident from the left at an angle of about -54° ; therefore, the specular beam and the peak in the intensity is at $+54^\circ$. The experimental distribution is shown by the dotted line, and the computed distribution, calculated from the measured surface profiles obtained by stylus, agrees very well with the experimental one. Therefore

Comparison of Stylus and Optical Measurements of Roughness Parameters

Surface	Measured by Stylus		Deduced from Optical Scattering	
	R_a	D	R_a	D
Brass 1	1.02	40.1	1.02	39.9
Brass 2	1.02	100.2	1.01	99.6
Brass 3	1.01	800	1.00	(800)
Nickel 1	1.03	100.2	1.01	100.2
Nickel 2	0.31	100.2	0.31	100.8
Nickel 3	2.98	100.1	2.99	99.3

Figure 6-9

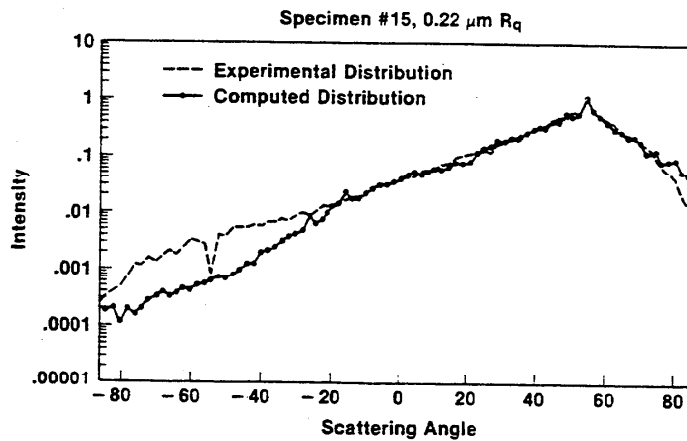


Figure 6-10

DALLAS Results

for the range of nine hand-lapped surfaces that we studied, the surface profile can be used to predict quantitatively the light scattering pattern. The small disagreement between the computed and experimental distribution is probably due to the fact that the stylus had limited resolution and could not resolve the finest surface structures, which scatter light to high angles in the left wing of the graph.

We are presently working on computer codes to calculate the rms roughness (R_q) and perhaps the autocorrelation length strictly from the scattering intensity patterns themselves [22]. When we have completed these studies and have determined what is the useful roughness range for the technique of optical scattering, as well as what kinds of manufactured surfaces it will be useful for, we plan to apply that knowledge to a practical instrument that can be used on-line in inspection or in real-time during a machining operation. One practical instrument available commercially is depicted here in Fig. 6-11. The small assembly on the right is a light scattering detector that is monitoring the surface condition of the part being held by a robot. This is an example of work going on at the inspection station at the AMRF in the Center for Manufacturing Engineering at NIST [14].

The instrument is an angular scattering instrument. A schematic diagram of its optical system is shown in Fig. 6-12. This was taken from the work of Brodmann et al.[5] All of the optics are located inside that housing shown in Fig. 6-11. The source is an infrared light emitting diode. The light is collimated and then focused by one side of the measuring lens into a 1.8 mm size spot on the surface. If the surface is smooth, the spot that is reflected back to the measuring lens is approximately the same size as the incident spot. If the surface is rough, however, the scattering pattern will be broadened and this broadening can be detected with the diode array shown in the upper right of Fig. 6-12. This instrument is easy to align and is very compact, but the question of its range and resolution is an important one. We have tested it for hand-lapped surfaces. The results [14] are shown in Fig. 6-13, where we plot the rms roughness for a number of surfaces measured by

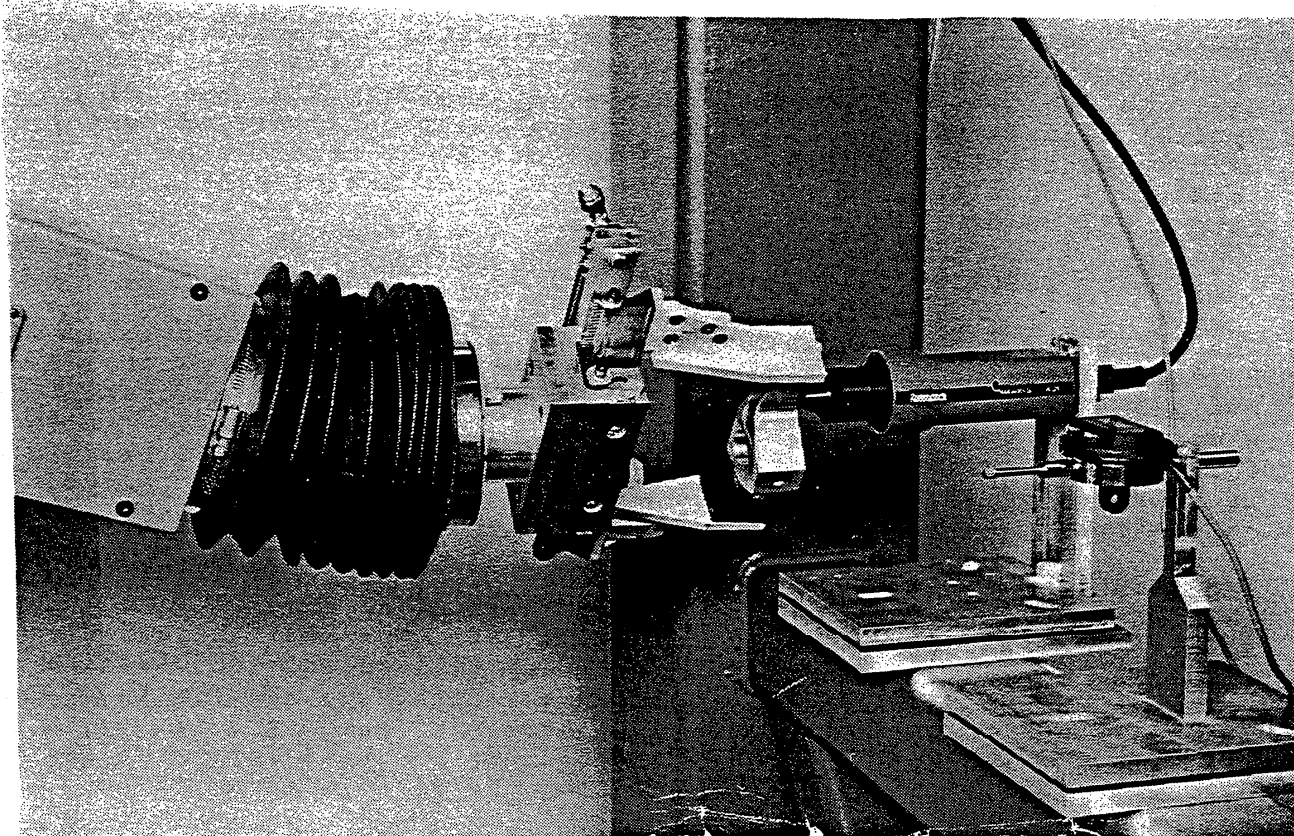


Figure 6-11

Surface Roughness Inspection System in AMRF at NIST

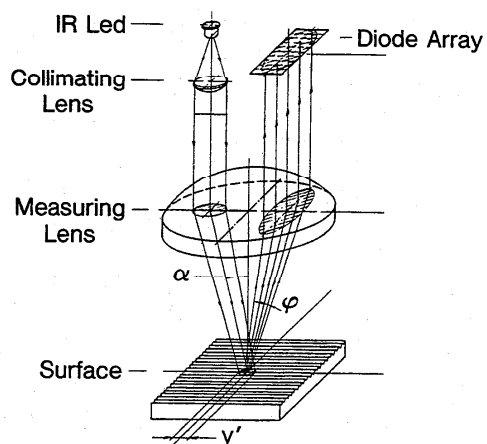


Figure 6-12

(from R. Brodmann et al. [5]) Schematic Diagram of Infrared Surface Roughness Probe

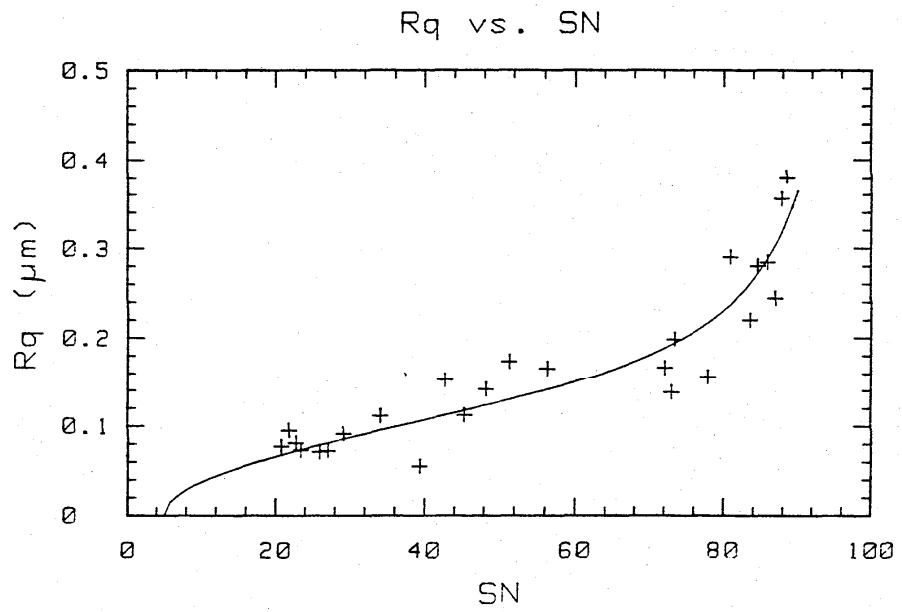


Figure 6-13

Comparison of Results Obtained with Stylus and Scattering Results

the stylus techniques vs. the optical scattering parameter S_N , which is used in the instrument as an indicator of the surface condition. S_N is proportional to the square of the width of the light scattering distribution measured by the instrument. Over the range of R_q from 0 to about $0.3 \mu\text{m}$, you can see a good correlation between roughness as measured conventionally and as measured by this light scattering technique [14]. The curved line is a best fit with two parameters. We will extend these studies to other kinds of surfaces besides those that have been hand-lapped.

ULTRASONICS

Blessing and Eitzen [23] have developed an ultrasonic scattering technique that has great potential for real-time measurement of surface roughness. It is conceptually similar to optical scattering except for the fact that a pulse of ultrasonic radiation illuminates the surface instead of a light beam. The radiation is incident at normal incidence, and the source transducer is also used to measure the reflected pulse intensity. This quantity varies inversely as the roughness height and hence is an indicator of roughness.

Figure 6-14 shows a schematic diagram of the instrument. The ultrasonic radiation propagates well along a stream of coolant fluid, such as might be used during a machining process. This capability gives the technique its potential usefulness for automated manufacturing.

The first prototypes have used a long ultrasonic wavelength ($150 \mu\text{m}$ typical). Hence, the regime of roughnesses studied so far have been complementary to those studied by the infrared technique discussed earlier. That is, the roughness height resolution of an ultrasonic probe with $\lambda = 150 \mu\text{m}$ is roughly the same as the range of the infrared probe with $\lambda = 0.8 \mu\text{m}$.

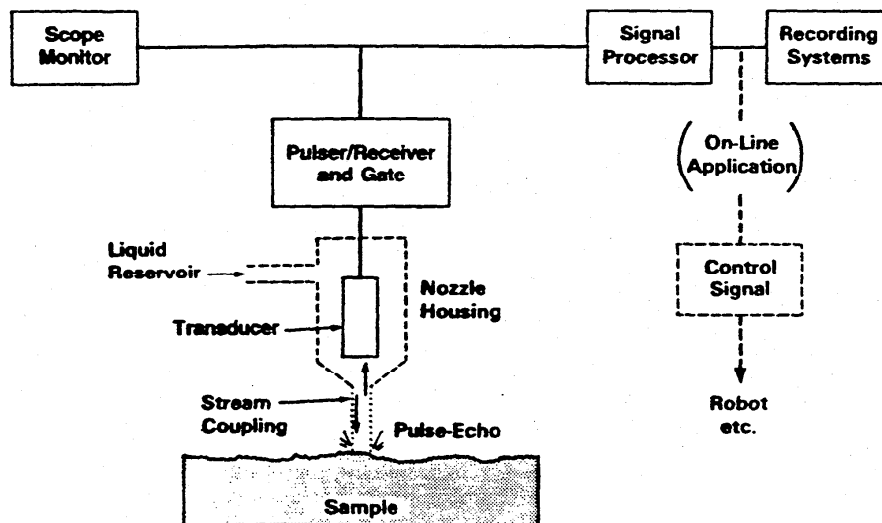


Figure 6-14

Schematic Diagram of Ultrasonic Scattering Instrument

(from Blessing et al. [23])

AREAL CAPACITANCE

The areal capacitance technique [24-26] was first developed about two decades ago. A schematic diagram is shown in Fig. 6-15. A flexible conducting plate is placed on a conducting surface with a thin insulator in between. The capacitance of the junction is a function of the distance between the two conductors which depends partly on the thickness of the insulator (t_d) but also on the surface roughness. Since the insulator is resting on the highest peaks of the surface, the rougher the surface the greater the distance, t_a , between the insulator and the average surface plane. Therefore, the measured capacitance should be an indicator of the surface roughness. However, this technique needs to be modeled to understand how roughness affects capacitance.

The sensing element conductor is about 1.2 mm wide and about 12 mm long. It has a flexible backing and is housed in a case with two shoulders that serve as stops when the element is pressed on the surface. The contact force is roughly 15N. When the response of the capacitance gauge is measured in a comparison experiment for a single family of surfaces, you can get good correlation between the roughness as measured by the capacitance gauge (appropriately normalized) and the R_a values measured by a stylus instrument. In Fig. 6-16, we plot the effective roughness R_C as measured by the capacitor vs. the roughness average R_a as measured by a stylus instrument for a family of ground surfaces. The two measured quantities correlate very well, except for the smoothest surface whose roughness of $0.025 \mu\text{m}$ is likely below the resolution of the capacitance instrument. The deviation of the R_C values from the straight line is 20% or less for the remaining seven surfaces. However, the correlation is not as good when we plot results for several types of surfaces. Altogether we tested 41 surfaces including sinusoidal and ruled surfaces, specimens that were replicas of ground, shaped, side-milled, and end-milled surfaces, as well as surfaces formed by electrical discharge machining. Figure 6-17 shows the spread in the results. Although there is general correlation between R_C and R_a , the variability in R_C for a given R_a value can be as high as a factor of 5 due to the fact that these

Capacitance Technique

$$C = \frac{kA}{\frac{t_d}{\epsilon_d} + \frac{t_a}{\epsilon_a}}$$

$$C \propto \frac{Aa}{t_a}$$



Figure 6-15

(from D.G. Risko)

Figure 6-16

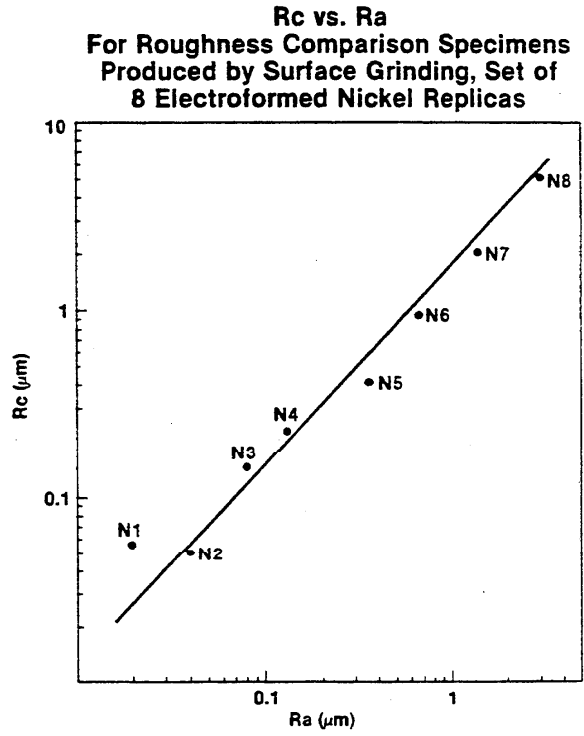
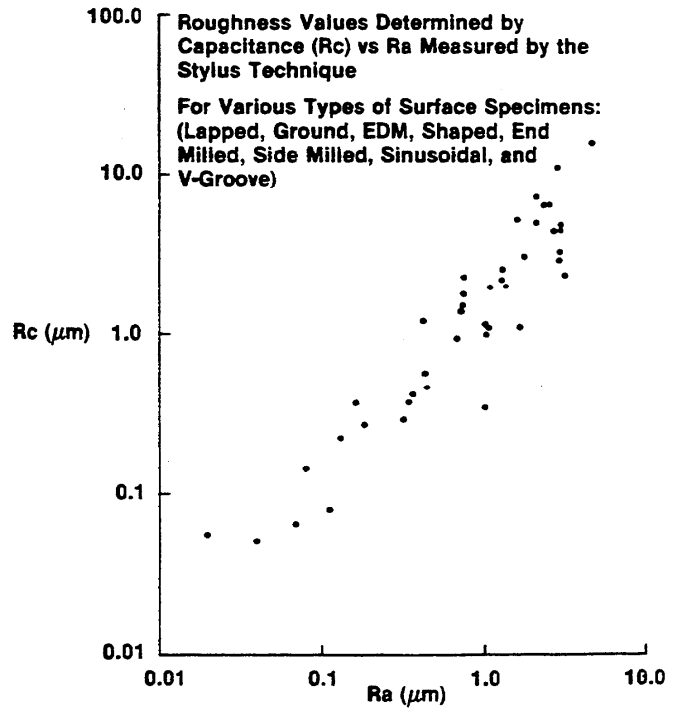


Figure 6-17



surfaces have different shapes because they were manufactured by different processes.

We tried to overcome the variability introduced by the shape factor by developing a fundamental model [24] for the way the capacitor senses the surface. The model took into account two things: a description of how each surface element affects the sensed capacitance and an elastic beam model to describe how the sensing element flexes when suspended between surface peaks. The resulting correlation is considerably better than a simple correlation between R_C and R_a . Figure 6-18 plots our predicted values of R_C , based on the model, vs. our measured values of R_C . For all the different varieties of surfaces, the agreement over several orders of magnitude is reasonably good. The most deviant point is about 50% away from the best-fit line itself. However, the spread in the data is still partly due to the fact that the model is being tested for several kinds of surfaces. The correlation is better for a single class of surfaces.

This parameter that we predicted from our model, R_C -calculated, seems to be equivalent to a parameter that characterizes peak height for a conventional surface profile. We call that parameter $R_p(750)$. To calculate it, one takes a sampling length 750 μm long and calculates the height difference from the highest peak to the mean-line over that sampling interval range. Then the $R_p(750)$ values for the various sampling intervals are averaged over the entire assessment length of the surface profile. In summary then, it seems that the areal capacitance instruments measure a surface roughness quality that is quite similar to the peak-to-mean line parameter R_p .

To summarize, we have observed a dramatic evolution of profiling instruments for measuring surface topography, particularly in the area of optical techniques, scanning tunneling microscopy, and atomic force microscopy. Commercial instruments are available in all of these areas.

In the field of area techniques, we have discussed areal capacitance sensing, ultrasonics, light-scattering angular distributions, and a form

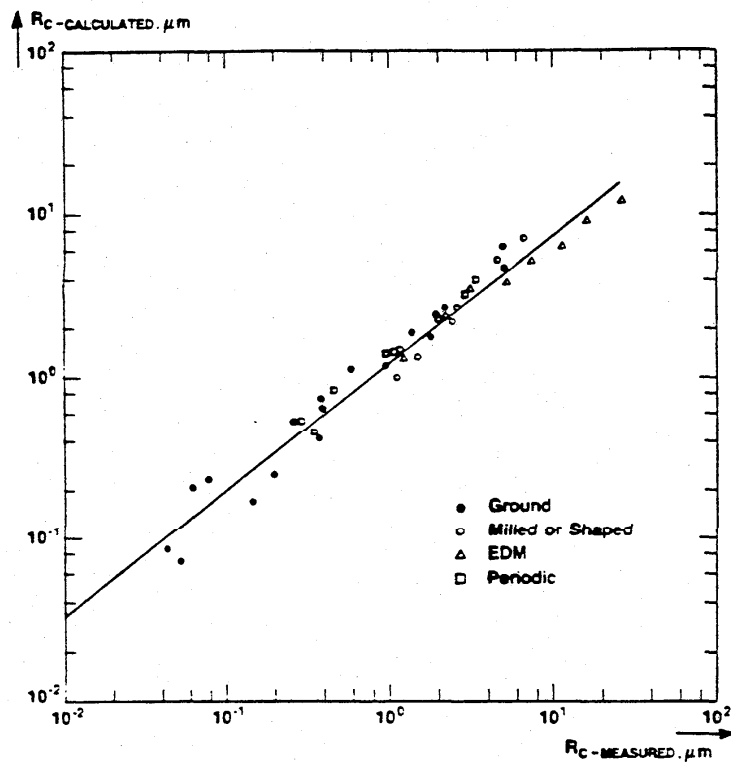


Figure 6-18

Results of Capacitance Modeling Experiment

of light scattering known as total integrated scatter. The latter is now the basis for an ASTM standard. Hence, we can point to progress in the standardization as well as the modeling of area techniques.

REFERENCES

OPTICAL SCATTERING

1. Detrio, J.A.; Miner, S.M. Standardized Total Integrated Scatter Measurements of Optical Surfaces, *Opt. Eng.* 24, 419 (1985).
2. Mitsui, K.; Sato, H. Frequency Characteristic of Cutting Process Identified by an In-Process Measurement of Surface Roughness, *CIRP Annals* 27 (1), 67 (1978).
3. Elson, J.M.; Bennett, H.E.; Bennett, J.M. Scattering from Optical Surfaces, in Applied Optics and Optical Engineering, Vol. 7 (Academic Press, New York, 1979) p. 191.
4. Stover, J.C.; Cady, F.M.; Sklar, E. Measurement of Low Angle Scatter, *Opt. Eng.* 24, 404 (1985).
5. Brodmann, R.; Gerstorfer, O.; Thurn, G. Optical Roughness Measuring Instrument for Fine-Machined Surfaces, *Opt. Eng.* 24, 408 (1985).
6. Silva, R.M.; Orazio, F.D.; Sledge, R.B. Automated Nondestructive PBS Measurements of Surface and Subsurface Defect Distribution in Silicon and Gallium Arsenide Wafers, *Proceedings 1985 Measurement Science Conference* (Jan. 17-18, Santa Clara, California).
7. Cunningham, L.J.; Braundmeier, Jr., A.J. Measurement of the Correlation between the Specular Reflectance and Surface Roughness of Ag Films, *Phys. Rev.* B14, 479 (1976).
8. Goodman, J.W. Statistical Properties of Laser Speckle Patterns, in Laser Speckle and Related Phenomena, Topics in Applied Physics, Vol. 9, J.C. Dainty, ed. (Springer-Verlag, Berlin, 1975) p. 9.
9. Asakura, T. Surface Roughness Measurement, in Speckle Metrology, R.K. Erf, ed. (Academic Press, New York, 1978) p. 11.
10. Uozumi, J.; Asakura, T. Granularity Growth of Laser Speckle and Its Application to Surface Inspection, *Optics and Laser Technology* 9, 177 (1977).
11. Ahlers, R.J. White-Light Method: A New Sensor for the Optical Evaluation of Rough Surfaces, *Opt. Eng.* 24, 423 (1985).

12. Saito, T.T.; Simmons, L.B. Performance Characteristics of Single Point Diamond Machined Metal Mirrors for Infrared Laser Applications, *Appl. Opt.* 13, 2647 (1974).
13. Endriz, J.G.; Spicer, J. Study of Aluminum Films, I. Optical Studies of Reflectance Drops and Surface Oscillations on Controlled-Roughness Films., *Phys. Rev.* B4, 4144 (1971).
14. Zimmerman, J.H.; Vorburger, T.V.; Moncarz, H.T. Automated Optical Roughness Inspection, in Optical Testing and Metrology II, Proc. SPIE 954, 252 (1989).
15. Baker, L.R. Areal Measurement of Topography, *Surface Topography* 1, 207 (1988).
16. Vorburger, T.V.; Teague, E.C.; Scire, F.E.; McLay, M.J.; Gilsinn, D.E. Surface Roughness Studies with DALLAS - Detector Array for Laser Light Angular Scattering, *J. Res. of NBS* 89, 3 (1984).
17. Sec. 2, Ref. 11.
18. Church, E.L.; Howells, M.R.; Vorburger, T.V. Spectral Analysis of the Finish of Diamond-Turned Mirror Surfaces, *Proc. SPIE* 315, 202 (1981).
19. Teague, E.C.; Vorburger, T.V.; Maystre, D.M. Light Scattering from Manufactured Surfaces, *CIRP Annals* 30/2, 563 (1981).
20. Vorburger, T.V.; Gilsinn, D.E.; Scire, F.E.; McLay, M.J.; Giaque, C.H.W.; Teague, E.C. Optical Measurement of the Roughness of Sinusoidal Surfaces, *Wear* 109, 15 (1986).
21. Vorburger, T.V.; Cao, L.X.; Giaque, C.H.W.; Raja, J.; Gilsinn, D.E.; Fullana, L. Optical Scattering from Rough Surfaces: Experiment and Theory, in Seventh International Colloquium on Surfaces, H. Trumpold, ed. (Technische Universitat, Karl-Marx Stadt, DDR, 1988), p. 308.
22. Marx, E.; Cao, L.X.; Vorburger, T.V. Determination of Surface Roughness from Scattered Light, to be published.

ULTRASONICS

23. Blessing, G.; Eitzen, D.G. Surface Roughness Sensed by Ultrasound, *Surface Topography* 1, 253 (1988).

AREAL CAPACITANCE

24. Lieberman, A.G.; Vorburger, T.V.; Giaque, C.H.W.; Risko, D.G.; Resnick, R.; Rose, J. Capacitance versus Stylus Measurements of Surface Roughness, *Surface Topography* 1, 315 (1988).

25. Sherwood, K.F.; Crookall, J.R. Surface Finish by an Electrical Capacitance Technique, Proc. Instn. Mech. Engrs. 182, Pt 3k, 344 (1967-68).
26. Brecker, J.N.; Fromson, R.E.; Shum, L.Y. A Capacitance-Based Surface Texture Measuring System, CIRP Annals 25 (1), 375 (1977).

PNEUMATIC

27. Hamouda, A.M. A Precise Pneumatic Co-axial Jet Gauging System for Surface Roughness Measurement, Prec. Eng. 1, 95 (1979).

ELECTRON DIFFRACTION

28. Hottier, F.; Theeten, J.B.; Masson, A.; Domange, J.L. Comparative LEED and RHEED Examination of Stepped Surfaces; Application to Cu (111) and GaAs (001) Vicinal Surfaces, Surface Science 65, 563 (1977).

SECTION 7 FUNCTION

We conclude this tutorial with a short discussion of surface function, a subject of great interest to engineers. The central theme here is to relate surface texture specifications to functional performance. However, knowledge in this area is not well organized. Therefore we will be showing a collection of case studies and examples, while emphasizing the need to systematize the information that is available in this field. In particular, we will show functional examples in optics, hydrodynamic drag, and aerodynamic drag, in turn. Then we will discuss surfaces that have been produced by metalworking for engineering components. We will conclude with a proposal about a surface texture information system.

OPTICS

Figure 6-2 showed the total integrated scatter measuring system which has been standardized by the ASTM. The device measures the amount of light scattered out of the specular beam by an optical component. This sort of measurement is appropriately related to the function of the component because in many types of optical instruments it is important to minimize the scattered or stray light. In this case, the measurement of TIS is appropriate for describing the function of an optical surface.

Figure 7-1 shows a set of surface quality standards for optical elements. These are five scratch standards [18] each with a different size scratch. They were developed for visual comparison [13] to describe the scratches on transmitting optical surfaces, like lenses or windows. The scratches may be compared by an observer with scratches on the optic itself under certain conditions. To the extent that scratches are important on optical surfaces, these standards are functional standards.

There is also a set of dig standards that can be compared with digs that might be found on optical surfaces. So in the optical industry, certain functional properties can be fairly well understood, and these can

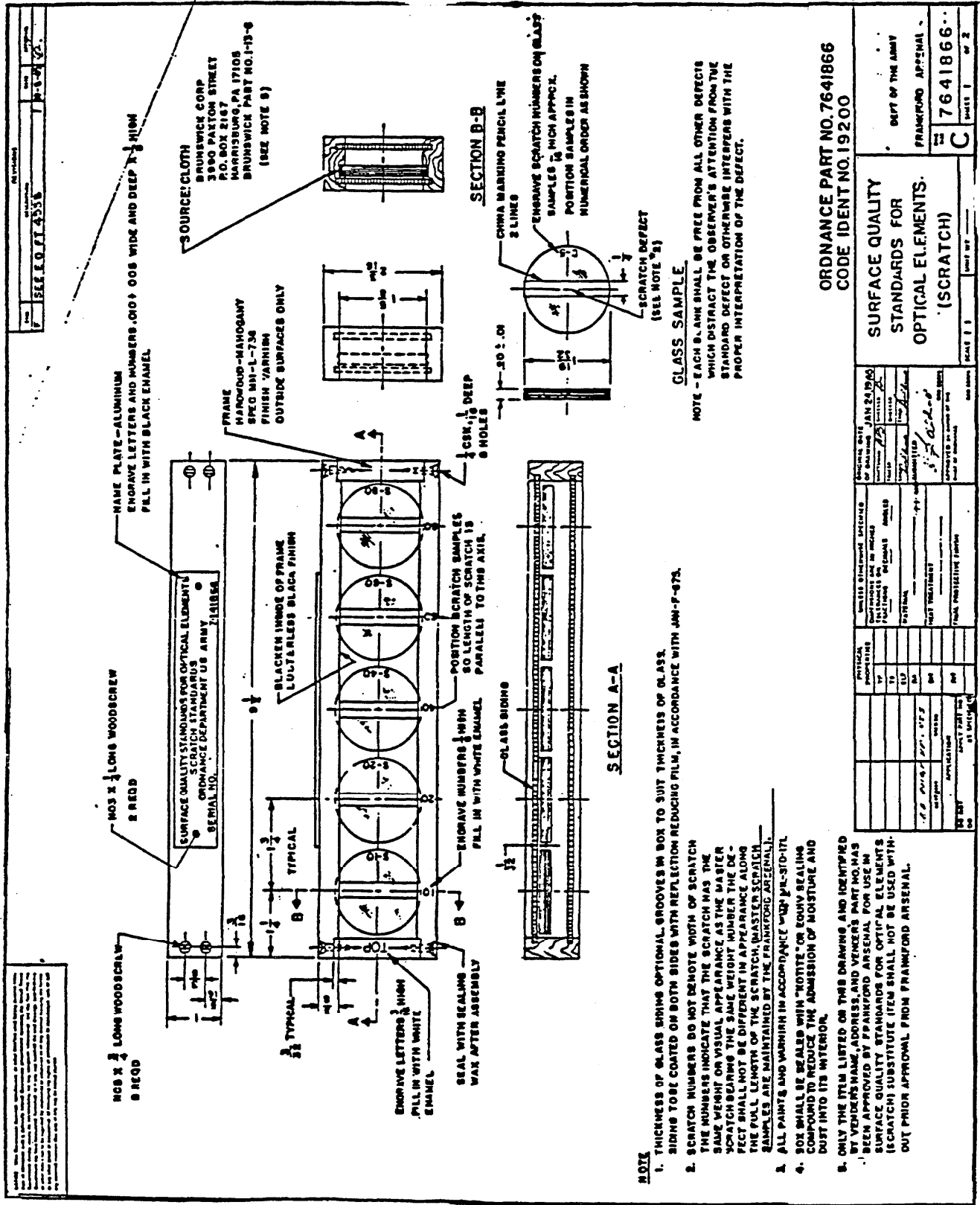


Figure 7-1

Drawing for Scratch Standards (from [18])

be quantified with standard specimens and standard measurement procedures. We should add that the scratch standards have been considered to be primarily useful for cosmetic purposes [13], and some contend that this cosmetic standard is not related to the true function of optical components. However, the presence of a scratch on an optical surface certainly increases the scattered light and that is a functional quality.

HYDRODYNAMIC DRAG

Figure 7-2 shows two disks of a set that was fabricated by the Navy for a hydrodynamic drag experiment. The disks were spun up to a high speed in water, and the torque on the shafts was measured with an instrument at the Naval Ship Research and Development Center. The torque is an indicator of the amount of hydrodynamic drag on the spinning disks. The roughnesses of the disks were also measured by us [12,17].

Figure 7-3 shows correlation between the measured drag coefficient and the R_a of the disks. The disks labeled P were coated with paints of differing roughness. The disks labeled T were of titanium with varying roughness patterns directly machined on them. You can see a strong correlation, between the drag coefficient C and R_a , although not a perfect one. The roughness average value, R_a , does not tell the whole story, as suggested by the spread of these data. If you also fold in the effects of peak spacing on the disks, you get a better correlation as shown by Fig. 7-4. Now the drag coefficient is plotted against R_a divided by the average wavelength or peak spacing of the disks taken to the $\frac{1}{2}$ power. There is a better correlation between the measured drag coefficient and this new surface parameter. We should add that $R_a/\lambda^{\frac{1}{2}}$ is an empirical parameter based on observations. The theoretical basis for this result needs to be further investigated.

AERODYNAMIC DRAG

Figure 7-5 is a photo of a model of the space shuttle, used in wind tunnel studies at NASA Langley Research Center. For accurate wind tunnel

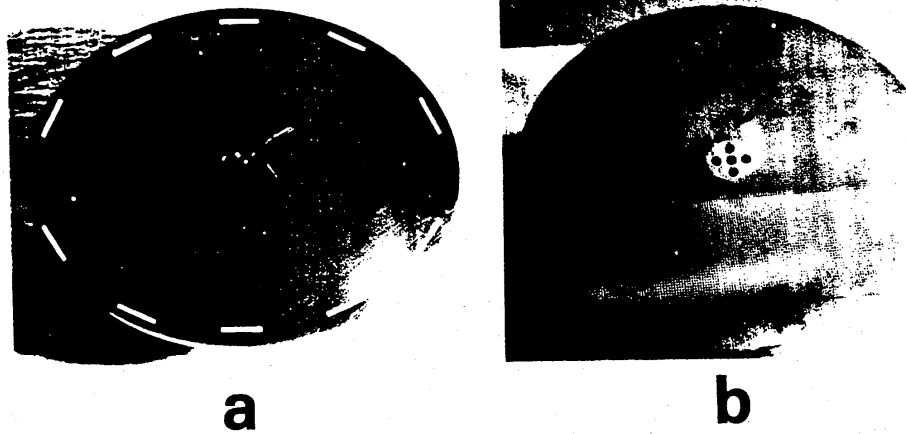


Figure 7-2

Titanium Disks Used for Hydrodynamic Drag Experiment

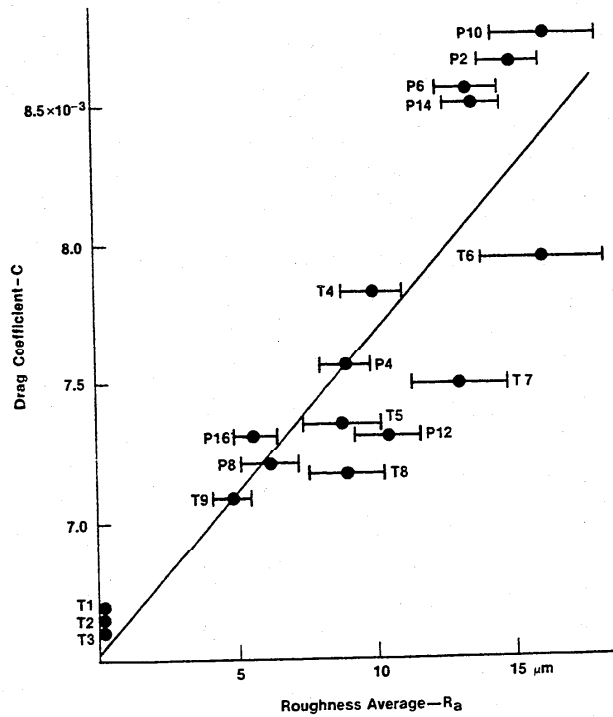


Figure 7-3

Results of Hydrodynamic Drag Experiment

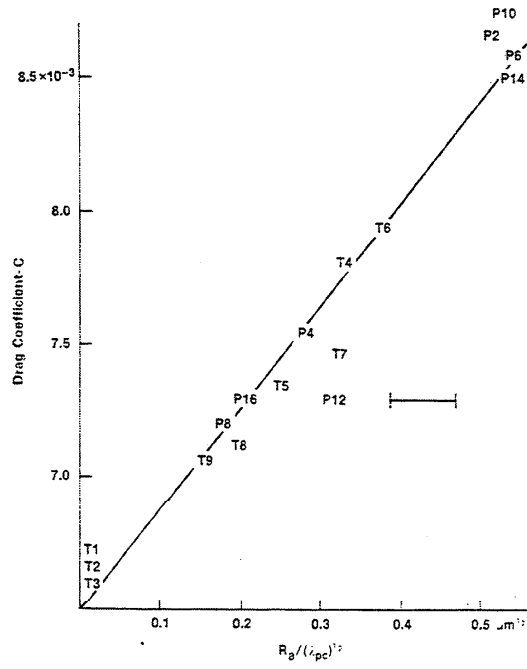


Figure 7-4

Results of Hydrodynamic Drag Experiment with Reanalysis

NASA
L-83-11,366

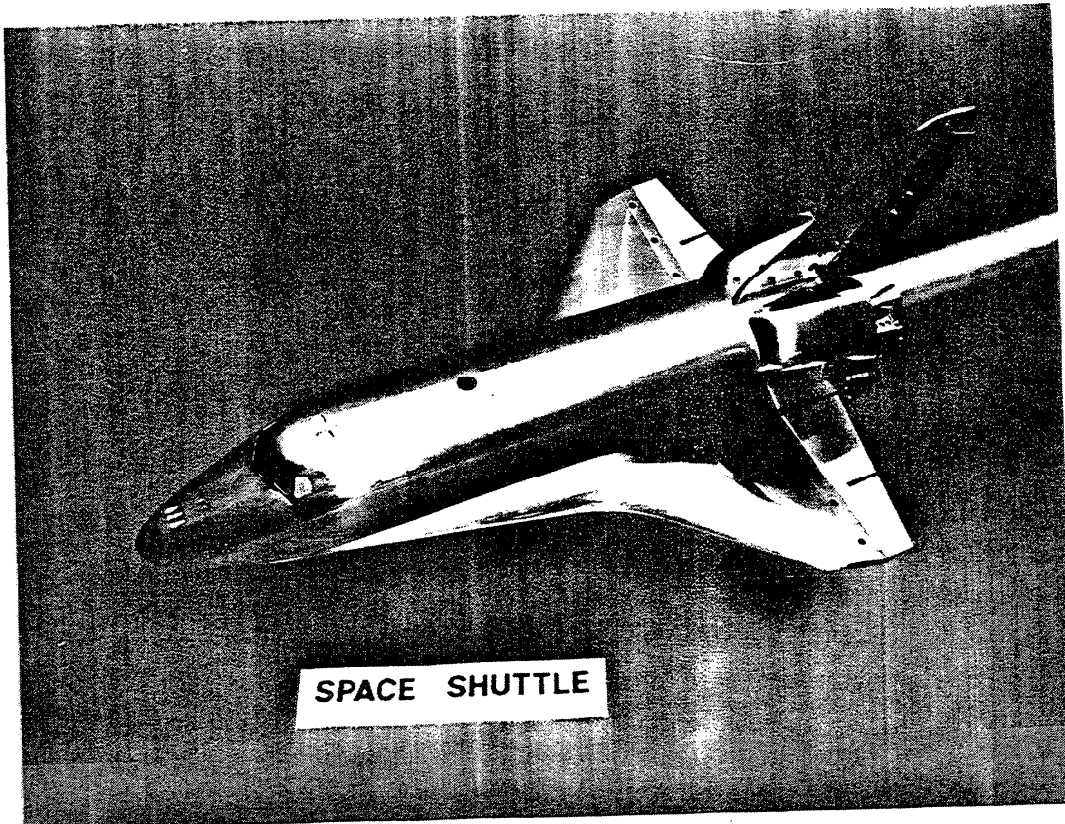


Figure 7-5
(Obtained from B.B. Gloss)

experiments on this and other aerodynamic models, the roughness of the model surfaces must be less than a certain admissible roughness height. This is shown in Fig. 7-6, where admissible roughness height in μ inch [19] is plotted as a function of the Reynolds number of the flow over the part. As the Reynolds number increases, you need to have smoother and smoother surfaces for accurate experiments. The graph is based on the work of Nikuradse more than 50 years ago [20]. In fact, further systematic work is required to understand this phenomenon better and to improve on the concept of admissible roughness height, a peak-to-valley parameter that is not well defined for random surfaces. Nevertheless, the overall point of the graph is well taken. As you increase the Reynolds number, you need to have smoother and smoother models in the tunnel. For NASA's highest performance wind tunnel, the National Transonic Facility (NTF), the surfaces of the model must have a roughness height less than 8 μ in.

METALWORKING

Measurements of surface roughness for metalworking components likely form the bulk of surface roughness measurements throughout the world. The automotive industry is one example where the manufactured surfaces are carefully specified. Figure 7-7 is a table of information, published by Young [21] about 13 years ago. It shows roughness specifications, in terms of arithmetic average roughness AA, an old expression for R_a , for a number of components on an automobile. These formed a part of specifications developed by an automobile manufacturer. It is likely true that they were drawn up empirically and were probably similar to specifications elsewhere in the automobile industry. However, there is no real collective body of knowledge that describes these types of specifications and the reasons for them. As far as we can tell, the information is scattered throughout the literature or is proprietary.

Figure 7-8 is information from a paper by Griffiths [14], who relied in part on work in Germany by Tonshoff and Brinksmeier [22]. The chart lists the correlations between surface physical properties and the various

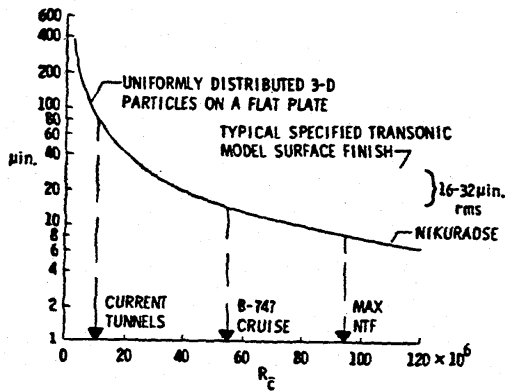


Figure 7-6
(from McKinney[19])

Figure 1. Admissible Roughness heights as a function of Reynolds number for typical NTF sized models. A mean chord of 0.20 m (0.65 ft.) was assumed. The line indicates the admissible peak-to-valley roughness heights based upon Schlichting's application of Nikuradse's measurements. The shaded band indicates root-mean-square roughnesses typically specified for transonic model surfaces.

Table : Surface Roughness of Automobile Motor Production Parts in Microinches AA

Component	Car No. 1		Car No. 2	
	Acceptable Roughness	Mfg. Process	Acceptable Roughness	Mfg. Process
Cylinder Block				
Cylinder Bore	16-20	Hone	20-25	Hone
Tappet Bore	60-75	Ream	80-120	Ream
Main Bearing Bore	60-80	Bore	130-150	Bore
Head Surface	40-50	Mill	190-210	Mill
Piston				
Skirt	45-55	Grind-Polish	40-50	Grind
Pin Bore	30-38		11-13	
Piston Pin	9-12	Grind-Lap	3-5	Grind-Lap
Crankshaft				
Main Bearing Journal	4-6	Grind-Polish	6-9	Grind-Polish
Connecting Rod Journal	4-6	Grind-Polish	6-9	Grind-Polish
Camsshaft				
Journal	4-6	Grind-Polish	14-18	Grind-polish
Cam	15-20	Grind-Polish	22-26	Grind
Rocker Arm Shaft	14-18	Grind	20-22	Grind
Rocker Arm				
Bore	29-32	Bore-Polish	30-40	Bore-Polish
Valves				
Intake Valve Stem	34-38	Grind	16-22	Grind
Intake Valve Seat	25-40	Grind	30-40	Grind
Exhaust Valve Stem	18-20	Grind	14-20	Grind
Exhaust Valve Seat	34-45	Grind	30-35	Grind
Tappet				
Face	4-5	Grind		
O.D.	14-18	Grind		
Hydraulic Lifter				
Face	22-25	Grind-Polish	15-20	Grind
O.D.	14-16	Grind-Polish	13-14	Grind

Figure 7-7
(from Young [21])

Cause of Failure	Surface Physical Properties						
	Yield Stress	Hardness	Strength	Fatigue Strength	Residual Stress	Texture	Micro Cracks
Plastic Deformation	●	●					■
Scuffing/Adhesion		●					
Fracture/Crack			●				○
Fatigue				●	○	○	●
Cavitation		○					○
Wear		●		■	○		■
Diffusion						○	
Corrosion		■			○	■	●

- Strong Influence
 - Traceable Influence
 - Supposed Influence
 - Additional Information
-) Original 1980
) Survey

Figure 1 Correlation between surface properties and failure causes.^{1,2}

Figure 7-8

(from Griffiths, [14])

Performance Parameter	Roughness	Waviness	Form	Layer	Laps & Tears	Chemistry	Metallurgy	Stress & Hardness
Sealing	●	○		○	○			●
Accuracy	●	○	○		○			●
Cleanliness	●				○	●		
Reflectivity	●	○		○	○	○		
Tool Life	●			○	●		●	●
Load Carrying	○	●						○
Creep	○					●	○	●
Magnetism						●	●	●
Electrical Resistance	●					○	○	
Assembly	○				○	●		○
Fluid Flow	●	○		○				
Joints	●	○		○				●

Figure 7-9

(from Griffiths, [14])

Figure 2 The influence of various surface aspects on functional performances.²

causes of failure -- plastic deformation, scuffing, etc. The circles are taken from Tonshoff and Brinksmeier and the squares from Griffiths' additional research. The surface texture itself enters in as a cause of plastic deformation, fatigue (to a lesser extent), and diffusion and corrosion. Griffiths also draws up a second chart (Fig. 7-9) that lists performance parameters vs. surface parameters. This chart discusses not only roughness and waviness, but also the metallurgy and chemistry of the surfaces and other qualities as well. Roughness is particularly important for sealing, for dimensional accuracy, for preserving the cleanliness of the component, and for optical reflectivity as we have seen before. Griffith's work, therefore, is one effort to systematize a body of knowledge on surface function.

One example of a new research result is from the work of Davis et al. [1,15]. who measured the 3-D topography of various places in a single-engine cylinder bore and related the topography to the component's wear. Based on those detailed results of the topography of the surface, they developed a chart showing oil volume in mm^3 vs. the amount of the surface that had been truncated by the wearing process. For an engine cylinder bore, oil volume is of crucial importance. Figure 7-10 shows data taken from their calculations based on the 3-D topographic maps. The oil volume is related to the volume of the surface valleys, calculated from their 3-D topographic measurements. The mathematical truncation process is a simulation of a wear process that cuts off the surface peaks. As the truncation proceeds, the oil volume in the valleys decreases. Based on their information and measurement results, Davis et al. predicted that the component begins to fail at a truncation level between 60-70%, because the oil volume has decreased to unacceptable levels.

Some comprehensive and systematic work on surface function for automobile components has culminated in the R&W system, developed by Bielle and others in the French automobile industry [10,11,16,23]. One motivation for their work was the importance to them of the distinction between roughness and waviness on a component. In order to specify a surface parameter closely related to the function of the component, you

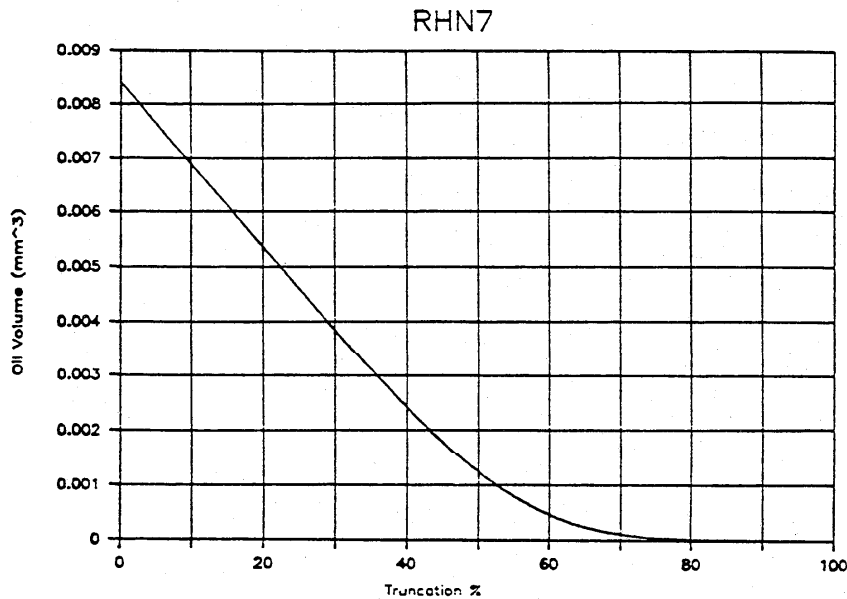
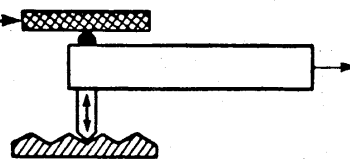


Figure 7-10
Oil Volume for Cylinder Bores (from Davis et al. [15])

R&W Approach — No Filtering

- Collect and Store Undistorted Surface Profiles Using Stylus Instruments with Flat Reference Datums



- Profiles are Digitized and Stored
- All “Filtering” is Done in the Analysis

Figure 7-11

had to distinguish in an appropriate way between roughness and waviness. To review, roughness consists of the closely spaced irregularities, such as may be produced by cutting tool marks or the grit of a grinding wheel; waviness consists of the more widely spaced irregularities that might be due to the vibration of the tool or workpiece. Roughness and waviness are caused by different aspects of production, and they likely have different effects on surface function. However, it is very difficult to characterize the distinctions between them mathematically. Bielle et al. attempted to overcome this difficulty.

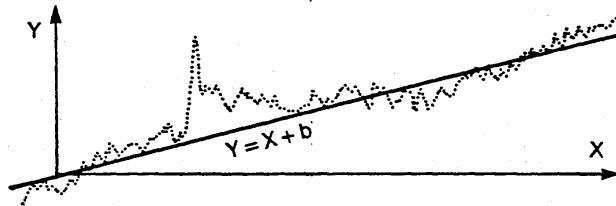
A second concern for them were the traditional methods of surface texture measurement, which made use of mechanical skids and RC electric filters that distorted the surface profiles, and the widespread use of velocity sensitive transducers rather than direct-profiling LVDT's. Bielle's approach (Fig. 7-11) to relate surface topography to function, therefore, called for undistorted measurements of surface profile using stylus instruments with flat reference datums. The profiles were then digitized and stored and all filtering was done in the analysis shown in Fig. 7-12. First, a least-squares line was fitted to the surface profile. Then the deviations with respect to that least-squares line were analyzed.

Bielle et al. applied a criterion for ignoring small peaks in the profile; then they grouped the remaining peaks and valleys into structures known as motifs or patterns, which are elemental peak-trough-peak sequences. The surface profile can be completely described by a succession of these peak-trough-peak sequences, and each of the motifs has two characteristic heights given by the legs on each side and a width extending from peak-to-peak. Then Bielle et al. applied a set of criteria to pick out the significant motifs. Using these rules, they combined motifs. The rules describe when to combine adjacent motifs to make a bigger one and when to keep them as separate and significant.

The resulting surface profiles are exemplified in Fig. 7-13 as a collection of motifs that can be characterized for their average roughness

Analysis:

1) Fit Least Squares Straight Line



2) Ignore Small Peaks

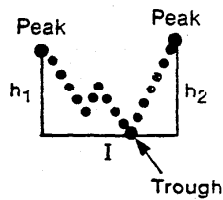
3) Identify Motifs:
Peak-Trough-Peak Sequences

Figure 7-12

Characterized by

- Width "I"
- Both Heights h_1 & h_2
- Characteristic "T"

(T = minimum of h_1 h_2)



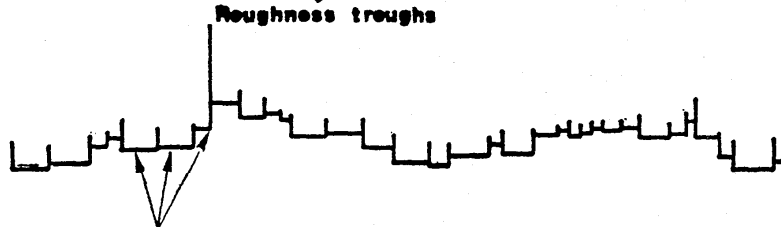
4) Combine Motifs



with 4 Conditions

**SEPARATION OF WAVINESS & ROUGHNESS
OF PROFILE TOP ENVELOPE LINE (T.E.L.)**

T.E.L. : line joining the peaks of roughness profile



Patterns retained = Roughness patterns

Figure 7-13
(from J. Bielle)

height R and their average roughness spacing AR (Fig. 7-14), two parameters considered to be closely related to certain functions of the surface.

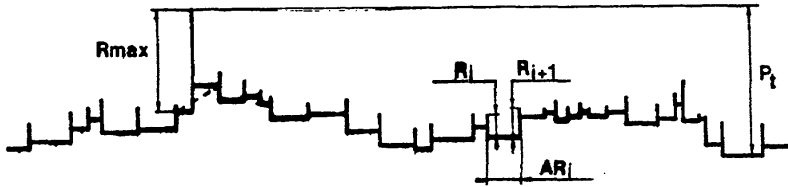
Once this elemental surface roughness pattern was generated, a waviness profile was developed by connecting the peaks of the motifs. Then the waviness motifs were constructed from the waviness profile, and the characteristic waviness height and spacing were calculated.

These parameters were correlated with function through an experimental study of the lifetimes of automotive parts in which 660 surfaces were measured, involving approximately 2000 profiles and 27,000 calculations of parameters. Based on this information, they developed an industrial standard and an examination for workers in surface quality control. They also kept fairly good control of drawing specifications. In particular, for each specification of a surface texture parameter, the function had to be specified and very often the machining process as well.

Figure 7-15 shows some of the key ideas that they developed. The left side of the table shows 18 different surface functions. Each of these functions has an appropriate symbol, and it was recommended that any specified value of a surface parameter be accompanied by the symbol of the function of the surface. Therefore, the designer had to understand the uses to which the surface would be put.

In addition, the chart shows the parameters that are considered to be important. An interesting example is resistance to hammering. Here the critical parameter is neither the roughness nor the waviness, but the bearing area curve calculated from the total profile. This is a way to quantify the deep cracks that can be harmful to surfaces that undergo a repeated hammering process such as a cam or cam follower.

CALCULATION OF P_t - R_{max} - R - AR



$$R = \frac{1}{m} \sum_{i=1}^{i=m} R_i$$

m : number of R_i's

$$AR = \frac{1}{p} \sum_{i=1}^{i=p} AR_i$$

p : number of AR_i's

Figure 7-14
(from J. Bielle)

SURFACE FUNCTIONS			PARAMETERS									
			ROUGHNESS			WAVINESS			TOTAL PROFILE			
DESIGNATIONS		SYMBOL	R	R _{MAX}	AR	W	W _{MAX}	W _L	AW	P _t	T _p (μ)	
TWO PARTS IN CONTACT	WITH RELATIVE DISPLACEMENT	SLIDING (LUB.)	FG	●			<.6R			○	●	
		SLIDING (DRY)	FS	●		○		●		○		
		ROLLING	FR	●			<.6R	●		○	○	
		RESISTANCE TO HAMMERING	RM	○		○	○			○		●
		FLUID FRICTION	FF	●		○				○		
	WITHOUT DISPLACEMENT	DYNAMIC SEALING	WITH SEAL	ED	●	○	○	<.6R	●		○	
			WITHOUT SEAL	ED	○	●		<.6R				●
		STATIC SEALING	WITH GASKET	ES	○	●		< R		○	○	
			WITHOUT GASKET	ES	○	●		< R	●			
		PRESS FIT	AC	○								●
ADHERENCE (BONDING)	AD	●							○			
INDEPENDENT SURFACE	WITH STRESS	TOOLS (CUTTING SURFACE)	OC	○		○	●		●			
		FATIGUE STRENGTHS	EA	○	●	○					○	
	WITHOUT STRESS	CORROSION RESISTANCE	RC	●	●							
		PAINT COATING	RE			○				○		
		ELECTROLYTIC COATING	DE	●	<2R	●						
		MEASURES	ME	●			< R					
		APPEARANCE (ASPECT)	AS	●		○				○		

- : MOST IMPORTANT PARAMETERS TO BE SPECIFIED
- : SECONDARY PARAMETERS TO BE SPECIFIED DEPENDING ON FUNCTIONS

Figure 7-15
(from J. Bielle)

A SURFACE TEXTURE INFORMATION SYSTEM

The above are only a few examples of surface topographic characterization and its relationship to surface function. Much of the information may be held as proprietary by companies, and the information in the literature is not well systematized. Therefore, we have been working with the ANSI standards committee to develop a surface texture information system (ASTIS) in order to relate surface texture specification to functional performance. ASTIS will be a systematic body of knowledge that would assist the designer to choose surface texture parameters for optimizing various surface functions. The ASTIS architecture is similar to a computerized tribology information system [24] presently under development.

ASTIS (Fig. 7-16) would consist of a functional database, a profile database, a characterization system, a knowledge development system, and an electronic bulletin board for sharing ideas. It would be used for a number of endeavors in addition to surface texture characterization (Fig. 7-17) such as product design, product testing, process development and diagnosis, and for information exchange.

The characterization system (Fig. 7-18) would have a menu of surface parameters and functions so that parameters such as amplitude, slope, and curvature; statistical functions such as the autocorrelation function; and parameters related to optical and capacitance methods of measurement could be calculated and intercompared. Various profile filtering methods would also be accessible to the user.

The profile database (Fig. 7-19) would involve the establishment of an atlas of surface profiles from different finishing processes, so that an engineer could access a surface profile in the atlas and then characterize that profile with the characterization system. Profiles would come from various places, such as the existing NIST profile database and the CIRP study by Peters and Vanherck.

A SURFACE TEXTURE INFORMATION SYSTEM

consisting of

- . FUNCTIONAL DATABASE
- . PROFILE DATABASE
- . CHARACTERIZATION SYSTEM
- . KNOWLEDGE DEVELOPMENT SYSTEM
- . ELECTRONIC BULLETIN BOARD

Figure 7-16

A SURFACE TEXTURE INFORMATION SYSTEM

intended use

- . PRODUCT DESIGN
- . PRODUCT TESTING
- . PROCESS DEVELOPMENT/DIAGNOSIS
- . SURFACE TEXTURE CHARACTERIZATION
- . INFORMATION EXCHANGE

Figure 7-17

A SURFACE TEXTURE INFORMATION SYSTEM

CHARACTERIZATION SYSTEM

- . MENU OF SURFACE PARAMETERS AND FUNCTIONS
 - . AMPLITUDE, SLOPE, CURVATURE
 - . AUTOCORRELATION, POWER SPECTRUM, CROSS COR.
 - . OPTICAL METHODS (PROFILE - SCATTERING)
 - . CAPACITANCE METHOD (PROFILE - CAPACITANCE)
 - . PARAMETERS BASED ON ISO, USA, DIN, FRANCE
JAPAN NATIONAL STANDARDS
- . FILTERING METHODS INCLUDED (CUTOFFS, MOTIF)
(CODES TO BE DOCUMENTED EXPLICITLY)

Figure 7-18

A SURFACE TEXTURE INFORMATION SYSTEM

PROFILE DATA BASE

- . TO ESTABLISH AN ATLAS OF SURFACE PROFILES
FROM DIFFERENT FINISHING PROCESSES
- . PROFILES FROM QIA PROJECT, NBS LIBRARY
- . PROFILES FROM CIRP STUDY
- . ESTABLISH GUIDELINES FOR STORAGE

Figure 7-19

A SURFACE TEXTURE INFORMATION SYSTEM
FUNCTIONAL DATABASE
. INITIAL STUDY (SEALING ,CYLINDER LINERS)
. FRENCH FUNCTIONAL SYNTHESIS
. LITERATURE SURVEY
. WORKING GROUPS

Figure 7-20

A SURFACE TEXTURE INFORMATION SYSTEM
KNOWLEDGE DEVELOPMENT SYSTEM
. WILL USE STATISTICS AND PATTERN
RECOGNITION TECHNIQUES
. WILL MAKE USE OF PROFILE DATABASE AND
CHARACTERIZATION SYSTEM
. WILL BE USED FOR PROCESS DEVELOPMENT
OR PROCESS DIAGNOSIS
. WILL BE USED FOR FUNCTIONAL CORRELATION
STUDIES IN PRODUCT LIFE TESTING

Figure 7-21

The functional database (Fig. 7-20) will be the heart of the system and will be developed with initial studies on sealing and cylinder liners. It will also use the French functional synthesis that we described before.

The knowledge development system (Fig. 7-21) will incorporate statistics and pattern recognition techniques and apply them to existing information such as the profile database and the characterization system or to the results of experiments in order to increase the functional knowledge of surfaces. In particular the knowledge development system will be useful for functional correlation studies in product life testing.

Lastly, an electronic bulletin board will facilitate information exchange in which current research results could be shared.

We project that the prototype ASTIS would function on a PC-AT, a PS-50 or a Sun-386, would likely be programmed in Turbo C and would use the Turbo Database. This would allow us to get the system up to speed very quickly. Once the start up phase is completed, the required resources would amount to about \$500K per year and would be based on users' fees.

In conclusion, information concerning surface function is appreciable, but not well systematized. It would be of great benefit to systematize and develop surface functional knowledge, and that is the purpose of the surface texture information system that we are proposing.

REFERENCES

FUNCTION

1. Sec. 4, Ref. 18.
2. Willn, J.E. Characterization of Cylinder Bore Surface Finish - A Review of Profile Analysis, *Wear* 19, 143 (1972).
3. Campbell, J.C. Cylinder Bore Surface Roughness in Internal Combustion Engines: Its Appreciation and Control, *Wear* 19, 163 (1972).

4. Lackenby, H. Resistance of Ships, with Special Reference to Skin Friction and Hull Surface Condition, Proc. Instn. Mech. Eng. 176, 981 (1962).
5. Malone, J.A.; Murtagh, M.M.; Ailman, M.J.; Baetsen, K.D.; Little, D.E. Ship Roughness Technology Program, Vol. 1, Dept. of Commerce Report MA-RD-930-81014 (Oct. 1980).
6. Bennett, J.M.; Burge, D.K.; Rahn, J.P.; Bennett, H.E. Standards for Optical Surface Quality Using Total Integrated Scattering, Proc. SPIE 181, 124 (1979).
7. Sec. 6, Ref. 1.
8. Madey, T.E. The Role of Steps and Defects in Electron Stimulated Desorption: Oxygen on Stepped W(110) Surfaces, Surface Sci. 94, 483 (1980), and references contained therein.
9. Furtak, T.E. Current Understanding of the Mechanism of Surface Enhanced Raman Scattering, J. Electroanal. Chem. 150, 375 (1983).
10. Scheffer, B.; Thurel, C. Donnees de base de la Realisation d'un Calculateur R et W, Mecanique, Materiaux, Electricite, No. 286, 19 (October 1973).
11. Bielle, J. Functional Needs, Machining Conditions, and Economics of Surface Finishing (translated by T. V. Vorburger and V. B. Roy), Prec. Eng. 7, 31 (1985).
12. Vorburger, T.V.; Scire, F.E.; Teague, E.C. Surface Roughness Measurements of Circular Disks and Their Correlation with Hydrodynamic Drag, NBS Tech. Note 1151 (U.S. Dept. of Commerce, Washington, DC, 1982).
13. Young, M. The Scratch Standard is Only a Cosmetic Standard, Laser Focus/Electro Optics, 138 (Nov. 1985).
14. Griffiths, B.J. Manufacturing Surface Design and Monitoring for Performance, Surface Topography 1, 61 (1988).
15. Davis, E.J.; Sullivan, P.J.; Stout, K.J. The Applications of 3D Topography to Engine Bore Surfaces, Surface Topography 1, 229 (1988).
16. Bhasker Rao, N.A.; Raja J. A Knowledge Based System of Surface Texture Parameters - a Preliminary Investigation, Surface Topography 1, 445 (1988).
17. Vorburger, T.V.; Scire, F.E.; Teague, E.C. Hydrodynamic Drag Versus Roughness for Rotating Disks, Wear 83, 339 (1982).

19. McKinney, L.W. Overview of National Transonic Facility Model Technology Program, in Cryogenic Wind Tunnel Models, NASA Conf. Publ. 2262 (NASA Langley, Hampton, VA, 1983).
20. Sec. 2, Ref. 44.
21. Sec. 2, Ref. 15
22. Tonshoff, H.K.; Brinksmeier, E. Determination of the Mechanical and Thermal Influences on Machined Surfaces by Microhardness and Residual Stress Analysis, CIRP Annals 29/2, 519 (1980).
23. Sec. 3, Ref. 34.
24. Jahanmir, S.; Ruff, A.W., Hsu, S.M. A Computerized Tribology Information System, Proc. ASM Conf. on Engineered Materials for Advanced Friction and Wear Applications (Gaithersburg, MD, March 1988).

Appendix A
April 1990

Measurement Conditions and Sources of
Uncertainty for NIST* Roughness and Step Height
Calibration Reports
*(FORMERLY NBS)

The property of surface roughness in the 5 μm Ra range and below and step heights in the 0.01 to 25 μm range are currently measured at the NIST by means of a minicomputer/stylus instrument system. Using an interferometrically measured step, the system is calibrated on each value of magnification employed during a measurement. Profiles of the calibrating step and the step or roughness area under test are stored in the minicomputer memory using 12 bit analog to digital conversion.

In measurement of roughness, surface profiles are taken with a lateral sampling interval of 1 μm over the traversing length of 4 mm. Ra values are then calculated as described in Appendix C of American National Standard ASME/ANSI B46.1-1985.

Two parameters of the instrumentation are important in the specification of roughness measurements. These are the stylus radius and the high pass electrical cutoff. We are continually refining our surface instrumentation and therefore, our own methods of specifying these two parameters are in a state of change.

The stylus radius is a difficult quantity to define, and we have recently been using an algorithm that is simpler than both the method found in the ANSI B-46.1-1985 standard and the method developed by us and reported previously in our article, "Measurements of Stylus Radii", available on request.

In our approach, a profile of the stylus is measured according to procedures discussed in the above article, and the stylus width is then calculated rather than the radius. The width is defined to be the distance between the two points of contact when the stylus profile is inscribed in a 150° angle. (See the enclosed illustration).

The stylus width according to this procedure has been measured to be $5.0 \pm 0.5 \mu\text{m}$. We intend to propose our new approach to the ANSI/ASME Committee B46 on the Classification and Designation of Surface Qualities as a standard approach to define stylus width instead of stylus radius.

The nominal cutoff of the high-pass electrical filter is 0.8 mm. Its transmission characteristics are in accordance with the 2RC filter described in ASME/ANSI B46.1-1985.

The above measurement conditions of stylus trace length, sampling interval, stylus width, and electrical filtering are the customary ones for our roughness measurements. Any unusual experimental parameters are given in the covering report.

In step height measurements, a straight line is fitted by the method of least squares to each side of the profile of the step, and the height is calculated

from the relative position of these two lines. The detailed experimental parameters of each measured step are given in the covering report.

Uncertainty of Ra Measurements:

The uncertainty quoted is the sum of the NIST system calibration uncertainty and a three-standard-deviations limit of variations about the mean value of data obtained from stylus traverses at ten uniformly distributed positions on the test specimen's surface.

There are six sources of calibration uncertainty in the NIST measurement process, and these may be described in terms of two categories: systematic uncertainty and random uncertainty. Systematic uncertainties result from those properties of the measurement process which are fixed prior to and during the procedure of obtaining data. Random uncertainties assess the variations in the data from one measurement to the next and from day to day.

Analytical and empirical studies of the components of the measurement process random uncertainty have been performed. These studies show that the net random uncertainty may be attributed to three sources:

- (1) The surface finish of the calibrating step. This leads to an uncertainty in stylus measurements of the calibration step to obtain the calibration constant for the instrument.
- (2) Variations in the calibrating constant due to sampling and digitizing processes, software computations, and nonlinearities in the stylus instrument transducer and in the interface hardware.
- (3) Variations in the measured Ra values due to the nonlinearities mentioned in (2).

A net random uncertainty for the measurement process is computed, for a particular Ra value and calibration step height, as the RMS sum of these components.

Sources of the systematic uncertainty are:

- (4) The uncertainty in the height of the calibrating step as determined from interferometric and stylus measurements.
- (5) Uncertainty in the horizontal resolution of the instrument. This is most often due to uncertainty in the stylus width. For very fine styli with good horizontal resolution, the resolution of the instrument itself may be limited instead by the frequency response of the electronics. Uncertainty in either quantity causes a small amount of uncertainty in Ra, which also depends on the roughness and form of the profile. The quoted uncertainties represent estimates for typical surfaces measured in the various roughness ranges.
- (6) Instrumental noise. This component always increases the Ra value and depends on the instrument itself. For the high resolution instrument, the noise is considerably lower than it is for the low resolution

instrument. This component is negligible for surfaces with Ra greater than 0.2 μm .

A net systematic uncertainty for the measurement process is computed, for a particular calibration step height, as the RMS sum of these three components.

The calibration uncertainty of the NIST system for measuring surface roughness is taken as the sum of the system's random uncertainty and its systematic uncertainty. The expressions used for each component depend on the calibrating step height H, and the Ra value itself, and on whichever instrument in our laboratory is used for the measurement. The calibration uncertainty (CU) as a function of the specimen Ra roughness is therefore given by the formulas shown in Table A.1.

Uncertainty of Step Height Measurements:

The quoted uncertainty of the step height measurements is the sum of the NIST system calibration uncertainty and a three-standard-deviations limit of variations about the mean value of data obtained in three stylus traverses at each of ten uniformly distributed positions on the step.

Calibration uncertainty in step height measurements arises from the same sources already described for roughness with the exceptions that components 5 and 6 are eliminated. Neither the horizontal resolution nor the instrumental noise causes any systematic uncertainty in the step height measurements. Instrumental noise, however, contributes to the random variation of the measurement results over the set of measurement positions. The calibration uncertainty is taken as the sum of the systems's random uncertainty and systematic uncertainty. The formulas which are used to calculate the calibration uncertainty depend on the height of the measured step (X) and the height of the calibration step (H) and are given in Table A.2.

The uncertainty reported by NIST represents only the estimated uncertainty in the NIST calibration of the customer's specimen. Additional uncertainties arising in the customer's use of the specimen (e.g., to transfer a calibration to another device) should be evaluated by the customer.

Additional information on the NIST surface measurement system is contained in the following articles which may be obtained from the authors.

E. C. Teague, Evaluation, Revision, and Application of the NBS Stylus/Computer System for the Measurement of Surface Roughness, NBS Tech Note 902 (U.S. Department of Commerce, Washington, D. C., 1976).

E. C. Teague, "Uncertainties in Calibrating a Stylus Type Surface Texture Measuring Instrument with an Interferometrically Measured Step", *Metrologia* 14, 39 (1978).

T. V. Vorburger, E. C. Teague, and F. E. Scire, "Fast Facility Available for Engineering Needs", *Dimensions/NBS* Nov., p. 18 (1978).

T. V. Vorburger, E. C. Teague, F. E. Scire, and F. W. Rosberry, "Measurements of Stylus Radii", *Wear* 57, 39 (1979).

T. V. Vorburger, Fastmenu: A Set of Fortran Programs for Analyzing Surface Texture, NBSIR 83-2703, U. S. Department of Commerce, Washington, D. C.(1983).

T.V. Vorburger and G.G. Hembree, "Characterization of Surface Topography," in Navy Metrology Research & Development Program Conference Report, Department of the Navy, p. 55 (Corona, CA, 1989).

D29:A13FEB87.DAT

TALYSURF 6 STYLUS RADIUS MEASUREMENT USING RAZOR BLADE AND PIEZO STAGE

PROF NO = 1

PTS 160 TO 1560

COMMENT - RAZOR BLADE POSITION #1

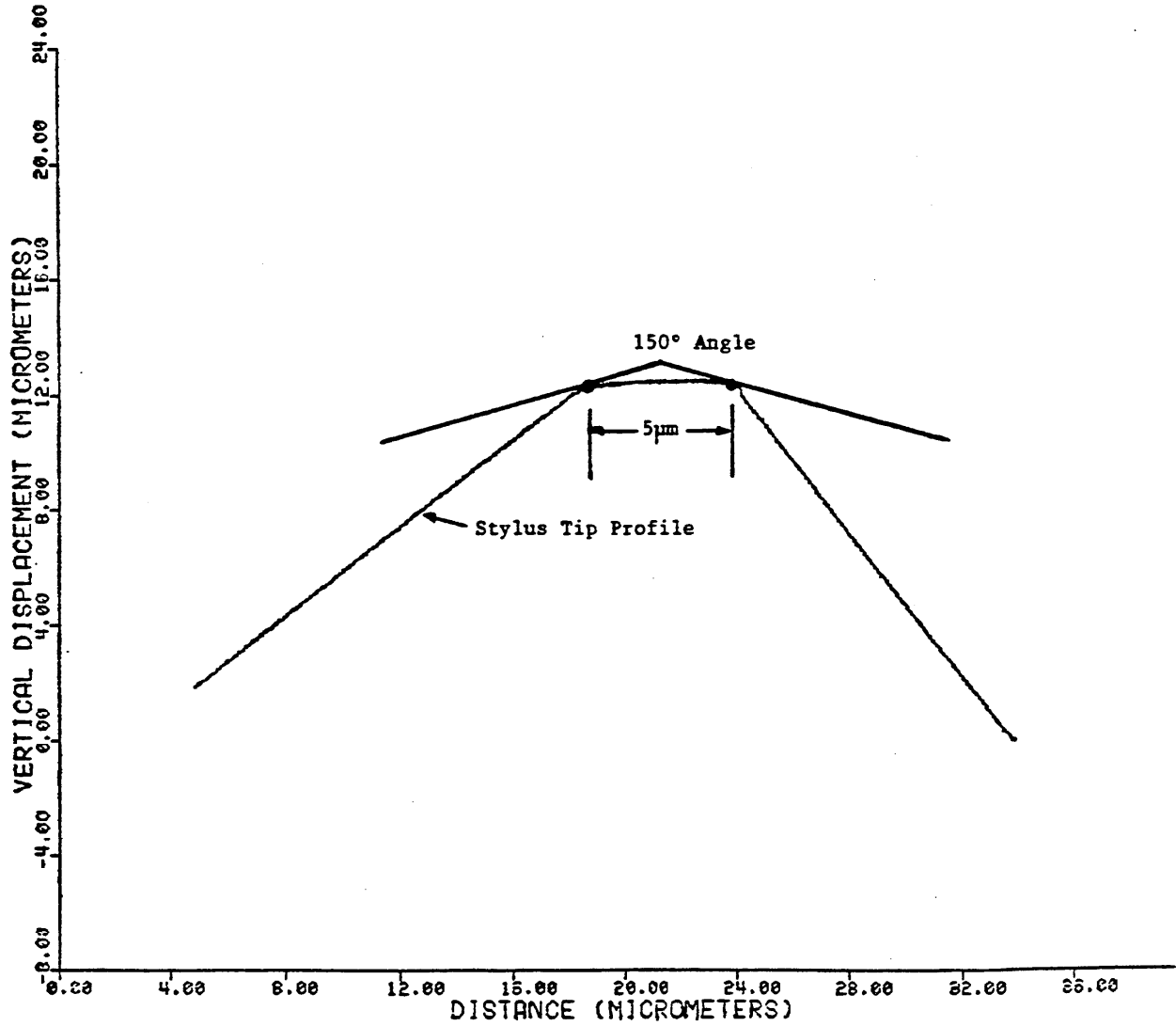


Table A.1

Calibration Uncertainty Formulas
for
NIST Roughness Measurements

R = measured Ra or Rq value
H = NIST calibration step
(all values expressed in nm)

H (instrument type)	1	2	3	4	5	6
29.1 (high resolution)	$[(1.2R/H)^2$	$+ (0.0055R)^2$	$+ (0.0055R)^2]^{1/2}$	$+ [(1.3R/H)^2$	$+ (0.25)^2$	$+ (0.16)^2]^{1/2}$
91.4 (high resolution)	$[(0.66R/H)^2$	$+ (0.004R)^2$	$+ (0.0054R)^2]^{1/2}$	$+ [(2.1R/H)^2$	$+ (0.25)^2$	$+ (0.16)^2]^{1/2}$
303 (high resolution)	$[(0.77R/H)^2$	$+ (0.0035R)^2$	$+ (0.011R)^2]^{1/2}$	$+ [(5R/H)^2$	$+ (4)^2$	$+ (0.16)^2]^{1/2}$
303 (long trace)	$[(0.77R/H)^2$	$+ (0.01R)^2$	$+ (0.014R)^2]^{1/2}$	$+ [(5R/H)^2$	$+ (6)^2$	$+ (8)^2]^{1/2}$
1015 (long trace)	$[(2.5R/H)^2$	$+ (0.01R)^2$	$+ (0.014R)^2]^{1/2}$	$+ [(9.3R/H)^2$	$+ (6)^2]^{1/2}$	
3042 (long trace)	$[(10R/H)^2$	$+ (0.01R)^2$	$+ (0.014R)^2]^{1/2}$	$+ [(12.4R/H)^2$	$+ (6)^2]^{1/2}$	
12.73×10^3 (long trace)	$[(27R/H)^2$	$+ (0.01R)^2$	$+ (0.014R)^2]^{1/2}$	$+ [(30R/H)^2$	$+ (6)^2]^{1/2}$	
22.90×10^3 (long trace)	$[(27R/H)^2$	$+ (0.01R)^2$	$+ (0.014R)^2]^{1/2}$	$+ [(30R/H)^2$	$+ (6)^2]^{1/2}$	

Table A.2

Calibration Uncertainty Formulas
for
NIST Step Height Measurements

X = measured step
H = NIST calibration step
(all values are expressed in nm)

H	Components			
	1	2	3	4
29.1	$[(1.2X/H)^2$	$+ (0.0055X)^2$	$+ (0.0055X)^2]^{1/2}$	$+ [1.3X/H]$
91.4	$[(0.66X/H)^2$	$+ (0.004X)^2$	$+ (0.0054X)^2]^{1/2}$	$+ [2.1X/H]$
303	$[(0.77X/H)^2$	$+ (0.0035X)^2$	$+ (0.0011X)^2]^{1/2}$	$+ [5X/H]$
1015	$[(2.5X/H)^2$	$+ (0.0035X)^2$	$+ (0.0025X)^2]^{1/2}$	$+ [9.3X/H]$
3042	$[(10X/H)^2$	$+ (0.004X)^2$	$+ (12)^2]^{1/2}$	$+ [12.4X/H]$
12.73×10^3	$[(27X/H)^2$	$+ (0.01X)^2$	$+ (0.01H)^2]^{1/2}$	$+ [30X/H]$
22.90×10^3	$[(27X/H)^2$	$+ (0.01X)^2$	$+ (0.01H)^2]^{1/2}$	$+ [30X/H]$